

**AQUITANIAN (LOWER MIOCENE) DEPOSITIONAL SYSTEMS: VINTON DOME,  
ONSHORE, GULF OF MEXICO, SOUTHWEST LOUISIANA**

---

A THESIS

PRESENTED TO

THE FACULTY OF THE DEPARTMENT OF GEOSCIENCES

UNIVERSITY OF HOUSTON

---

IN PARTIAL FULFILMENT

OF THE REQUIREMENTS FOR THE DEGREE

MASTER OF SCIENCE IN GEOLOGY

---

BY

MORENIKE OLAYINKA COKER

DECEMBER 2006

**AQUITANIAN (LOWER MIOCENE) DEPOSITIONAL SYSTEMS: VINTON DOME,  
ONSHORE, GULF OF MEXICO, SOUTHWEST LOUISIANA**

---

MORENIKE OLAYINKA COKER

APPROVED:

---

DR. KURT MARFURT, CHAIRMAN

---

DR. JANOK BHATTACHARYA, PROFESSOR

---

MR. GREGORY JONES, STRATIGRAPHER, EXXONMOBIL

---

DEAN, COLLEGE OF NATURAL SCIENCES AND MATHEMATICS

## **ACKNOWLEDGEMENTS**

My gratitude goes to the Almighty God for His infinite power, guidance and grace in accomplishing this program. My special thanks go to my committee members, Dr. Kurt Marfurt, Dr. Janok Bhattacharya and Mr. Gregory Jones (Exxonmobil) for their guidance, readiness, open-mindedness and contributions to my thesis. I also acknowledge the support of Dr. Charlotte Sullivan, Dr. Michael Murphy and Dr. Donald Van Nieuwenhuise for their useful discussions and module reviews along the course of the study. The following companies are also acknowledged for their assistance in providing biostratigraphic data: E. H. Stork, JR. and Associates, Paleo Control, Inc., Paleo Data, Inc., Shell Offshore Inc., and Unocal Corporation.

## **DEDICATION**

I dedicate this thesis to all my children, Michael Oladapo, Christopher Oluwaseun, Francis Oluwafunmbi and Agnes Morenike Oluwakemi, my husband and my parents, for all their support during the Master's degree program at the Geosciences Department of the University of Houston.



**AQUITANIAN (LOWER MIOCENE) DEPOSITIONAL SYSTEMS: VINTON DOME,  
ONSHORE, GULF OF MEXICO, SOUTHWEST LOUISIANA**

---

AN ABSTRACT OF A THESIS  
PRESENTED TO  
THE FACULTY OF THE DEPARTMENT OF GEOSCIENCES  
UNIVERSITY OF HOUSTON

---

IN PARTIAL FULFILMENT  
OF THE REQUIREMENTS FOR THE DEGREE  
MASTER OF SCIENCE IN GEOLOGY

---

BY  
MORENIKE OLAYINKA COKER  
DECEMBER 2006

## ABSTRACT

Biostratigraphic, geophysical, sequence-stratigraphic, and well data evaluation of the complexly faulted Vinton Dome field in the northwest Gulf of Mexico basin resulted in an improved Upper Oligocene and Lower Miocene stratigraphic architecture and provided new insights into the Chattian and Aquitanian depositional systems. Well control and modern seismic attribute analysis reveal the relation between the depositional environment, structural patterns and salt tectonics.

The structural setting of the Miocene shelf is the result of the hereditary Upper Oligocene structural design, and substantial evolution of sediment dispersal onto a thick column of the Anahuac shale and onto unstable salt bodies. The dome is characterized by a counter-regional fault, and three peripheral fault sets, each having a different outline and basis for its formation. Fine scale isotropic polygonal faults, averaging 200 ft (~ 60 m) in size, exist throughout the dome. Imaging of fine polygonal structures has been rarely documented in the Gulf of Mexico basin, although larger scale polygonal faults have been reported in the North Sea Basin.

Salt movement had set the stage for thinning and thickening of the Upper Chattian strata, creating unconformities, slumps, and onlap against the salt plug, whereas the Aquitanian is characterized by syn-deposition, and an unconformity as a result of sea-level fall and increased sedimentation, perhaps also caused by the salt withdrawal processes. Stratigraphic evaluation of the Upper Chattian reveals shale deformation structures that resemble sinuous sandy channel deposits that could contribute to pitfalls in seismic interpretation.

During sea level falls in the Late Oligocene to Early Miocene, the depocenter shifted from the west to the south with unconformities characterizing the southern parts of the dome. Transgressive systems tracts represented by the Late Oligocene Anahuac shale deposits are overlain by the highstand systems tracts of the Early Miocene Aquitanian deltaic sandstones.

# TABLE OF CONTENTS

<b>CHAPTER ONE: INTRODUCTION</b>	-----	1
1.1 REGIONAL GEOLOGIC SETTING	-----	2
1.2 PREVIOUS STUDY	-----	8
1.2.1 General Stratigraphy	-----	8
1.2.2 Vinton Salt Dome	-----	12
1.3 STUDY AREA	-----	13
 <b>CHAPTER TWO: METHOD OF STUDY</b>	 -----	 22
2.1 CHALLENGES	-----	22
2.2 DATA	-----	23
2.3 WELL TO SEISMIC TIE	-----	25
2.4 MAPPING TECHNIQUES	-----	28
2.5 SEISMIC ATTRIBUTES	-----	30
2.5.1 Attributes Sensitive to Structure	-----	31
2.5.2 Amplitude Attributes	-----	33
2.5.3 Waveform Similarity Attributes	-----	33
 <b>CHAPTER THREE: SALT TECTONICS AND STRUCTURAL DEVELOPMENT</b>	 -----	 36
3.1 PRINCIPLES AND APPLICATIONS	-----	36
3.1.1 Observations and Discussions on Structure of Vinton Dome	-----	39
3.2 STRUCTURAL EVALUATION	-----	46
3.2.1 Salt Shape	-----	46
3.2.2 Faults	-----	48
3.2.2.1 Major Faults	-----	48
3.2.2.2 Polygonal “Mosaic” Fractures	-----	56
3.2.3 Discussion on Faults	-----	63
3.2.4 Impact on Sedimentation	-----	64
3.2.5 Appendices	-----	70

<b>CHAPTER FOUR: INTEGRATED INTERPRETATION</b>	-----	74
4.1    APPLIED BIOSTRATIGRAPHY	-----	74
4.2    LOG INTERPRETATION	-----	80
4.3    SEQUENCE STRATIGRAPHY	-----	90
4.3.1    Sequence Stratigraphic Analysis by Well Logs	----	91
4.4    SEISMIC INTERPRETATION	-----	97
 <b>CHAPTER FIVE: CONCLUSIONS</b>	-----	115
 <b>REFERENCES:</b>	-----	118

# CHAPTER ONE

## INTRODUCTION

Small compartmentalized reservoirs are becoming increasingly economic in complexly faulted producing areas, such as the Vinton Salt Dome area. Production in the Vinton Dome, Onshore Gulf of Mexico has continued for over a century, but few published studies have focused on the geology of the shallow Miocene strata, which were presumed wet, partly due to the early-favored highly prolific and deeper Oligocene reservoirs, and largely due to lack of imaging technology to identify small by-passed fault compartments (Thompson & Eichelberger, 1928). Nevertheless, the Miocene strata are locally highly prolific at Vinton Dome, with ten acre fault blocks producing as much as 1 million barrels of oil (SONRIS Database Access, 2006).

New seismic attribute technology, developed at the University of Houston, has the potential to identify small or subtle subsurface features. My study tested the applicability of these new volumetric seismic attributes on deltaic-shelfal Aquitanian and Chattian strata constrained by biostratigraphic data. Attributes including coherence, curvature, and amplitude gradients, can be used to identify channels, channel belts, fault compartments, polygonal faults, deformation structures, subaqueous channels and prodelta turbidites. Using seismic, biostratigraphic, and a variety of well and engineering data, I am able to identify depocenters, depositional systems tracts, facies migration and stacking patterns, and their relations to salt tectonism.

My study not only characterizes the deposition of the Lower Miocene sandstones at Vinton Dome, it also highlights shale deformation structures that could otherwise simply be interpreted as fluvial structures, which may contribute to pitfalls in seismic interpretation, and also helps to develop workflows for navigating through the abundance of attributes available to seismic interpreters.

## **1.1 REGIONAL GEOLOGIC SETTING**

The Vinton Dome is located on the northern Gulf of Mexico shelf. The basin initialized in the Middle Jurassic during the break up of the North American lithospheric plate from the South American and African plates as a result of seafloor spreading associated with the break up of the Pangean supercontinent. (Salvador, 1987; Worall & Snelson, 1989). Regional subsidence, influx of marine waters, and restricted seawater circulation resulted in the deposition of a thick sequence of Jurassic evaporite deposits. These evaporite deposits (Figure 1) are thought to have been originally contiguous, but were later separated into a northern and southern belt by continued seafloor spreading during the Mid-Late Jurassic (Marton & Buffler, 1993; McBride *et al.*, 1998).

The northern salt, typically referred to as the Louann salt, is the major source of salt migration in the northern Gulf of Mexico. Following the evaporite deposition, clastic and carbonate sediments were deposited onto the salt resulting in basinward and upward migration of the salt (Salvador, 1987; Watkins *et al.*, 1996). The Cenozoic era was a period of extensive deposition of terrigenous sediments to the

basin (Galloway, 2001) (Figure 2). The northern part of the Gulf of Mexico basin was fed from the west, northwest, and north by sediments delivered by a major complex of avulsing river systems and reworked coastal sediments (Worall & Snelson, 1989).

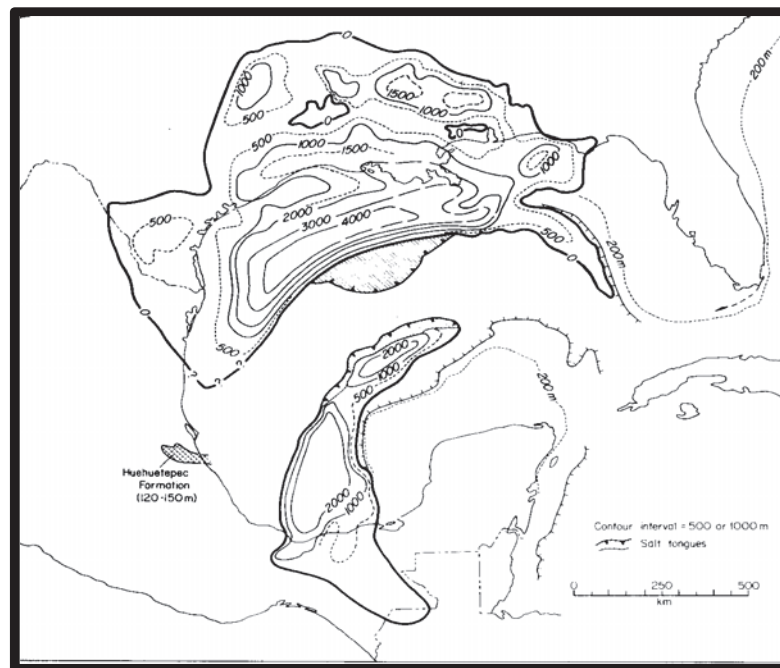


Figure 1: Paleogeographic map of the Middle Jurassic salt belt before Cenozoic deposits (Salvador, 1987)

The Miocene stratigraphic interval in the Gulf of Mexico is marked by 2 supersequences (Figures 3 & 4), each beginning with a gradual transgression, and ending with an abrupt regression (Fillon & Lawless, 2000). The first supersequence began below the Basal Miocene and ended at the middle Middle Miocene. The second supersequence extended beyond the Miocene into the Pliocene (Fillon &



Lawless, 1999). Periods of slow transgression due to gradual sea-level rise allow sediments to accumulate on the shelf and to gradually aggrade, while conforming to accommodation provided by salt withdrawal. Periods of major regression are marked by the formation of major disconformities or major by-pass of the shelf and deposition onto basin slopes and the adjacent abyssal plains.

However, sediments can be transported from the Gulf of Mexico shelf to reach the basin floor, by major by-pass during regression (at lowstands of sea-level), and also by gradual fill and spill processes primarily controlled by salt tectonics (Hamiter *et al.*, 1997; Combellas-Biggot & Galloway, 2002) as illustrated in Figure 2. Though sediment accumulation rate was non-uniform, especially during the Early Miocene, accumulation is expected to be greatest on the shelf during periods of rising sea level.

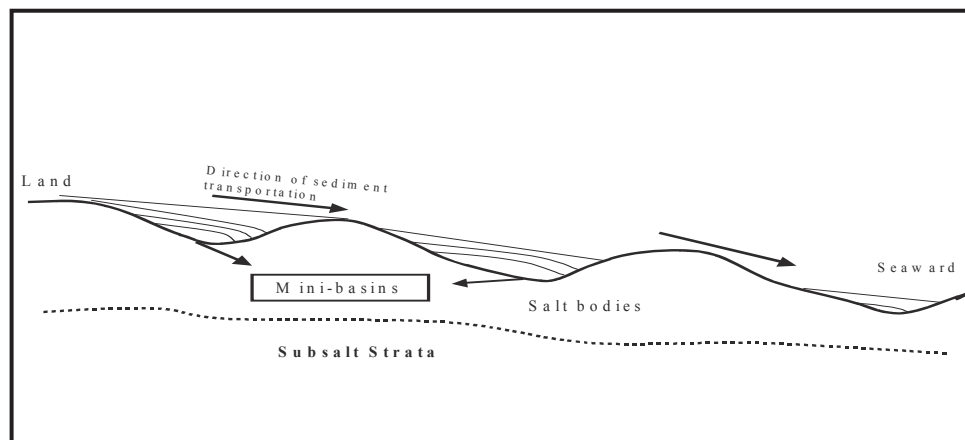


Figure 2: Illustration of sediment deposition and transportation along fill and spill minibasins on salt bodies. Not drawn to scale.

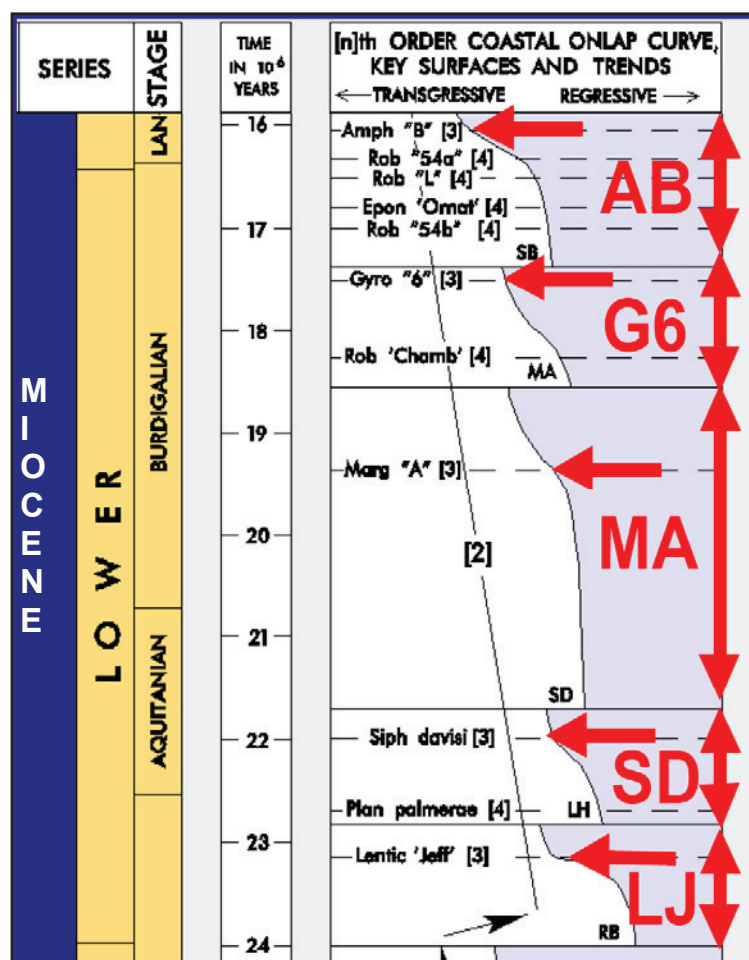


Figure 3: Sea Level and Depositional Cycles of the Lower Miocene (after Fillon *et al.*, 1997)  
 LJ – *Lenticulina jeffersonensis*; SD – *Siphonina davis*; MA – *Marginulina ascensionensis*; G6 – *Gyroidina* “6”; AB – *Amphistegina* “B”.

List of Abbreviations for Figures 3 and 4; LH – *Lenticulina hansen*; SD – *Siphonina davis*; MA - Marg A – *Marginulina ascensionensis*; Rob ‘chamb’ - *Robulus chambersi*; G6 - Gyro “6” – *Gyroidina* ‘6’; Epon ornat – *Eponides ornata*; Rob ‘L’ – *Robulus L*; AB - Amph ‘B’ – *Amphistegina* ‘B’; Cib Op – *Cibicides opima*; Cris “W” – *Cristellaria* ‘W’; Cris “I” – *Cristellaria* ‘I’; Big hum – *Bigenenerina humblei*; Tex “W” – *Textularia W*; Cib carst “1” – *Cibicides carstensi* ‘1’; Cib inflat – *Cibicides inflata*; Tex “L” – *Textularia* ‘L’; Rob “E” – *Robulus* ‘E’

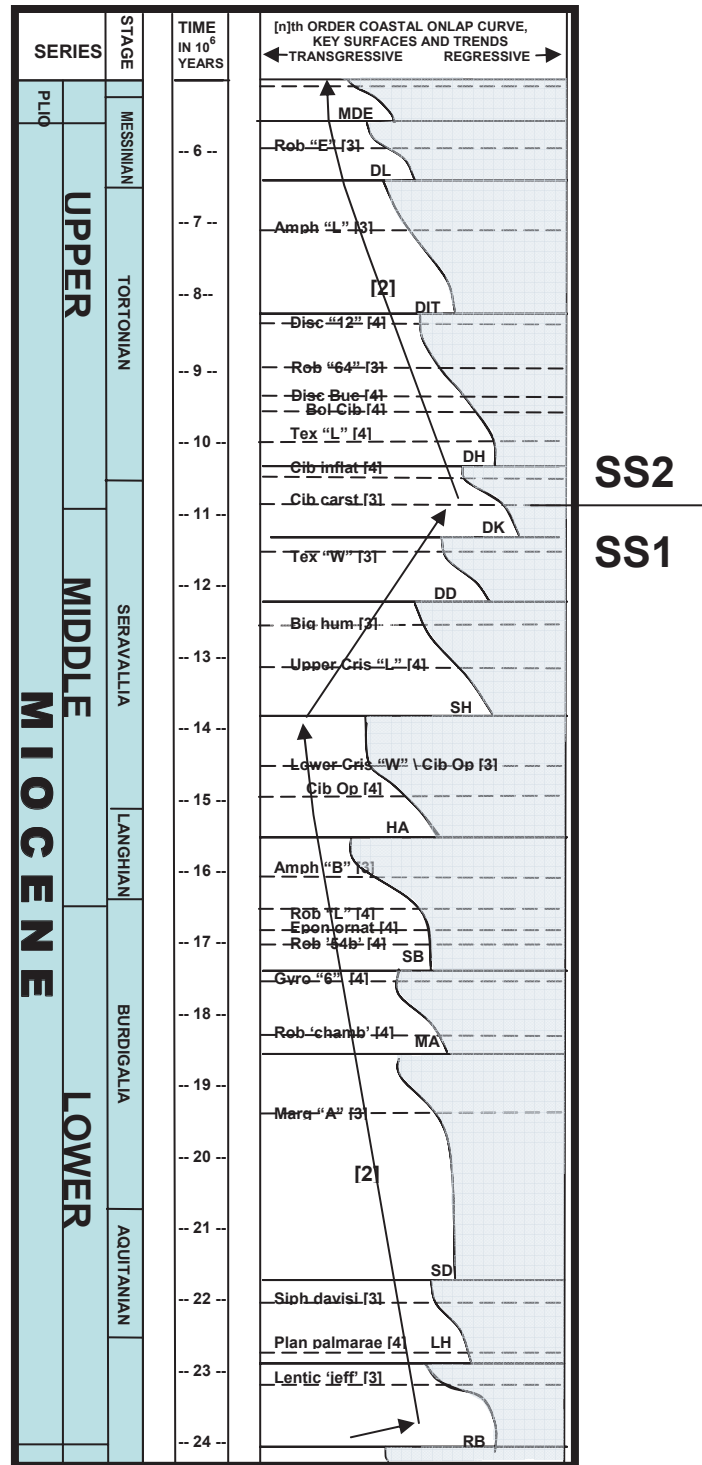


Figure 4: Coastal Onlap Curve, Miocene, Northern Gulf of Mexico  
(Modified after Fillon, 1997) SS = Supersequence

*Lenticulina jeffersonensis* and *Cibicides carstensi* biozones marked the bases of the 1st and the 2nd supersequences in the Miocene. Previous biostratigraphic work defined the Lower Miocene section as being bracketed by the *Lenticulina jeffersonensis* and *Amphistegina “B”* biozones ( Breard *et al.*, 1993; 1994; 1996; & Fillon & Lawless, 1999), the Middle Miocene by *Cibicides carstensi* biozone while the top of the Upper Miocene is capped by *Robulus “E”* biozone (Figure 5).

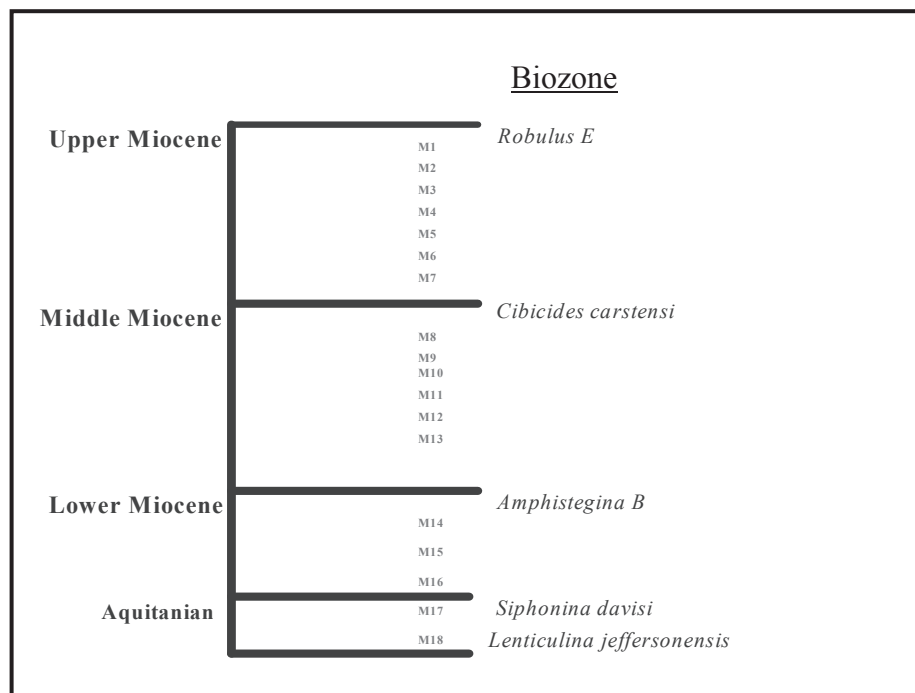


Figure 5: Schematic diagram showing spatial biozones of the Miocene packages, Vinton Dome. M = numbered sands as per company reports.

## 1.2 PREVIOUS STUDY

### 1.2.1 General Stratigraphy

Previous regional and local studies done on the northern Gulf of Mexico (e.g. Curtis, 1970, Edwards, 1994, Blood & Crastley, 1995, Galloway *et al.*, 2000) are typically based on thousands of well logs, 2D and 3D seismic data, biostratigraphy, and in some cases, outcrops. The Lower Miocene framework study by Galloway (1986) identified outcrops of gently dipping, coastward-thickening sections of interbedded sandstones and mudstones in South Texas, northwest shelf, of the Gulf of Mexico basin. The wave-dominated north Padre delta system in South Texas included the extensive wave-reworked Matagorda barrier and strandplain complex that extended to Louisiana.

The Early Miocene was a period during which the depocenter of the ancestral Mississippi delta system was located onshore, near the present day coastline in southwest Louisiana (Hunt & Burgess, 1995 & Galloway 2000). The LM1 and LM2 through to MM7 chronozones (Figures 6) recorded eastward onshore migration, whereas only the outer fringes of deltaic and submarine fan facies are observed offshore. In the northwest Gulf of Mexico, the Early Miocene was a period of onset of deposition onto a thick column of the Anahuac shale revealing substantial evolution in sediment dispersal.

The 3<sup>rd</sup> order sequences previously established in the Lower Miocene supersequence are marked by the *Lenticulina jeffersonensis*, *Siphonina davisi*, *Marginulina ascensionensis* (Marg “A”), *Gyrodina* “6”, *Amphistegina* “B”, and lower

*Cristellaria* “I” biozones (Haq *et al.*, 1988; Fillon & Lawless, 2000; & Witrock *et al.*, 2003) (Figure 7). The basal Miocene is the *Lenticulina jeffersonensis* sequence deposited during the Liebusella regression, a major regression that terminates the 2<sup>nd</sup> order Late Oligocene Anahuac sequences reportedly consisting of on-shelf retrogradational shallow coastal systems such as wave-dominated deltas and barriers. The 2<sup>nd</sup> order early Miocene sequences, however, are on-shelf progradational shallow coastal systems (Fillon & Lawless, 2000; Trevino *et al.*, 2003).

The Anahuac Shale Formation in the Upper Oligocene sequence symbolizes the maximum landward shift of shorelines during the Late Oligocene. It is recognized below by *Marginulina vaginata*, in the middle by *Heterostegina texana* and at the top by *Discorbis gravelli*. The *Heterostegina texana* biozone, however, is a limestone unit in the middle of a marine shale facies, a period of carbonate build up (reef) that occurred in the Late Oligocene as far west as the Houston salt basin (Galloway *et al.*, 2000). The period was characterized by a decrease in sediment supply that provided conducive conditions such as clear and clean waters for carbonate development. On the western Louisiana shelf, patch reefs developed on the top of salt domes and in the southeast, carbonates build up as thick as 1300 ft (400 m) (Krutack & Beron, 1990; Liu *et al.*, 1997). The condition was terminated by an increase in clastic sediment influx at the onset of the Early Miocene.

Depositional systems in the Early Miocene in the NW Gulf of Mexico are identified as wave dominated thick sand-rich strand plain and barrier shore zone systems. This was followed by progradation of the fluvial dominated Calcasieu delta

onto an initially highly unstable collapsing continental margin creating an extensive sandy delta-fed apron and the principal LM1 & LM2 depocenter (Galloway, 1986). Thereafter, accumulation rates became low and clastic deposition spread onto the NE shelf (Figure 7). The west Gulf margin thereafter regressed to a narrow clastic shelf and progradational slope apron (Galloway, 2000).

SYSTEM	SERIES	ATLAS CHRONO-	CHRONO-ZONES	BIOCHRONZONES
QUATERNARY		Pleistocene		
TERTIARY	Plio-cene	UP	UP-L	Sangamon Fauna
			UP-L-4	Trimosina A 1st
		LP	UP-L-3	Trimosina A 2nd
			UP-L-2	Hyallnes B/Trimosina B
		LP	UP-L-1	Angulogerina B 1st
			MPL-2	Angulogerina B 2nd
		LP	MPL-1	Lenticulina 1
			LPL	Valvulina H
		LP	LPL-	Bulminella 1
			LP	Textularia X
TERTIARY	Miocene	UM3	UM-3	Robulus E/Bigenerina A
			UM-2	Cristellaria K
		UM8	UM-1	Discorbis 12
			MM9	Bigenerina 2
		MM7	MM-8	Textularia W
			MM-7	Bigenerina humbeli
		MM4	MM-6	Cristellaria I
			MM-5	Cibicides opima
		MM1	MM-4	Amphistegina B
			MM-3	Robulus 43
		LM4	MM-2	Cristellaria 54/Eponides 14
			LM-1	Gyroldina k
		LM3	LM-4	Discorbis b.
			LM-3	Marginulina ascensionensis
		LM2	LM-2	Siphonina davis
			LM-1	Lenticulina hansen
		OL	LM-1	Lenticulina hansen
			LM-1	Lenticulina hansen

Figure 6: Chronostratigraphic subdivisions and biostratigraphic zones used for the Gulf of Mexico. (Modified from Seni *et al.*, 1995)

Time (mya) (not to scale)	CHRONOSTRATIGRAPHY				BIOSTRATIGRAPHY		MMS CHRONOZONE	
	SYSTEM	SUBSYSTEM	SERIES	STAGE	FORAMINIFERAL PLANKTIC AND BENTHIC REGIONAL AND LOCAL MARKERS	CALCAREOUS NANNOPLANKTIC REGIONAL AND LOCAL MARKERS	PROPOSED	CURRENT
16.40	TERTIARY	NEOGENE	MIOCENE	BURDIGALIAN	Camerian 1, Robulus 54B = Cristellaria 54 Saracenaria sp. / "D" Gyrodina "K"/9/4 Catapsydrax stainforthi Catapsydrax dissimilis, Robulus chambersi, Discorbis bolivarensis/"B", Cristellaria "A" Marginulina ascensionensis/"A"	Sphenolithus belemnos Reticulofenestra gartneri Sphenolithus disbelemnos Orthorhabdus serratus	MUL	M
20.52					Globigerina binaensis Gyrodina 8 Siphonotularia fredsmithi	Triquetrorhabdulus carinatus, Triquetrorhabdulus challenger Discoaster caliculosus increase	MML	LM4
23.80				AQUITANIAN	Siphonina davisii Planulina palmerae Globigerinoides primordius  Lenticulina hanseni Lenticulina jeffersonensis, Cristellaria "R", Globorotalia kugleri, Globigerina angulosuturalis	Discoaster saundersi  Sphenolithus dissimilis  Cyclargolithus abisectus Helicosphaera recta	MLL	LM2 LM1
					Robulus "A" Discorbis gravelli Hetrostegina texana	Sphenolithus delphix		

Figure 7: Biostratigraphic chart of the Gulf of Mexico, Lower Miocene  
(Modified from Witrock *et al.*, 2003).



### 1.2.2 Vinton Salt Dome

The Vinton salt dome contains a core of massive cap rock, rock salt, gypsum, and anhydrite, in succession (Thompson & Eichelberger, 1928), with the cap rock extending over the rock salt (Figure 8). Of particular interest to geologists are salt domes in the deltaic, delta fringe, continental shelf and sandy upper slope areas of the northern Gulf of Mexico because they tend to provide trapping mechanism for hydrocarbons, and can also be economically beneficial because they sometimes contain quality salt, dolomite, limestone, gypsum, and anhydrite.

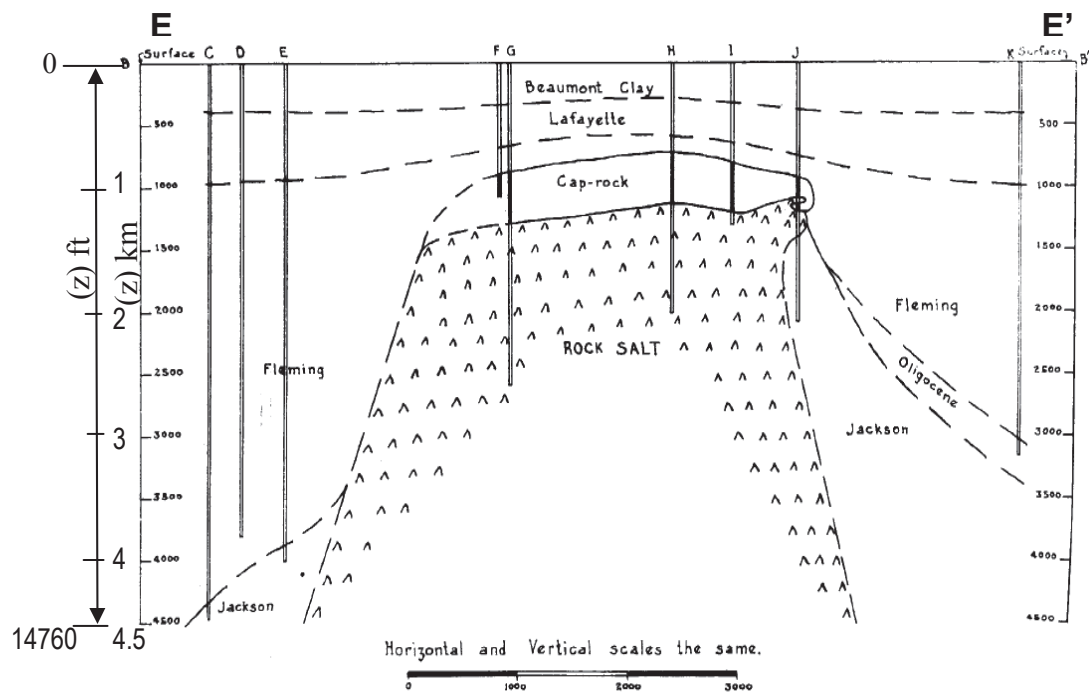


Figure 8: A cross-section of Vinton dome showing the position of cap rock.  
Scale in feet. (after Thompson & Eichelberger, 1928)

### 1.3 STUDY AREA

The Vinton Dome area, also known as the Ged Field covers an area of approximately 156 km<sup>2</sup> in the Calcasieu Parish, Southwestern Louisiana (Figure 9).

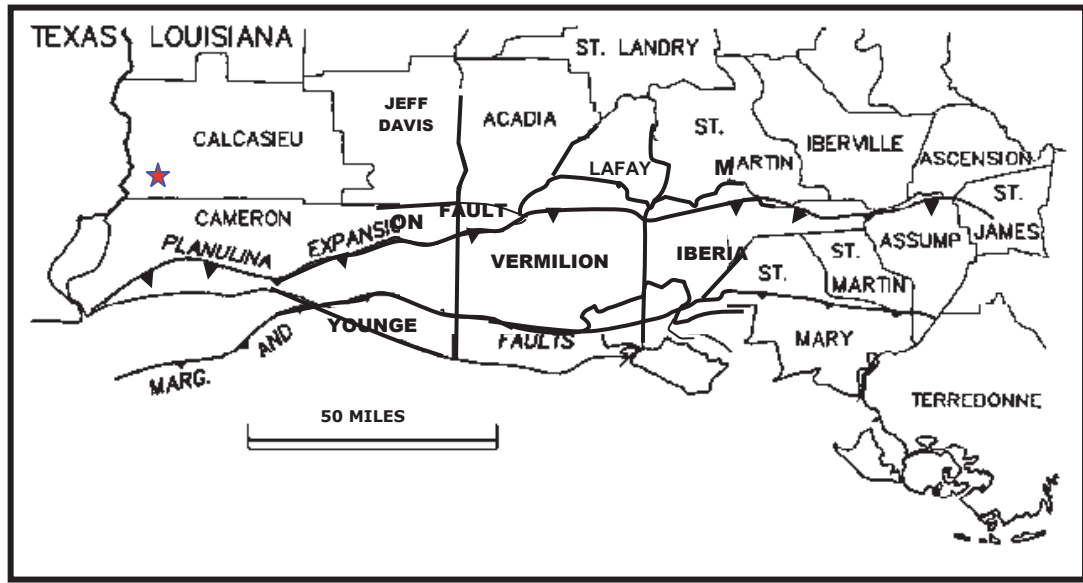


Figure 9: ★ Vinton Dome location, Northwest Gulf of Mexico, Southwest, Louisiana (modified from Edwards, 1994).

Biostratigraphic picks in the Miocene section of Vinton Dome area are scanty and are largely confined to a pilot study of the Aquitanian stage. In this study, the top of the Aquitanian stage is placed at *Siphonina davis* (Haq *et al.*, 1988; & Styzen, 1996; & Witrock *et al.*, 2003) (Figures 6 & 7) and the base is hinged on the *Discorbis gravelli* pick. In general, the basal Miocene may be defined by Top Oligocene fossils, *Discorbis gravelli* (Trevino *et al.*, 2003) or *Heterostegina texana* (Ye *et al.*, 1995; Galloway, 2000). Based on well log analysis, the depositional environments are broadly fluvial-deltaic, and my best attempt to determine these

environments is based on the environmental preferences of foraminifera reported from drilled wells, and the depositional patterns indicated by log curve shape. Paleo markers, reported from 12 wells at the Vinton Dome are listed below, along with their published environmental preferences (Vail & Wornardt, 1991; Breard *et al.*, 1993; 1994; 1996) (Figure 10). Based on the biostratigraphy, the Miocene strata of the Vinton Dome area seem to consistently lie in a relatively shallow marine, inner shelf environment.

Foraminiferal marker	Environment	water depth
<i>Siphonina davisi</i>	<i>Inner Neritic</i>	<i>0' - 100'</i>
<i>Discorbis gravelli</i>	<i>Deep Inner Neritic</i>	<i>&lt; 100'</i>
<i>Heterostegina texana</i>	<i>Inner Neritic</i>	<i>0' -100'</i>
<i>Marginulina vaginata</i>	<i>Deep Inner Neritic</i>	<i>&lt; 100'</i>

Paleobathymetry (in feet)	Paleoenvironment	
0-100	Inner Neritic	Neritic
100-300	Middle Neritic	
300-600	Outer Neritic	
600-1200	Upper Upper Bathyal	Upper Bathyal
1200-1500	Lower Upper Bathyal	
1500-3000	Middle Bathyal	Middle
3000-4500	Upper Lower Bathyal	Lower Bathyal
4500-6000	Lower Lower Bathyal	
Below 6000	Abyssal	

Figure 10: Paleobathymetric zonation (Vail & Wornardt, 1991; Breard *et al.*, 1993).

There are very few published studies on Vinton Dome and on the Miocene sections of the area. Regional studies done by Curtis (1970), Edwards (1994), and Galloway (1996 & 2000) presented a general overview of the geology of the northwest Gulf of Mexico area. Thompson & Eichelberger (1928), however, were modest in details of the geology of the dome considering the few available wells, lower quality data, and older geological concepts in the early 20<sup>th</sup> century. There are few or no published articles on the Miocene depositional models in the Vinton Dome area. Therefore, this study will provide an understanding of the Aquitanian depositional systems and insight for future studies of the Miocene depositional systems in the northern Gulf of Mexico.

The general study of the northwest Gulf of Mexico conducted by Galloway *et al.*, (2000) placed the Vinton dome area on the Miocene shelf, which was the location of deltaic, shallow marine and shelfal sediments, as also indicated by the biostratigraphy and paleogeography (Blood & Crastley, 1995 & Galloway *et al.*, 2000). The following figures reveal the evolution of the northwest Gulf of Mexico through the Miocene including the approximate paleogeographic position of the Vinton Dome area. During the Chattian, the dome was situated below the shelf, while in the Aquitanian, the dome was located on the fluvial dominated system of the Calcasieu Delta in the Red river dispersal axis (Figures 11-15 and Table 1).

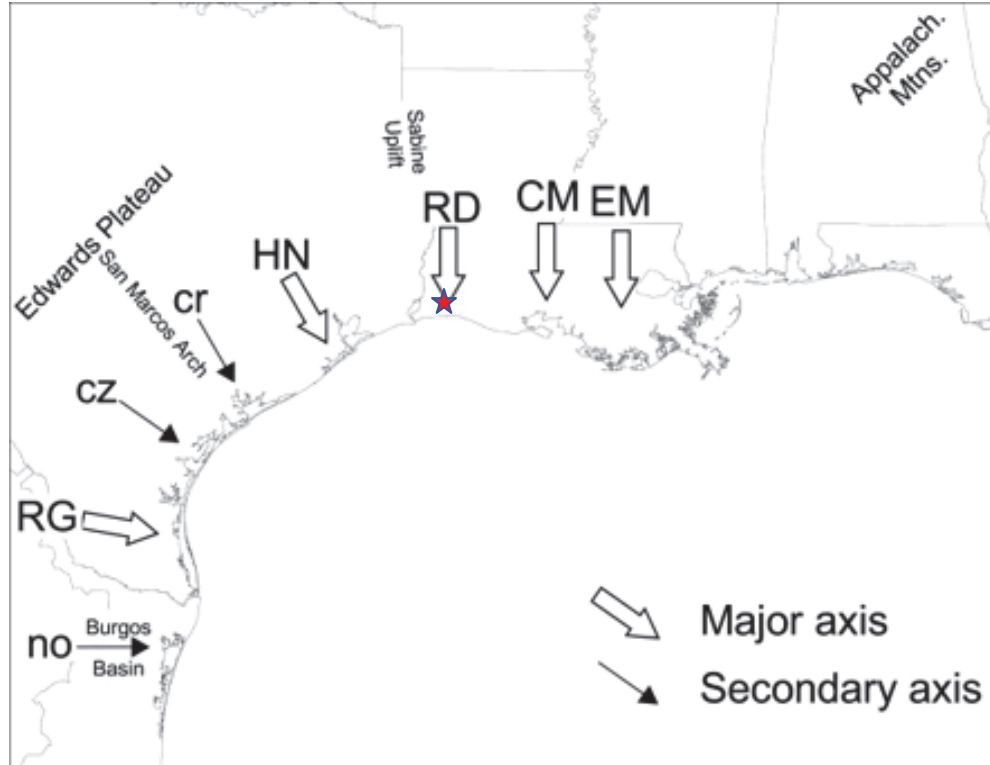


Figure 11: Basin-margin structural features and principal (caps) and secondary (lower case) Cenozoic sediment dispersal axes of the Gulf of Mexico basin: no = Norias; RG = Rio Grande; cz = Carrizo; cr = Corsair; HN = Houston; RD = Red River; CM = Central Mississippi; EM = East Mississippi (Modified after Galloway *et al.*, 2000). Vinton area was located on the Red River dispersal axis.

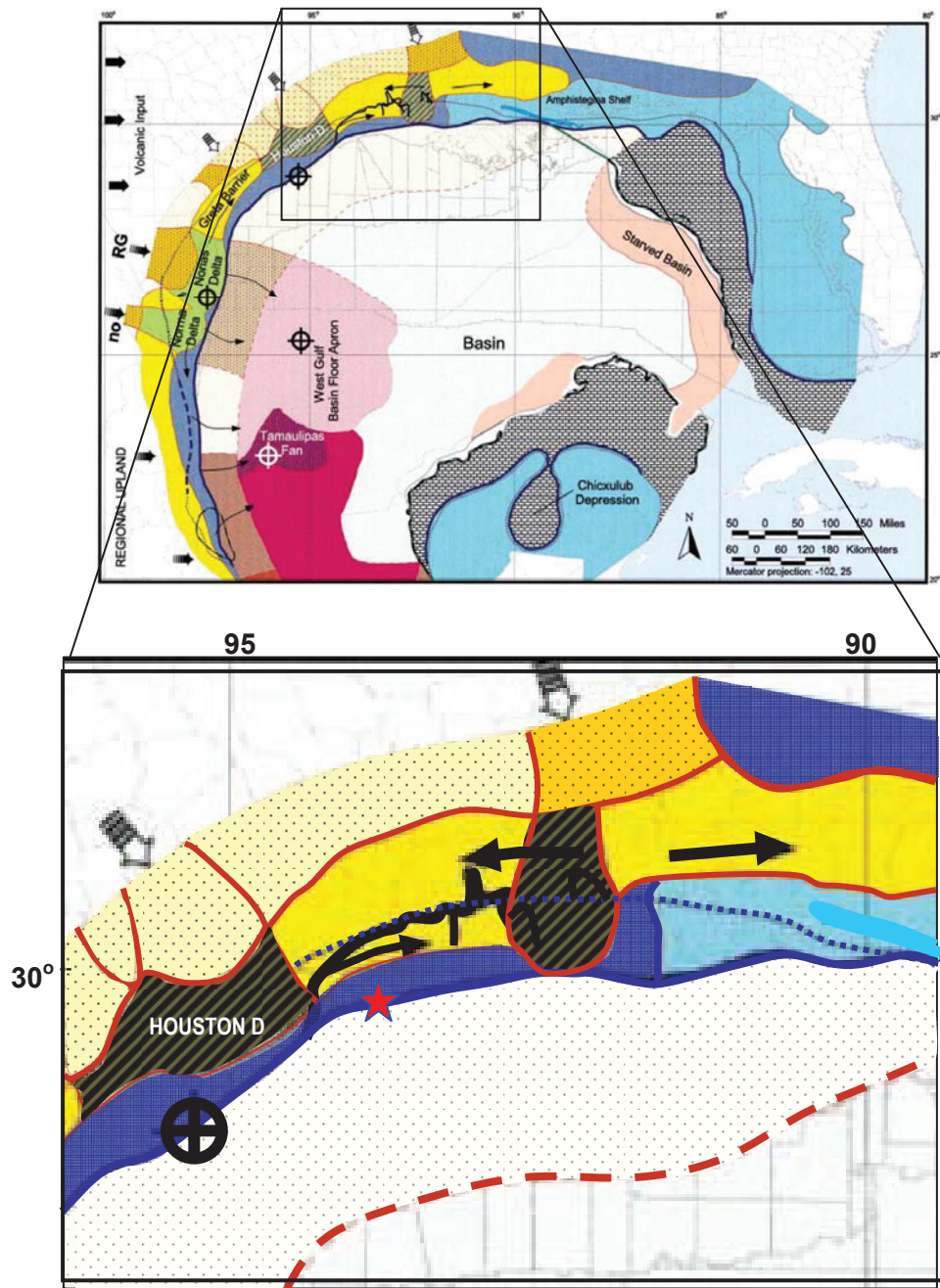


Figure 12: Paleogeography of the Late Frio/Vicksburg (OF-F, 28-25 Ma) depositional episode. See Table 1 for explanations of symbols and abbreviations (Modified after Galloway *et al.*, 2000).

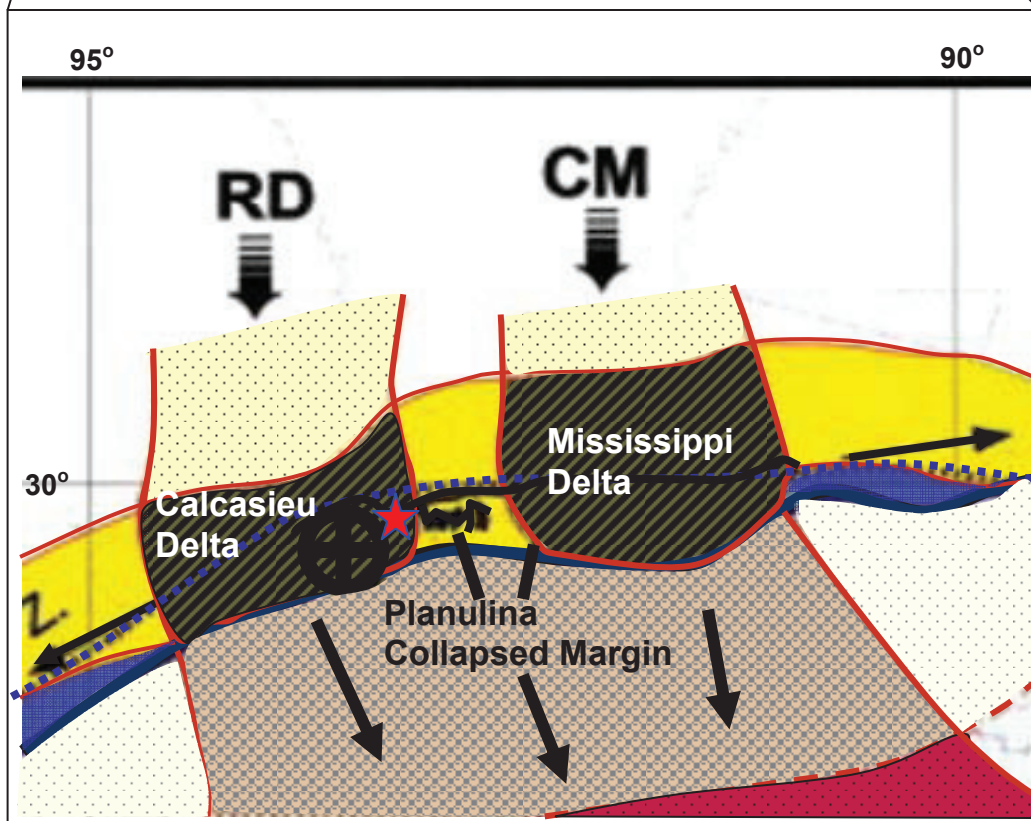
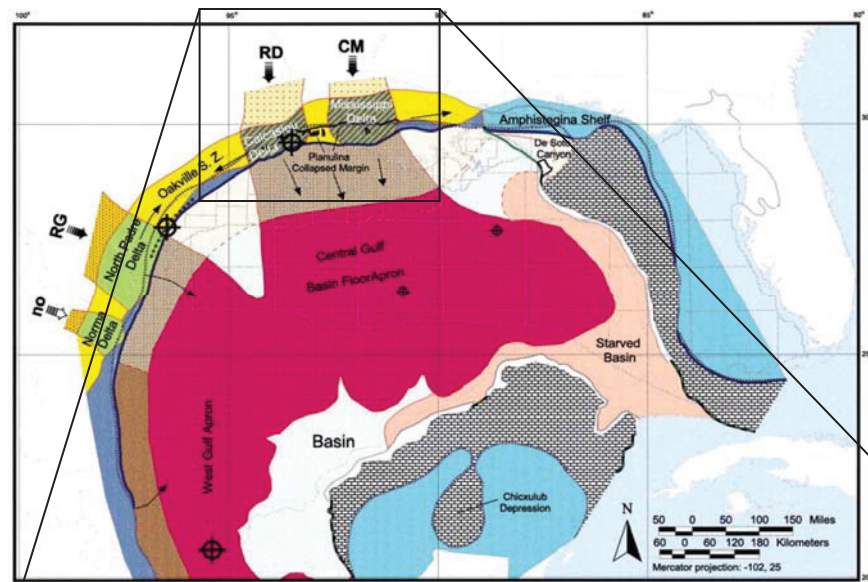


Figure 13: Paleogeography of the Miocene (LM1, 25-18 Ma) depositional episode. See Table 1 for explanations of symbols and abbreviations (Modified after Galloway *et al.*, 2000). Vinton area was situated on the eastern edge of the Calcasieu Delta.



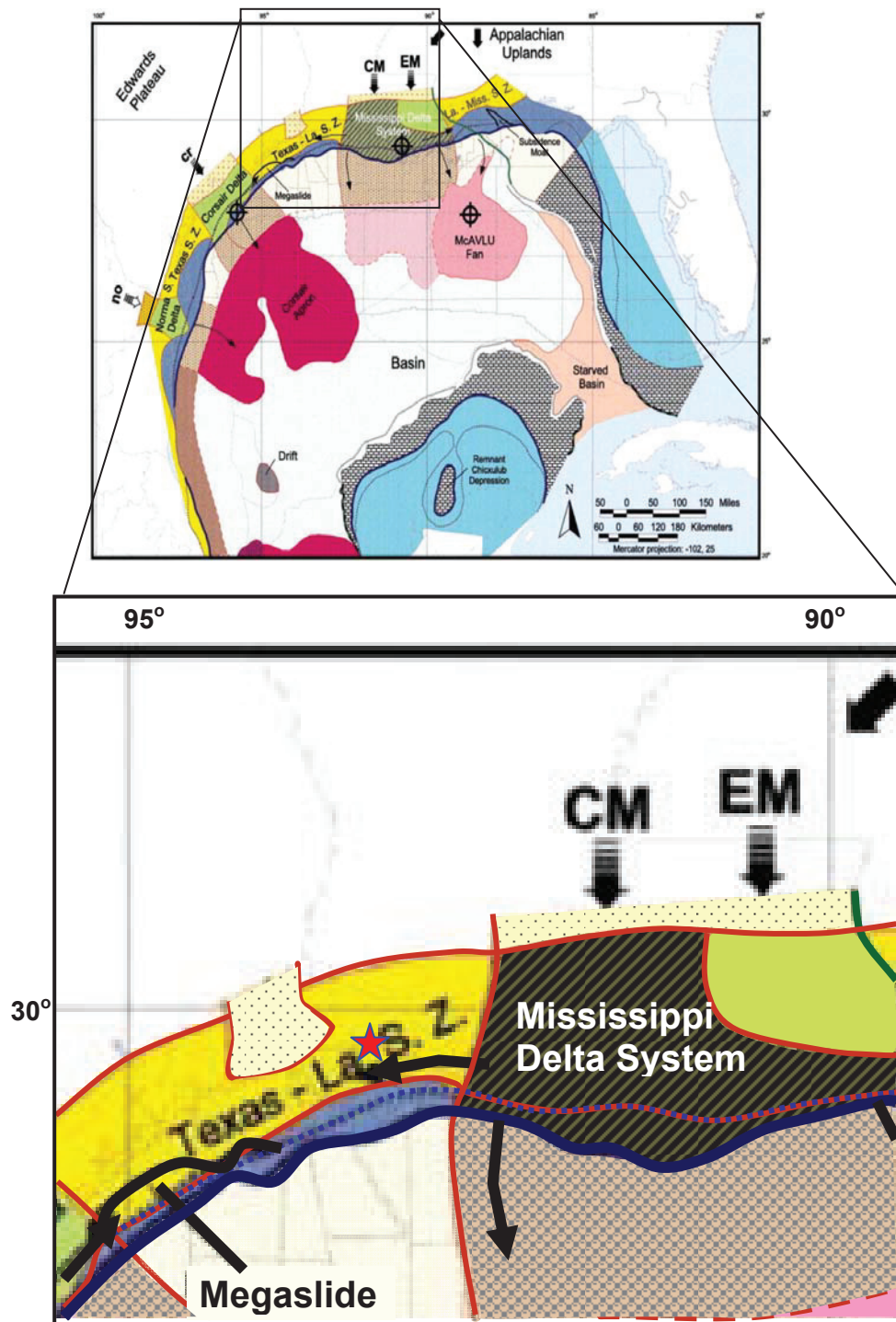


Figure 14: Paleogeography of the middle Miocene (MM-I, 15.6-12 Ma) depositional episode. See Table 1 for explanations of symbols and abbreviations (Modified after Galloway *et al.*, 2000). Vinton area was situated on the Mississippi delta system.



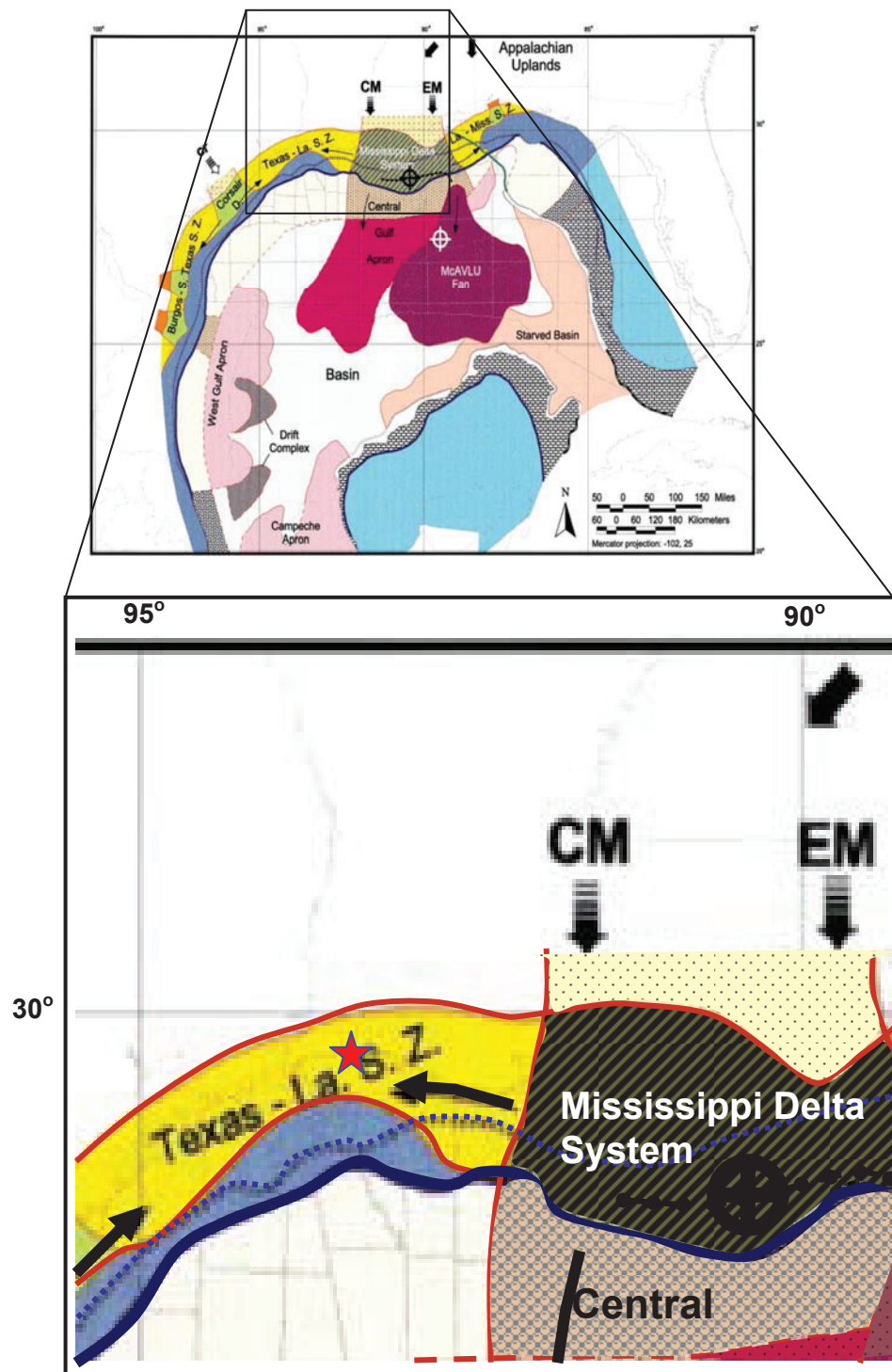











Figure 15: Paleogeography of the late Miocene (UM-K, 12-6.4 Ma) depositional episode. See Table 1 for explanations of symbols and abbreviations (Modified after Galloway *et al.*, 2000). Vinton area was situated on the west of the Mississippi delta system.

## Depositional Features

	Shelf margin at maximum progradation
	Relict shelf margin of underlying depiside
	Other relict shelf margin
	Relict Cretaceous shelf margin
	Outline of submarine canyons, megaslides, and embayments
	Pinch out or truncation
	Regional depoaxis
	Regional depocenter
	Sediment transport

## Depositional Systems

	Fluvial undifferentiated
	Bed – load dominated fluvial
	Mixed – load dominated
	Suspended – load dominated fluvial
	Fluvial – dominated delta
	Wave – dominated delta
	Shore zone
	Siliciclastic shelf
	Carbonate shelf
	Slope system
	Progradational delta-fed apron
	Progradational shelf-fed
	Retrogradational apron
	Bypass slope
	Carbonate ramp
	Basin floor apron
	Sandy basin floor
	Sandy – rich fan
	Sandy fan
	Muddy fan
	Mass transport complex
	Contourite drift
	Basin
	Starved basin
	Non-deposition

Table 1: Explanation of symbols for paleogeographic maps (Figures 11-15). Maps show depositional systems, sediment dispersal axes, generalized depocenters, and selected depositional and erosional features (Re-drafted after Galloway, 2000).

## **CHAPTER TWO**

### **METHOD OF STUDY**

#### **2.1 CHALLENGES**

The Vinton Dome area is mainly characterized by salt intrusion and related faulting. As a result, synthetic seismograms generated near the salt are of limited benefit due to highly disturbed beds, high bed dips, severe faulting, and poor seismic resolution. The synthetic seismogram generated at the periphery of the area, where the salt impact is low, is of best quality. Since the main structural traps are against the salt body, which is at the center of the dome, the well data are not uniformly distributed across the area. The majority of the wells are close to the salt body and the southwestern part of the survey does not have wells. Therefore, the apparent distribution of well information, interpretation, and well to seismic ties, is biased by the location of the 546 logged wells.

Due to the low seismic resolution and unavailability of core data and wellbore images of the complex area, major challenges are the:

(1) prediction of sand body geometries as a result of the salt influence and severe faulting; (2) stratigraphic sequencing of the Aquitanian due to the limited seismic vertical resolution of 4<sup>th</sup> order sequences, amalgamation of shelfal and fluvial deposits in the restricted accommodation on the shelf, and the resultant recognition of smeared facies distribution within the 3<sup>rd</sup> order sequences; (3) presence of sporadic sandstone bodies; (4) complex fault system; and (5) timing of the salt movement and prediction of the subsequent sediment deformation by the salt.

## 2.2 DATA

The stratigraphy and structure of the Aquitanian were mapped using 60-65 Hz resolution 3-dimensional (3D) surface phase rotated seismic data, 546 well logs, and the limited available biostratigraphic data, using a Geoframe 4.0.4. workstation software. The workflow is shown in figure 16. The radial 3D seismic survey covers an area of 156 square km and consists of 666 crosslines starting from line 1 in the north-south direction and 655 inlines starting from line 1000 in the east-west direction. The peak frequency of the seismic data is 40 Hz. Calculated lateral and vertical resolution are 125 ft (38 m) and 44 ft (13.4 m) respectively at 7500 ft (23 m). Imaging of subsurface bodies using conventional seismic amplitude is therefore subjected to the tuning thickness based on the lateral and vertical data resolution. The seismic data were processed with 3001 samples per trace at a 2 millisecond sampling interval. The seismic data were rotated 90° from the original zero phase and interpretation was performed directly on 90° phase rotated data. Pure 90° phase rotation (Quadrature) data were needed for maximum amplitude extractions of centers of beds of interest, which were otherwise on zero crossings when well to seismic ties were carried out on zero phase data. The rotation then makes the seismic response symmetrical to the beds rather than to the top or base of the beds, giving seismic events a more geological definition.

The Vinton Dome area has a lot of wells. However, out of 546 wells, only 144 wells passed through the Aquitanian and only the basic logs (SP or GR, IES, DT and density) were available. Some wells did not reach the *Siphonina davisi* surface

which is the shallowest flooding surface within the interval of interest. Other wells in the database did not have adequate stratigraphic data because of shortcomings such as, faulted out beds, washouts in logs, salt area, indefinable top or base of interval of interest. Only vertical wells were selected for correlation.

A relatively small fraction (about 12 wells) of the stratigraphically useful wells contained biostratigraphic data. GR logs were not common in the well data, therefore SP logs were utilized. Density logs did not accompany sonic logs in the log suites. Two checkshot surveys on the dome were used to approximate the time/depth relationship. Conversion of depth to time indicates that one millisecond is equivalent to approximately 3.72 feet (1.15 m).

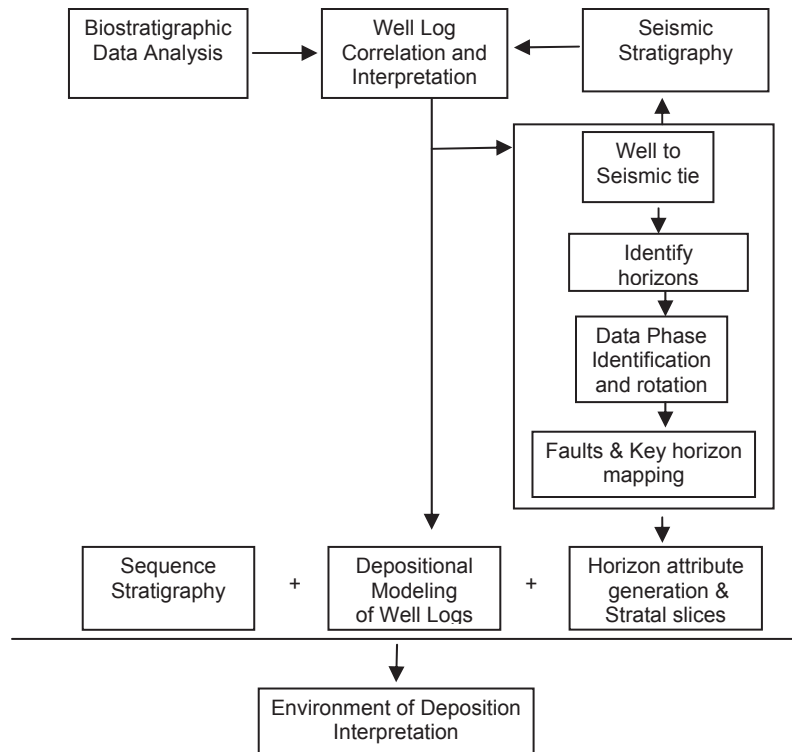


Figure 16: Flow chart of interpretation methodology

### 2.3 WELL TO SEISMIC TIE

In order to calibrate seismic data with well data, synthetic seismograms are normally generated using sonic and density logs. In the absence of density logs, we may assume a simple empirical relationship between density and velocity to generate synthetics (Rekoske & Hicks, 1992). Synthetic seismograms are a one-dimensional model of acoustic energy traveling through the layers of the Earth and are used for correlation and wavelet processing of seismic data. Statistical relations that exist between velocity, density, and resistivity employ the use of Gardner's equation that relates density with velocity, or Faust's equation that relates resistivity with velocity. Faust's equation usually needs extensive stretching and squeezing which may introduce further errors to sonic curves; therefore, the use of Gardner's equation is preferred except when sonic logs are not available (White & Simm, 2003).

In the entire survey, only two well log suites contained sonic logs and these are without the density logs. Therefore, I used Gardner's equation and ran the synthetic seismogram using a checkshot from a nearby well to calibrate the sonic log. The accuracy of time relationships between horizons is the goal, and was achieved, since time is based solely on velocity and depth. Although, reflector amplitude which is based on impedance (density times velocity) would be imprecise, it would not impinge on the validity of the synthetic, considering its relation with time or depth (White & Simm, 2003).

The sonic logs were edited and conditioned for calibration using the WellEdit module in the Geoframe software. This meant reformatting the logs where obvious erroneous values of velocity are spotted, which could create artificial acoustic

impedance contrasts and could result in the creation of false reflections on the synthetic seismogram. Salt bodies typically offer high velocity which could be very influential on the overall result of synthetic seismogram. As a result, the sonic log at the periphery of the salt dome was preferred to the one at the salt flank.

Generation of the synthetic seismogram was performed using the Geoframe synthetic module. The synthetic module permits the tie of time data (seismic data) to depth data (well data) by integrating the velocity profile. Impedance log and reflection coefficient curves were generated from the velocity profile. The reflection coefficient curve was convolved with a seismic wavelet to produce a synthetic seismic trace. The synthetic seismogram was generated using a  $+90^\circ$  - phase wavelet because the seismic data are in  $+90^\circ$  phase (Zeng & Hentz, 2004). This was then compared with the actual seismic traces at the borehole to ensure it represented the adjacent seismic section (Figure 17). No bulk time shift was required for the best fit between the theoretically and field-derived waveforms (Figure 18).

Checkshot guided depth-to-time conversion enabled accuracy of other well to seismic ties and the seismic interpretation. Through paleo and regional correlations, interpretation and mapping were then carried out. Key seismic stratigraphic surfaces delineating previously established 3<sup>rd</sup> order surfaces were interpolated between wells and extrapolated beyond well control into the large 3D survey area by integrating the seismic information. Local maximum flooding zones (MFZ) associated with the top of the faunal marker, *Siphonina davisii* and *Discorbis gravelli*, *Heterostegina texana* and *Marginulina vaginata* were identified on the well logs, and the interpretations of

the reflections were extrapolated across the 3D survey. Query checks were carried out on all wells. The result was a successful tie with the well markers in all other boreholes (within +/- 10 ms.). Velocity variations in the severely faulted salt dome and pitfalls in biostratigraphic picks could be responsible for inconsistent marker-horizon ties (discussed in the biostratigraphy section).

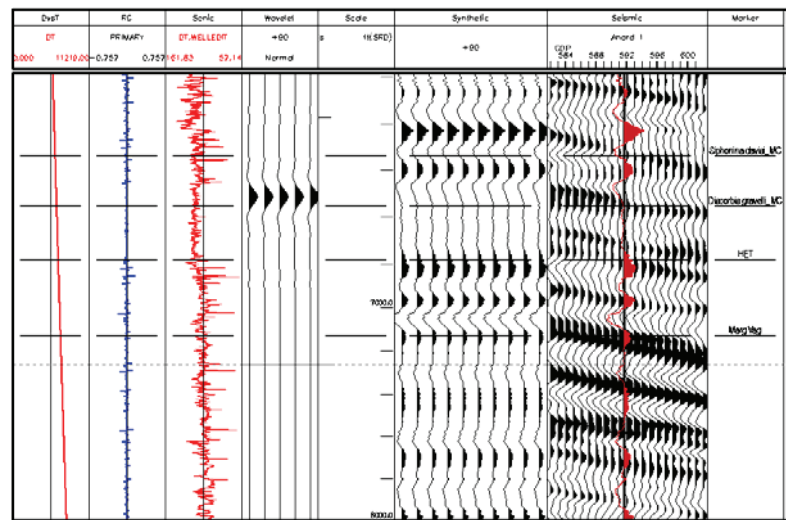


Figure 17: The synthetic seismogram view.

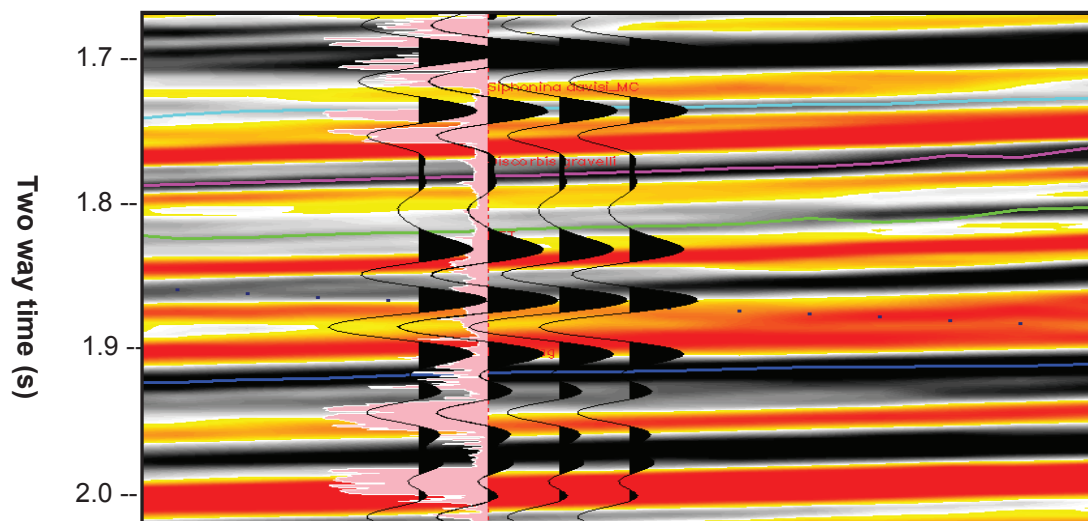


Figure 18: A good-tie obtained between the synthetic seismogram and the seismic data.



## **2.4 MAPPING TECHNIQUES**

In order to establish the evolution of the Vinton Dome area during the Early Miocene, I performed a detailed interpretation and mapping of the Upper Oligocene and Lower Miocene horizons. First, I mapped faults that are associated with the Top Oligocene to Lower Miocene interval to ensure proper correlation of the 3<sup>rd</sup> order sequences (faults are discussed in chapter 3) and key horizons were manually picked using a 1 x 1 grid of inlines and crosslines of the survey. A coarser grid such as 20 x 20 grid interpretation would have been ideal in higher resolution seismic data and in a less structurally complex area. However, finer grids are necessary for achieving detailed accuracy, to compensate for the low resolution of seismic data and in order to avoid the use of the Geoframe Autopix module for the automatic pick of highly faulted and salt impacted horizons. Autopix, a 3D autopicker, is usually employed for computer-assisted picking of events in areas that are between manually-picked control grids. It tracks events along bedding planes and is most useful in areas with fairly good lateral continuity. Eradication of mis-ties through loop ties of the horizons was also achieved by the 1 x 1 grid interpretation. These horizons were then interpolated and snapped to the closest event.

Horizons were generated via the seismic interpretation of reflecting sequences, which are characterized by distinct waveforms. These waveforms were used for correlation, facilitated by seedpoints (previous picks in crosslines or inlines) and were also used for correlation across faults, and verification that the reflections were picked correctly. Changes in these waveforms can be correlated with changes in thickness of intervals, in number and thickness of beds, and/or seismic reflection

doublets. Horizon slices generated from seismic and attribute volumes were used for detailed interpretation of the area. Horizon amplitudes were generated and further compared to other attribute-based slices. Horizon slices were analyzed in seismic attribute volumes to create window-based attributes around the events. These surface-derived attributes enable the stratigraphic evaluation of interpreted seismic sections (Rijks & Jauffred, 1991).

Stratal slices were also generated by flattening attribute volumes on manually -picked horizons, which enabled intermediate time slices of stratigraphic packages. Such slices allowed further insights into sand body geometries and their changes over short periods of time. Flattening volumes upon marker horizons approximately restores the horizon to the time of deposition and largely removes the effect of subsequent deformation of extensional tectonic events, assuming that the horizon had a nearly horizontal depositional surface.

A series of isochores and interpretative maps for each stratigraphic package were generated. These isochores helped to establish sand depocenters. I ran GeoQuest horizon dip maps, and AGL time and horizon extractions of curvature on each maximum flooding zones of the *Siphonina davisi*, *Discorbis gravelli*, *Heterostegina texana* and *Marginulina vaginata* fossils of the previously established 3<sup>rd</sup> order sequences to examine any evidence of compaction over sand lobes and sand filled channels. Extracted amplitude maps for the most sand rich intervals determined sand body geometries, and enabled comparison with curvature attributes and coherent energy gradients maps to assist in the identification of channels, sand bodies, faults,

and other geologic features. Coherence images generated from applications of coherence cubes to 3D seismic data reveal unbiased interpretation of events and faults in the system. The remarkable tie in the details of faults and highly distorted stratigraphic features confirmed the results of the interpretation of time and attribute based slices.

## **2.5 SEISMIC ATTRIBUTES**

Seismic attributes quantify measures of seismic characteristics of interests. They quantify amplitude and morphological features that are observed in seismic data through a suite of deterministic calculations performed on a computer. They are very useful in resolving smear that has been caused by the effect of seismic data migration, and they increase the visibility of geometrical characteristics of seismic data. Seismic attribute generation and analysis are used primarily to reveal patterns associated with the depositional environments. The diversity of seismic attributes can be overwhelming; therefore, attributes must be selected to relate to the objectives of the study. Target oriented attributes such as time attributes provide information on structure; amplitude attributes, on stratigraphy and reservoir; and waveform similarity attributes, on faults and depositional features. These attributes provide complimentary imaging that enables us to map subsurface geological features. (Brown, 1996; Arenson *et al.*, 1999; Welper, 2000; Rader & Medvin, 2002; Brown, 2005; Chopra & Marfurt, 2005; Barnes, 2006).

### 2.5.1 Attributes Sensitive to Structure

Attributes that are sensitive to structure include curvature, dip and azimuth, which are a class of reflection attributes derived from horizons interpreted in 3-D seismic volumes. Horizon attribute mapping help define depositional features and are typically used for detailed fault interpretation – to locate subtle faults that are not easily recognized on vertical sections in data volume. These subtle faults are important because they may possibly compartmentalize conventional reservoirs, and therefore would have significant effect on fluid movement in the subsurface.

*Curvature:* Curvature quantifies the degree to which the surface deviates from being planar. Mathematically, it is the reciprocal of the radius of a circle that is tangent to the given curve at a point. Curvatures are second order derivatives of the curve; consequently, the more curvy the bend, the larger the curvature (Roberts, 2001; Chopra & Marfurt, 2006) (Figure 19). Most positive curvature measures positive bending of a surface and emphasizes anticlinal surfaces such as ridges. The most negative curvature, however, measures negative bending of a surface and emphasizes synclinal features such as faults, fractures, joints, and channel axes. Curvature images provide detailed information in structural and stratigraphic interpretation and are particularly useful in mapping faults that are otherwise smeared during seismic data migration.

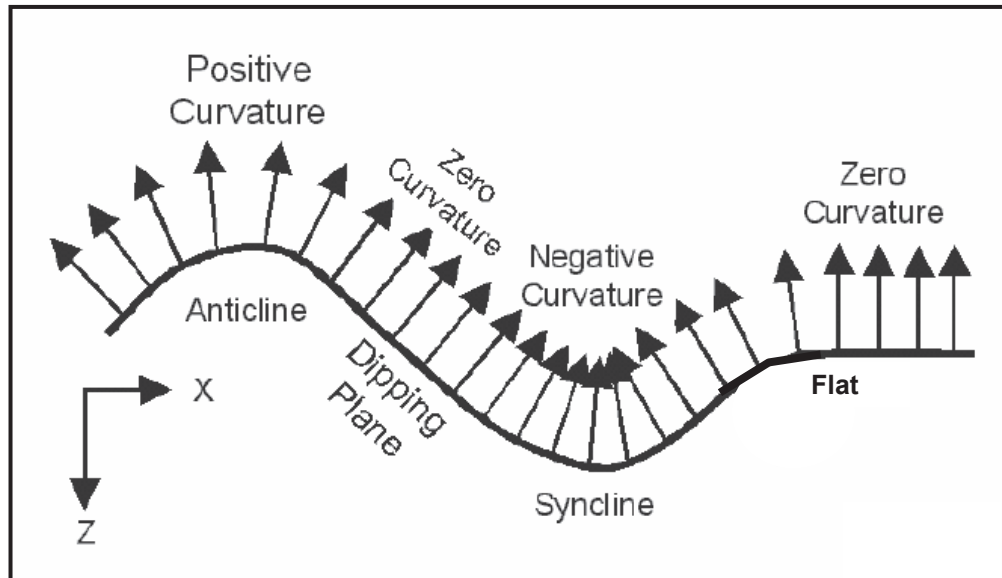


Figure 19: Sign convention for curvature attributes. The black arrows on curvilinear surface represent vectors, which are normal to the surface. Where these vectors are parallel on flat or planar dipping surfaces, the curvature is zero. Where the vectors diverge over anticlines, the curvature is defined as positive and where they converge over synclines, the curvature is defined as negative. (Modified after Roberts, 2001).

Seismic attributes - K negative and K positive long wavelength curvature attributes developed at the University of Houston Allied Geophysical Laboratory are better able to detect subtle faults and features when compared to images from coherence slices. Seismic attributes images derived from K positive and negative long wavelength curvature offer additional important fault details when applied to horizon based seismic volumes.

*Dip and Azimuth:* True dip is the magnitude of angles measured downwards from the horizontal to the surface while the azimuth is the direction that the surface points, ranging from 0 to 360°, and is measured perpendicular to the geologic strike, in the direction of maximum downward dip. Therefore, dip azimuth is measured from the

North and combines dip and azimuth through a circular two dimensional color bar whereby azimuth controls the hue and dip controls the intensity.

### **2.5.2 Amplitude Attributes**

Amplitude attributes in 3-D seismic mapping are only achievable with a fully interpreted horizon, interpolated and snapped to the event. They are used for defining subsurface depositional bodies and may also delineate reservoirs. High amplitude values may be indicative of hydrocarbons. Amplitude extractions co-rendered with coherence attributes yield outstanding details of structural and depositional features, lithological changes and may reveal definitive features such as gas chimneys. Horizon amplitudes delineate reservoirs and features better than RMS (root mean square) attributes (Brown, 2005).

### **2.5.3 Waveform Similarity Attributes**

Coherence is a measure of waveform similarity that images discontinuities (rather than reflections) as a result of lateral changes in geological subsurface features in the 3-D seismic data (Figure 20). These changes may be caused by faulting, fracturing, diagenesis, erosion, fluvial systems, or changes in rate of sedimentation. This attribute is able to detect trends and subtle changes in a waveform of a seismic trace when compared over the entire survey and therefore provides the means of viewing faults and stratigraphic features in non-interpreted seismic data without the influence of time or bias of interpretation. This process is

especially advantageous in the reconnaissance stage of a mapping project, by providing indications of depositional environments and patterns that can be easily seen aerially and may require further investigation. When horizon slices of coherence cube volumes are combined with other attributes such as amplitudes, they can reveal facies changes and detailed depositional environments. It also provides better image for viewing channels and other depositional features that avoid structural highs generated by salt domes, especially channels that change direction across faults, radial faults associated with salt domes, complex and en-echelon faults (Arenson *et al.*, 1999).

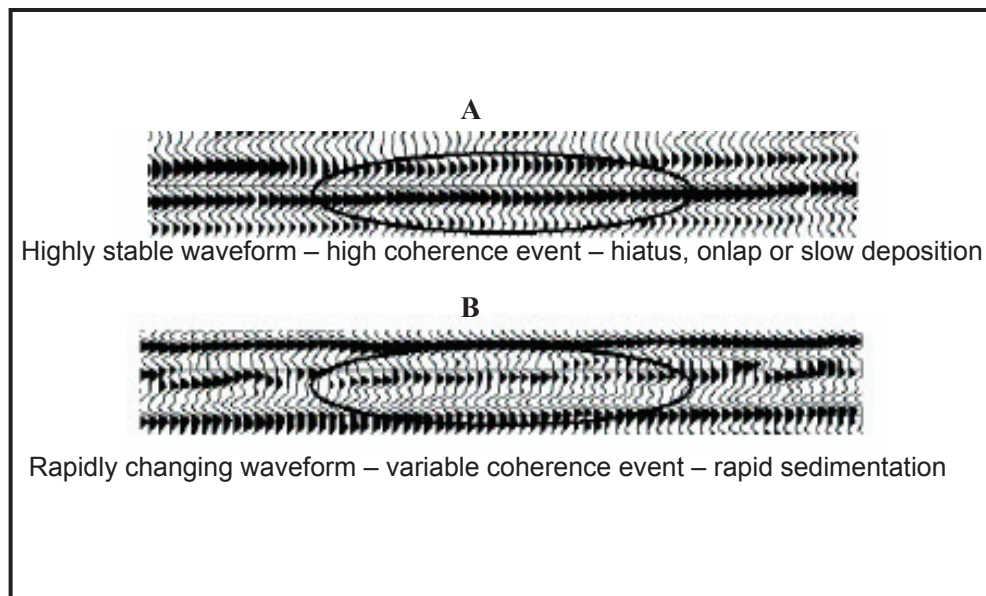


Figure 20: Oval A shows continuous reflectors with stable waveforms indicating areas of high coherence. Oval B shows reflectors with varying waveforms indicating areas of low coherence (Arenson *et al.*, 1999).

High coherence areas are shown as white to light gray and may indicate slow rates of deposition including shales, carbonates, and hemipelagic environments whereas, low or non-coherence areas are shown as dark gray to black, enabling faults to be easily recognizable. Areas of low coherence include faults, salt edges, reef edges, channel edges, slumps, and high porosity areas resulting from rapid sedimentation of sand deposition. Coherence maps have played a major role in the recognition of depositional environments and can assist inter-related features to be more distinctively recognized (Taner & Sheriff, 1977; Chopra & Marfurt, 2005). In this study, coherence attributes were used to map out faults, channels, mudflow gullies, and their associated muddy prodelta lobes, which were otherwise difficult to decipher in time slices.



## CHAPTER THREE

### SALT TECTONICS AND STRUCTURAL DEVELOPMENT

#### 3.1 PRINCIPLES AND APPLICATIONS

The Miocene in the Louisiana coast is one of the thickest wedges of terrigenous clastic sediments fed by a complex river system in the northern Gulf of Mexico. In the Early Miocene, active salt tectonics restricted deposition to the shelf (Figure 21) with the salt reinforcing the prograding slope, thereby trapping sediments on the shelf (Fillon & Lawless, 2000). High bulk accumulation of shelf sediments onto the salt during the Early Miocene has led to salt detachments and basinward migration of the autochthonous salt (Worall & Snelson, 1989; Watkins *et al.*, 1996). Continued progradation of shelf sediments onto Louann salt bodies eventually created weak points and paved ways for deposition along fill and spill minibasins to the deeper slopes and basin floors (Watkins *et al.*, 1996; Galloway, 2001).

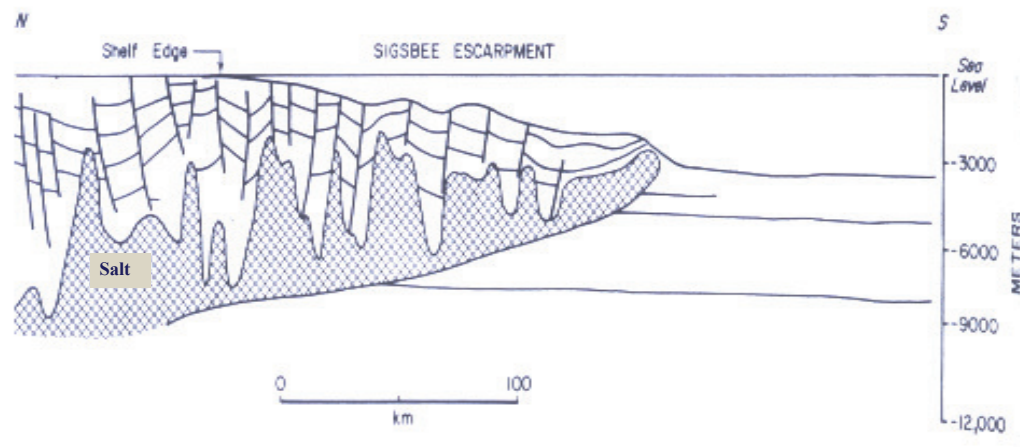


Figure 21: Cross-section showing southward squeezing of Louann Salt caused by loading and progradation of shelf sediments. (after Salvador, 1987)

The center of Vinton Dome is a salt plug that crops out at the surface with a depression at the center, occupied by Gray Lake. Previous work by Watkins *et al.* (1996) interpreted these salt types to be detached from the autochthonous Louann salt bodies, which were deformed through progradation and loading of shelf sediments onto the salt. The resulting detached salt lobes pushed upwards through the overlying sediment packages to form salt domes.

However, recent studies on salt movement provide other possible explanations by which salt could migrate. Hamiter *et al.* (1997) proposed that “the migrating mechanism has been the movement of the salt wedge and that the overlying sediments have been relatively passive riders, driven only by gravity. This causes the continental margin, certainly the shallower half, to slip downslope with salt as a prime mover or lubricant.” The growth faults and salt diapirism are mutually reinforcing (Hamiter *et al.*, 1997). Salt movement causes extension in overlying sediments thereby increasing the possibility of salt rising to the surface. Other explanations proposed by Rowan (2000) include passive diapirism, movement triggered by contraction, and/or movement by strike-slip faulting. Mohriak *et al.* (1995) suggested that the salt lobes could possibly be formed by a combination of progradation and extension of overburden on salt.

The purpose of this study is to define the evolutionary stage of salt movement in the Early Miocene, show evidence of salt creep across a counter regional or antithetic fault and the consequence on the depositional history of the dome.

Consequently, the study may illuminate some of the models and the mechanisms that have been attributed to salt movement.

Deposition on diapiric structures plays a major role in the associated fault pattern. Consequently, fault patterns provide important clues to the history of the salt movement, and also the depositional history of the associated strata. A classification of fault types and diapiric structures (Fails, 1990) has been employed to understand fault patterns on salt domes. Domes can be classified into three types: Penetrant - which are shallow piercement salt domes that extrude or protrude to near surface by piercing overlying strata, semi-penetrant – which are shallow, buried salt domes that pierced to a shallow depth but have since remained inactive, and non-penetrant - which are deep-seated, buried and inactive salt domes (Figure 22).

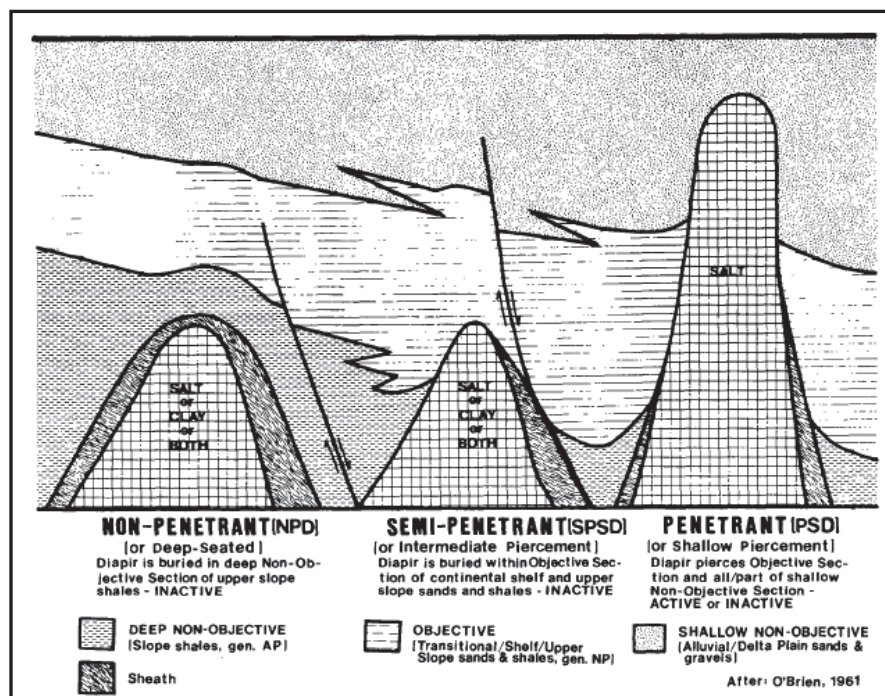


Figure 22: Salt dome classification (after Fails, 1990).

Fails (1990) further classified fault patterns associated with salt domes into three types:

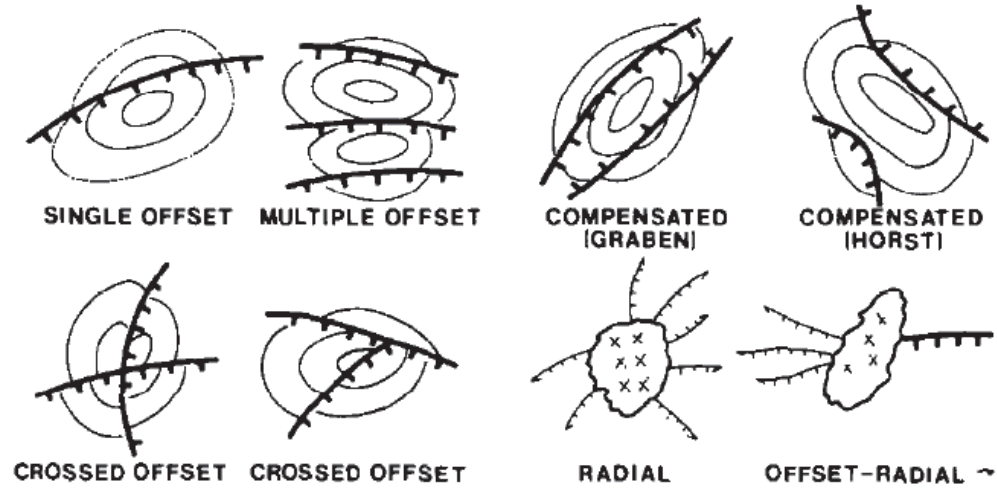
- single or multiple offset consisting of one or more semi-parallel faults, downthrown in the same direction.
- compensated faults consisting of two or more semi-parallel faults, downthrown in opposite directions, forming grabens or horsts, and
- crossed offset, consisting of two or more faults in crossed orientation.

Diapiric structures fall into one or more combination of these fault patterns and orientations (Figure 23).

#### **3.1.1 Observations and Discussion on Structure of Vinton Dome**

The structure of Vinton Dome is characterized by a multi-style fault pattern – a combination of single offset and offset radial fault pattern (Figure 24). The master fault lies in a northeast-southwest, transverse direction, downthrown to the north, indicating that it is a counter-regional fault. The southeast faults are parallel almost in an en-echelon pattern while the northeast faults are divergent with their tips converging toward the center of the dome. The west faults are relatively small and are positioned closely to the northwest and west of the master fault.

# **BASIC FAULT PATTERNS-COASTAL SALT BASIN DIAPIRIC STRUCTURES**



**SINGLE PHASE** Fault Patterns are shown above.

**MULTIPLE PHASE** Fault Patterns are combinations of:  
Offset plus Compensated or Crossed Offset plus Compensated Basic Patterns

Figure 23: Fault pattern classification for Coastal Salt Basin diapiric structures, including salt domes (after Fails, 1990).

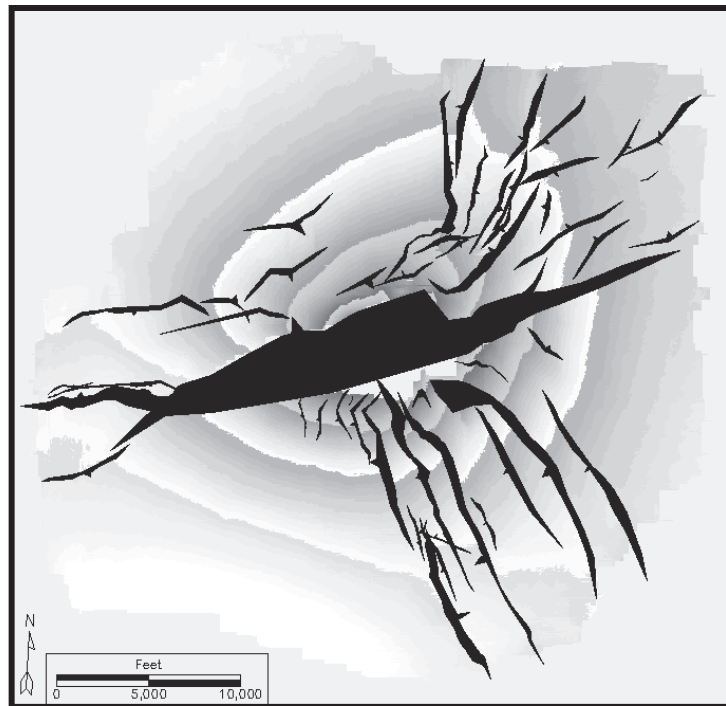


Figure 24: Interpreted Vinton Dome faults in Aquitanian strata.

Stratal geometries related to salt diapir evolution have been addressed by only a few researchers, such as Seni & Jackson (1983), Fails (1990), Pate & Dunbar (2000), Vendeville *et al.* (2003) and Yin & Groshong (2003). The most common model consists of three evolutionary stages of salt movement: pillow, diapir and post diapir. The pillow stage is the first stage which often begins as low-amplitude dome-like swells (Nettleton, 1934). The diapir stage is the second stage associated with subsidence and thickening of the denser overburden near the rising salt. The third and final stage is the post diapir stage in which the diapir continually rises while the overburden thins directly above the diapir crest. Restoration of the sections involving salt structures is complicated because it is often difficult to understand fully the dynamics of the system (Lerche *et al.*, 1996) that are attributable to dynamical parameters which are rarely accurately known; therefore intrinsic uncertainties are introduced in any model based on assumptions concerning the dynamical behavior of salt and sediments.

Seni & Jackson (1983) described salt movement and diapirism as involving flow of salt into a growing structure, creating a withdrawal basin which is generally classified to include rim synclines, primary, secondary, and tertiary peripheral sinks (Figure 25). Primary peripheral sinks form during the pillow growth, secondary sinks or rim synclines form during the diapir growth, while the tertiary sinks form during the post diapir stage.

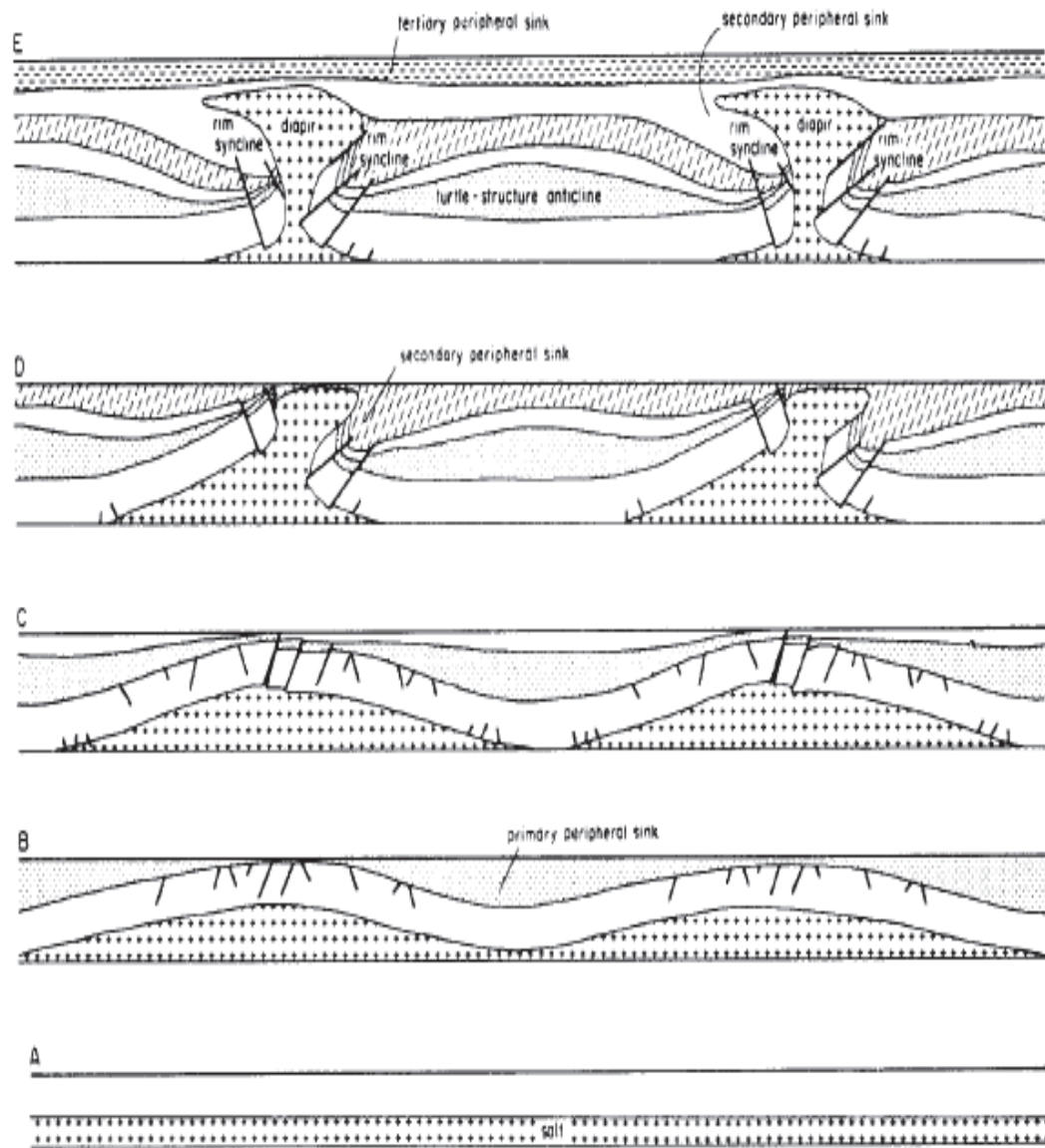


Figure 25: Structural evolution of salt pillows, salt diapirs, their peripheral sinks, and turtle structure (after Seni & Jackson, 1983).



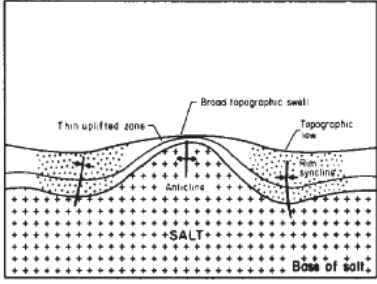
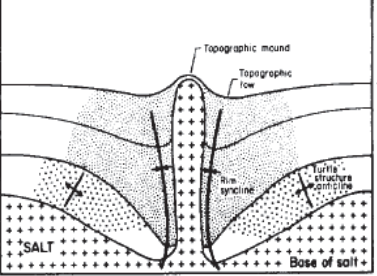
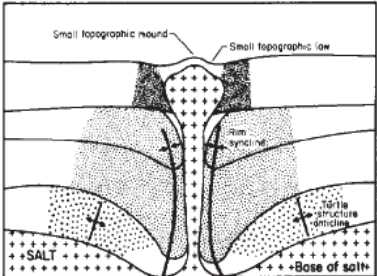
GROWTH STAGE	UPLIFTED AREA	WITHDRAWAL BASIN
<p data-bbox="574 296 643 317"><b>PILLOW</b></p> <p data-bbox="402 323 472 344">Not to scale</p>  <p data-bbox="402 636 570 657">Primary peripheral sink</p>	<p data-bbox="833 275 906 296">Geometry</p> <p data-bbox="833 310 1109 426">Sediments above pillow are thin over broad, equidimensional to elongate area. Maximum thinning over crest. Area extends 100 to 400 km<sup>2</sup> (40 to 150 mi<sup>2</sup>), depending on size of pillow. Percentage thinning, 10 to 100%.</p> <p data-bbox="833 541 878 562">Facies</p> <p data-bbox="833 577 1109 695">Thin, sand-poor, fluvial-deltaic deposits over crest of pillow include interchannel and interdeltic facies. Erosion common. Carbonate deposits on crest would include reef, reef-associated, and high-energy facies.</p>	<p data-bbox="1125 275 1198 296">Geometry</p> <p data-bbox="1125 310 1401 520">Sediments are overthickened in broad to elongate primary peripheral sink, generally located on updip side of salt pillow. Axial trace of sink parallels axial trace of elongate uplift, generally separated by 10 to 20 km (6 to 12 mi). Sink attains 300 km<sup>2</sup> (120 mi<sup>2</sup>) in extent, depending on size of pillow. Percentage thickening, 10 to 30%. Recognition of primary peripheral sink may be hindered by interference of nearby salt structures.</p> <p data-bbox="1125 541 1170 562">Facies</p> <p data-bbox="1125 577 1401 730">Thick, sand-rich, fluvial-deltaic deposits in primary peripheral sink include channel axes and deltaic depocenters. Aggradation common in topographically low area of sink. Carbonate deposits in sink would include low-energy facies caused by increase in water depth.</p>
<p data-bbox="574 764 643 785"><b>DIAPIR</b></p> <p data-bbox="402 812 472 833">Not to scale</p>  <p data-bbox="402 1117 581 1138">Secondary peripheral sink</p>	<p data-bbox="833 743 906 764">Geometry</p> <p data-bbox="833 779 1109 863">Strata largely absent above dome. An 8 to 50 km<sup>2</sup> (3 to 20 mi<sup>2</sup>) area around diapir is thinned, depending on size and dip on flanks of dome.</p> <p data-bbox="833 957 878 978">Facies</p> <p data-bbox="833 993 1109 1087">Facies immediately over dome crest not preserved because of piercing by diapir of all but the youngest strata. Sand bodies commonly pinch out against dome flanks.</p>	<p data-bbox="1125 743 1198 764">Geometry</p> <p data-bbox="1125 779 1401 936">Sediments are thickened up to 215% in secondary peripheral sink. Sinks up to 1,000 km<sup>2</sup> (390 mi<sup>2</sup>) in extent are equidimensional to elongate, and they preferentially surround single or multiple domes; several sinks flank domes; percentage thickening ranges from 50 to 215%.</p> <p data-bbox="1125 957 1170 978">Facies</p> <p data-bbox="1125 993 1401 1171">Expanded section of marine facies dominates, including limestones, chalks, and mudstones; generally sink is filled with deeper water low-energy facies caused by increased water depth. Elevated saddles between withdrawal basins are favored sites of reef growth and accumulated high-energy carbonate deposits.</p>
<p data-bbox="558 1247 659 1268"><b>POST-DIAPIR</b></p> <p data-bbox="402 1295 472 1316">Not to scale</p>  <p data-bbox="402 1600 570 1621">Tertiary peripheral sink</p>	<p data-bbox="833 1241 906 1262">Geometry</p> <p data-bbox="833 1276 1109 1360">Strata thin or absent in small 10 to 50 km<sup>2</sup> (4 to 20 mi<sup>2</sup>) area over crest and adjacent to dome; area depends on size of dome and dip of flanks.</p> <p data-bbox="833 1434 878 1455">Facies</p> <p data-bbox="833 1470 1109 1625">Facies and strata over crest of dome not preserved in places of complete piercement. Modern analogs have interchannel and interdeltic facies in uplifted area. Mounds above dome include thin sands. Carbonate strata would include reef or high-energy deposits; erosion common.</p>	<p data-bbox="1125 1241 1198 1262">Geometry</p> <p data-bbox="1125 1276 1401 1413">Sediments within 20 to 200 km<sup>2</sup> (8 to 80 mi<sup>2</sup>) tertiary peripheral sink are thickened 0 to 40%, commonly by &lt; 30 m (100 ft). Axial trace of elongate to equidimensional sink surrounds or flanks a single dome, or connects a series of domes.</p> <p data-bbox="1125 1434 1170 1455">Facies</p> <p data-bbox="1125 1470 1401 1549">Modern analogs have channel axes in sink. Aggradation of thick sands common in subsiding sink. Carbonate strata would include low-energy facies.</p>

Figure 26: Schematic stages of dome growth and variations in associated strata above and around salt structures (after Seni & Jackson, 1983).



Geometry and facies classification of the three stages of growth (Figure 26) (Seni & Jackson, 1983) are useful tools for studying the Aquitanian in the Vinton Dome area. Evidence of turtle structure anticline and rim syncline near the salt in the Late Oligocene to Early Miocene (Figure 27) showed that the Aquitanian strata in the dome were formed in the post pillow stage. The close proximity of the strata to the salt, thinning near the salt and thickening on the peripheries suggest that the Aquitanian strata were formed in the diapir stage.

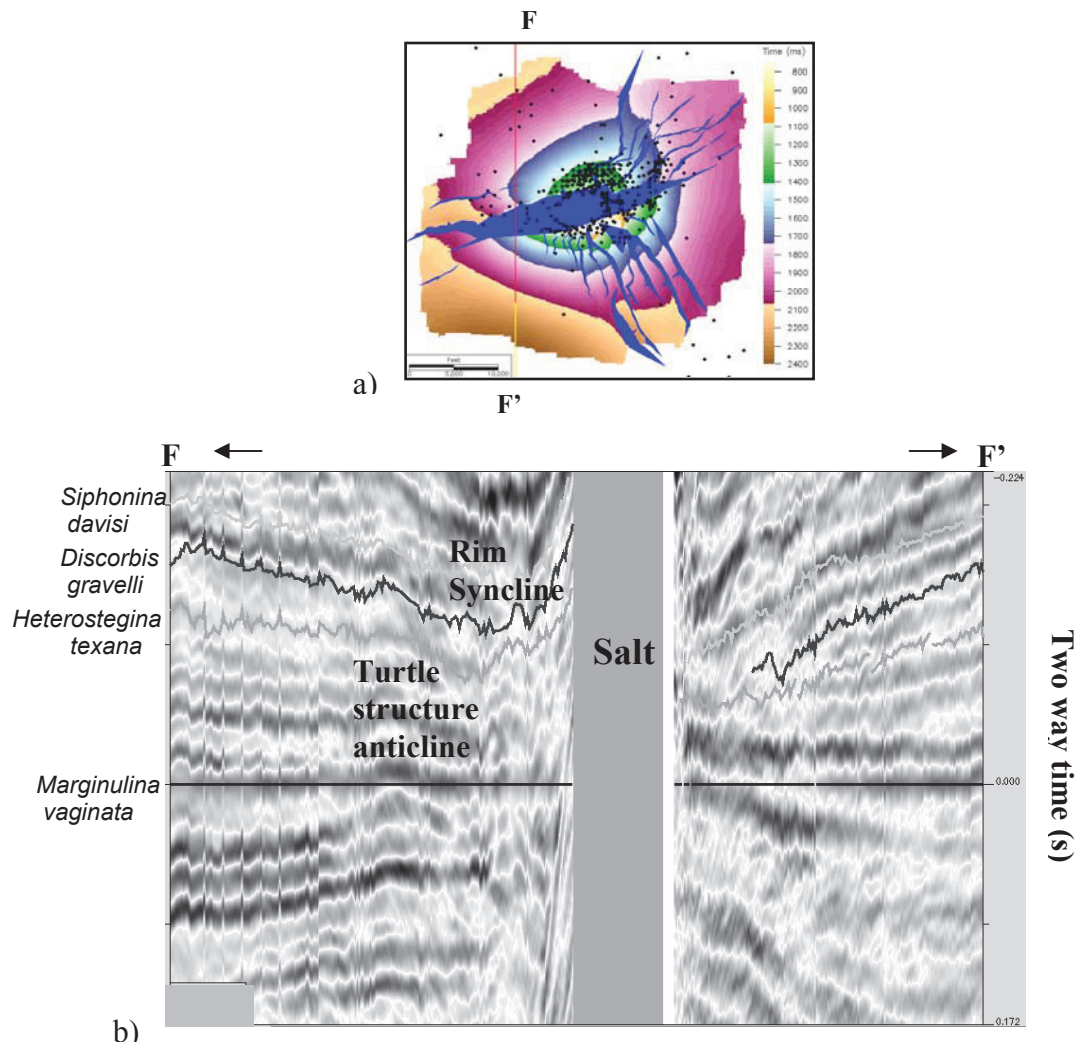


Figure 27 a & b: Basemap and crossline position of seismic profile showing flattened *Marginulina vaginata* horizon slice, evidence of rim syncline and turtle anticline Structures in Late Oligocene to Early Miocene, Vinton Dome.

The Vinton dome area is characterized by intercalated layers of sandstones and shale. The upward thrust of the salt plug affected both the stratigraphy and structure of the area resulting in thinning of beds near the flanks of the salt and thickening towards the edge of the dome. The thickening at the periphery of the dome is attributed to slumping and syn-depositional thickening (Figure 28). Dip of beds range from  $85^{\circ}$  near the margin of the salt to near horizontal at the periphery of the study area.

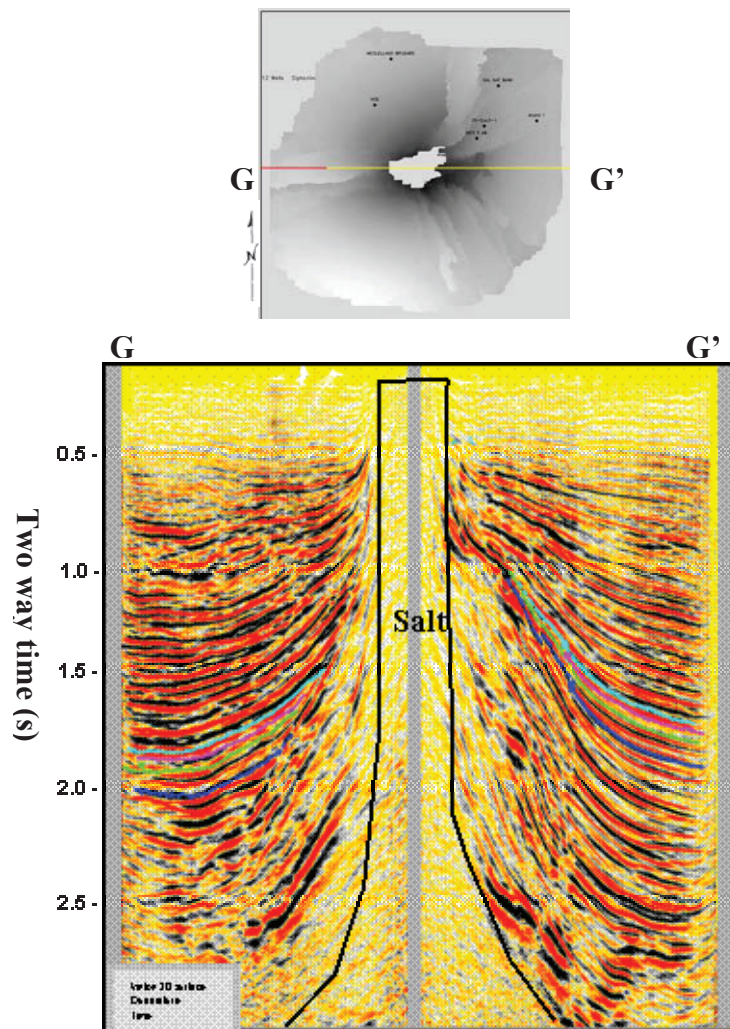


Figure 28: Seismic profile showing high dip of beds due to impact of Vinton salt. Turquoise blue line represents the Lower Miocene.

## **3.2 STRUCTURAL EVALUATION**

The top of salt was mapped in depth by Thomas & Eichelberger (1927) using well logs (Figure 9). Over the years, the advent of 3-dimensional seismic data has permitted better imaging of geometries, internal architecture of subsurface bodies, and more accurate estimates of margins than can be achieved from well logs, subject to vertical and lateral resolution of the seismic data. I performed a detailed interpretation and mapping of the structure of Vinton salt in 3D seismic data (in time) (Figure 29). Though the salt body was not imaged in the 3D seismic data, nonetheless, boundaries of salt were derived from salt - sediment contacts.

### **3.2.1 Salt Shape**

The Vinton salt boundaries are circular to ellipsoidal in plan view (Figure 29). The piercement point of the salt is circular while the diapir becomes more ellipsoidal with depth to 3250 ms. The salt is not detached from the underlying salt body and can be classified as a penetrant salt dome (Figure 28). The Lower Miocene salt boundaries (red polygon) trend northeast – southwest with two elongate boundaries in the northeast – west direction, and a circular boundary in the south direction (Figure 29). The north – south direction has dimensions of 8850 ft (2697 m) and the northeast – southwest direction, 14,100 ft (4298 m). The Vinton strata are asymmetrical on opposite sides of the salt, largely caused by salt tectonics and displacement by a counter regional fault. The positions of the Aquitanian strata on

the sides of the diapir differ significantly in time between 125ms and 375 ms (Figure 28).

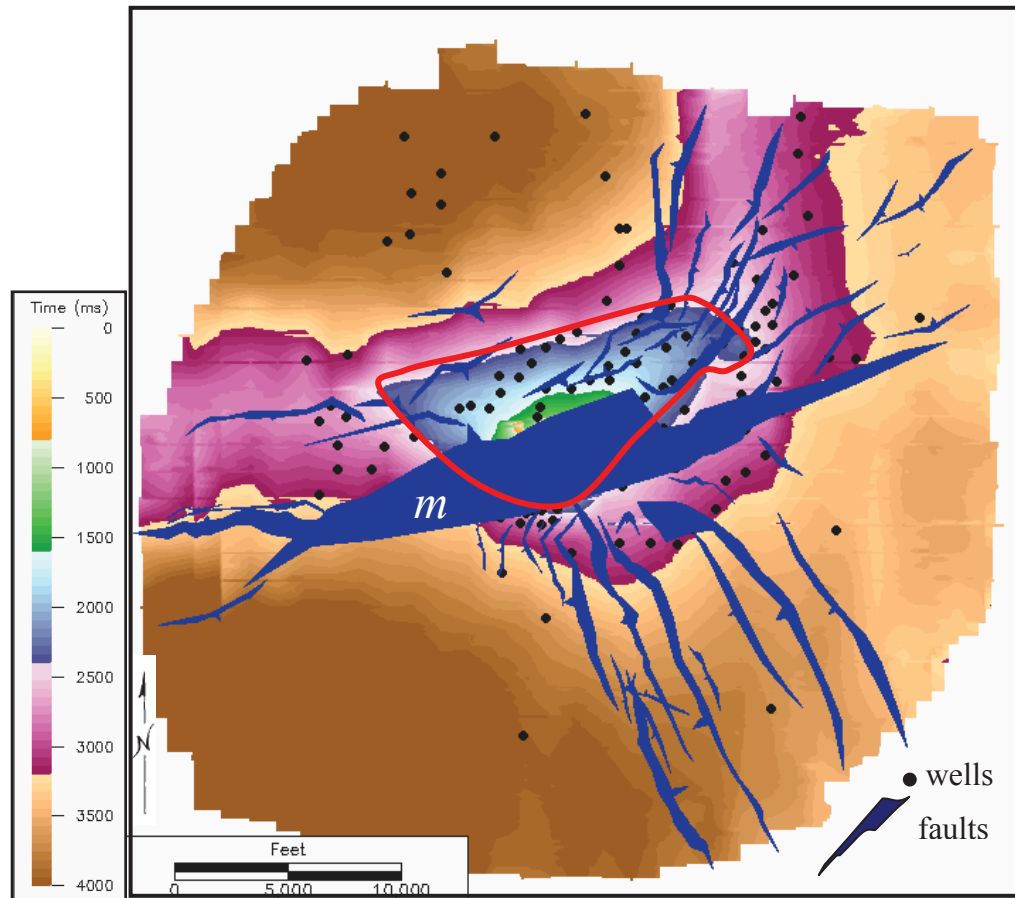


Figure 29: Time map of top of Vinton salt. Red line indicates Early Miocene salt boundary. Faults are overlaid on top of salt map.

### 3.2.2 Faults

#### 3.2.2.1 Major Faults

The master fault **m**, which is genetically antithetic to a regional growth fault, is a normal fault and dips inland to the north, subdividing the dome into two seemingly equal parts (Figures 29 and 30). The fault trends parallel to the ellipsoidal direction of the salt and its length is almost the diagonal of the dome. It strikes N 75° E, with dip of 45° and throw of approximately 1400 ft (427 m). The fault continued to grow and increase in length from the Late Oligocene to the Early Miocene.

Peripheral fault sets in the dome are normal and consist of divergent, en echelon, and parallel fault patterns. The northeast faults splay in one of the direction of the salt's ellipsoidal axis. They strike between N 5° W and N 80° E, and dip between 45° and 60° with throws ranging from 7 ft (2 m) to 175 ft (53 m). These faults are generally shallower than the southeast faults.

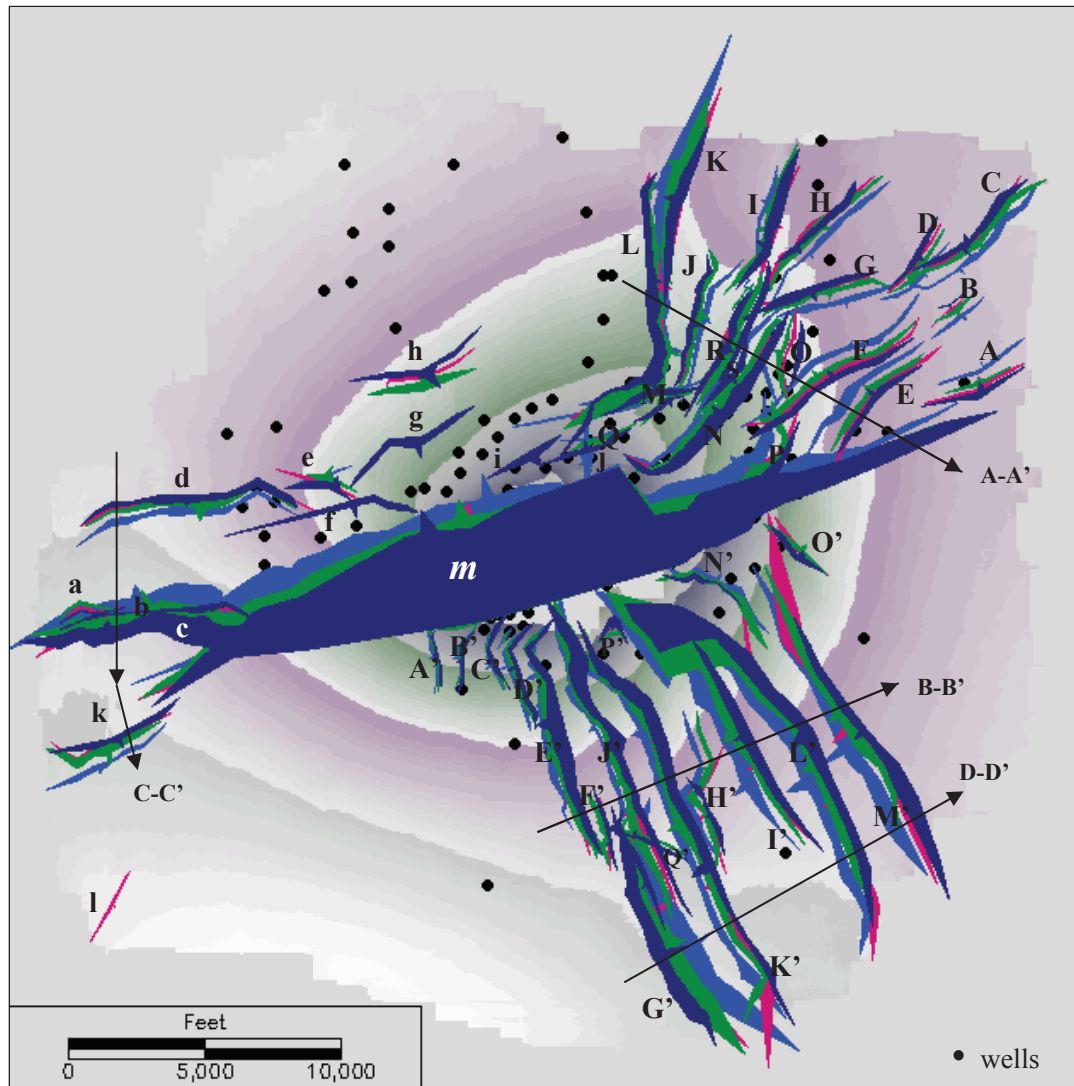
The positions of maximum displacement of the southeastern faults are deeper than those of the northeastern faults, suggesting that their origins may be deeper-seated. Only some of the faults were active in the Early Miocene (Figures 30-34). Active faults during the Early Miocene are northeast faults **m**, E, O, S, and i, southeast faults G' and K', and west faults b, c, f, and g (Figure 30).

Variations in thickening and thinning of strata enable determination of fault throws which in turn indicate the active faults. I tested the origin and timing of

Vinton Dome faulting by comparing throws and thickness variations across faults. Thickening of strata adjacent to the southeast fault set shows that the active faults strongly control sedimentation in the Aquitanian (Figures 30-34, cross-sections B-B' & D-D').

The southeast faults are arranged in an en echelon pattern, forming half grabens. Faults dip between 30° and 45° to the west with the exception of fault **K'**, which dips to the east creating a graben in conjunction with the opposite fault **G'** (Figures 32 & 34). The graben was a major area of sediment ponding, forming the thickest part of the study area. Faults strike N 5° W to N 40° W and throws range from 65 ft (20 m) to 445 ft (136 m).

Faults in the west of the area are relatively short, parallel, and appear to be complimentary to the master fault, **m**. They are situated to the west and northwest of the master fault, in the western ellipsoidal direction of the salt (Figure 29). Some of the west faults set (faults d, e, g and f) serve as boundaries of a major channel belt that parallels the master fault (as will be shown in section 2.2.4). The faults strike N 85° E to N 90° E and dip 30° with throws between 100ft (30.5 m) to 380 ft (116 m). Evolution of these faults strengthens during the Early Miocene (Figure 30) with faults b, f, g, and i emerging in the Early Miocene, whereas, other faults had been in place earlier than the Late Oligocene.



Picture 30: Early Miocene time-structure map showing fault development with depth and cross-sections A-A', B-B', C-C' and D-D' across fault sets. Change in fault color signifies different horizons. Navy Blue - *Siphonina davis* (Topmost); Wine – Top Anahuac; Green – *Heterostegina texana*; Light Blue – *Marginulina vaginata*. Fault tips outside survey are extrapolated.



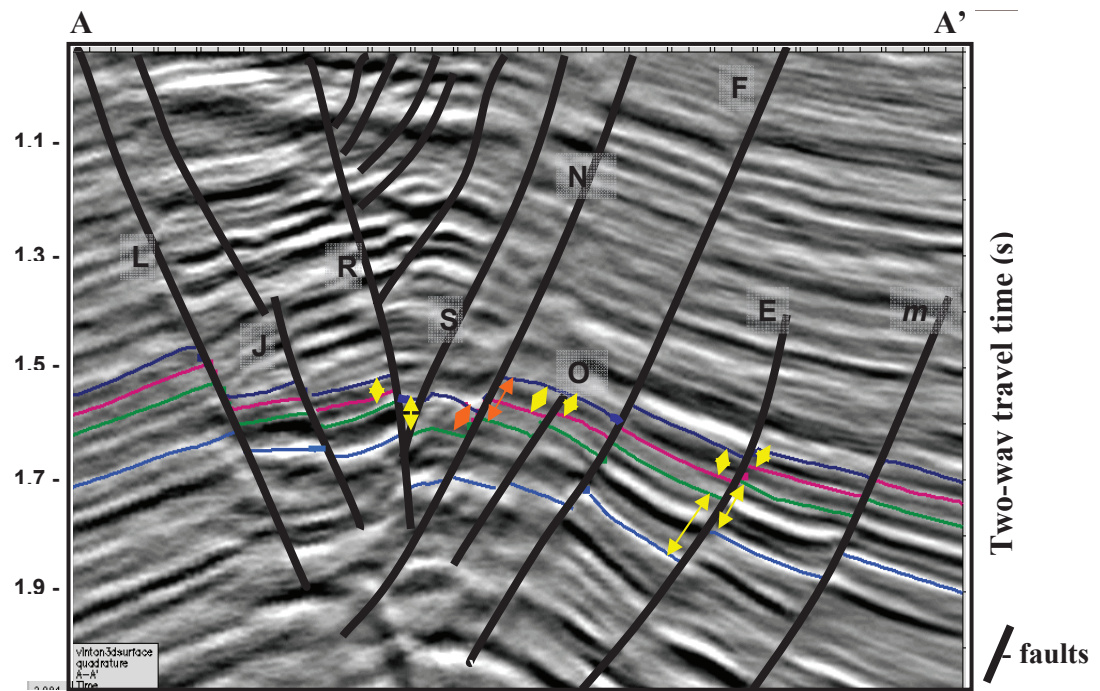


Figure 31: Seismic profile showing the A-A' cross-section across the northeast divergent faults. Double headed arrows express strata thickness variations.

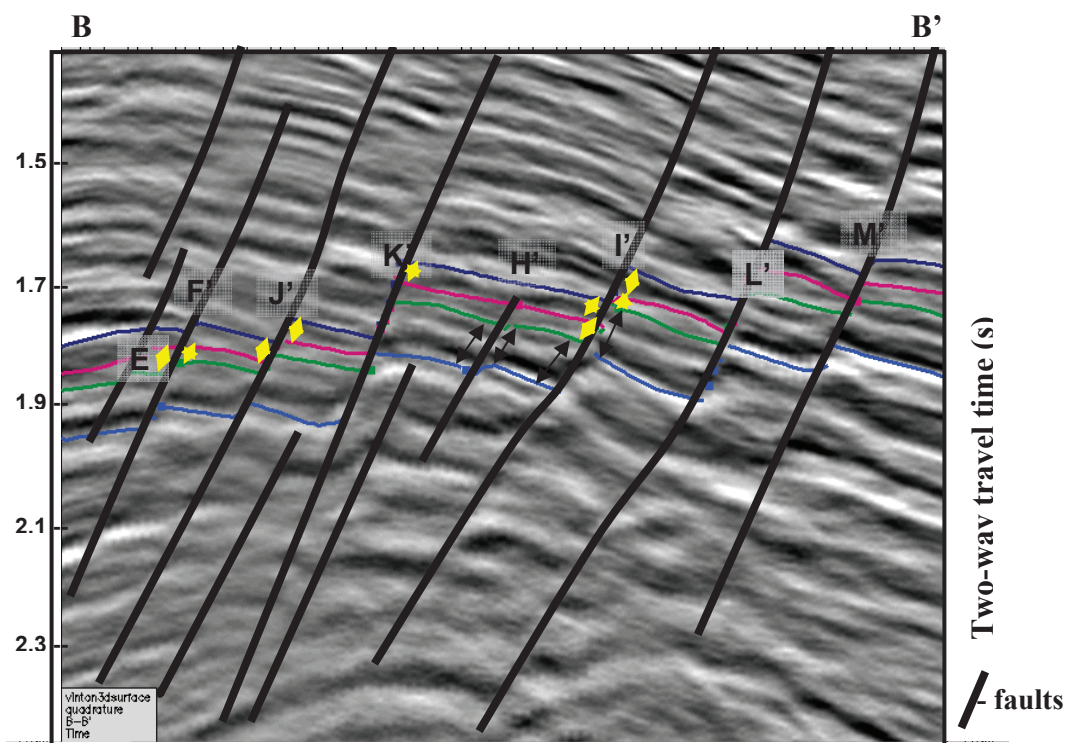


Figure 32: Seismic profile showing the B-B' cross-section across the southeast faults.



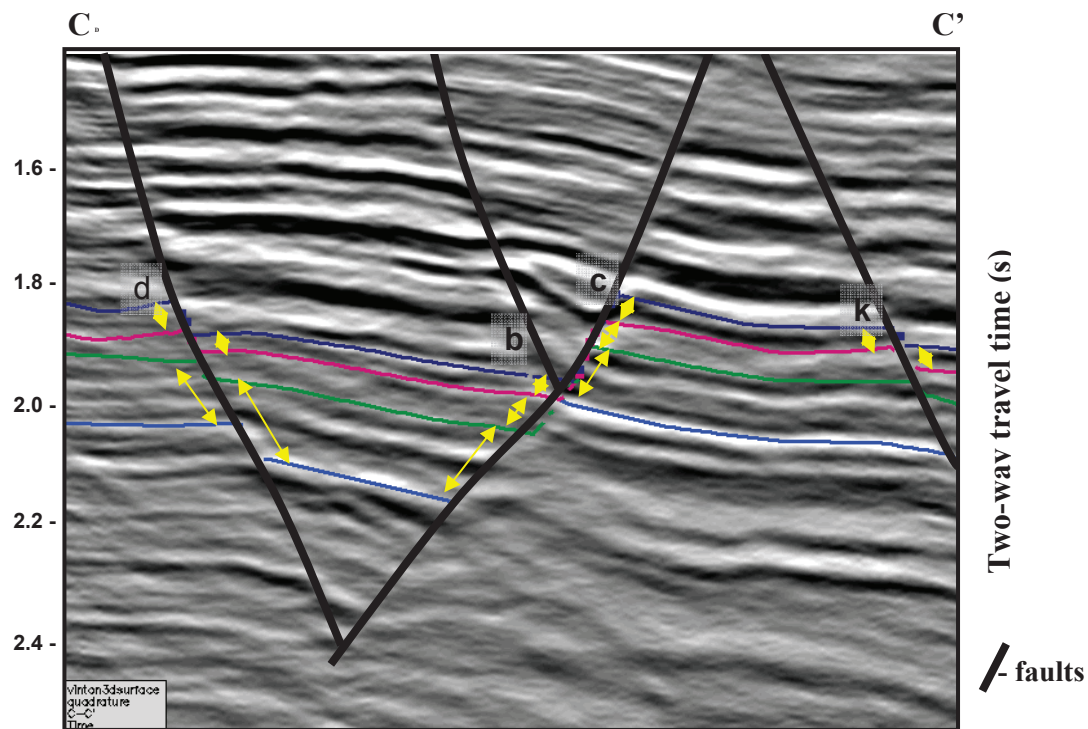


Figure 33: Seismic profile showing the C-C' cross-sections across the west faults.

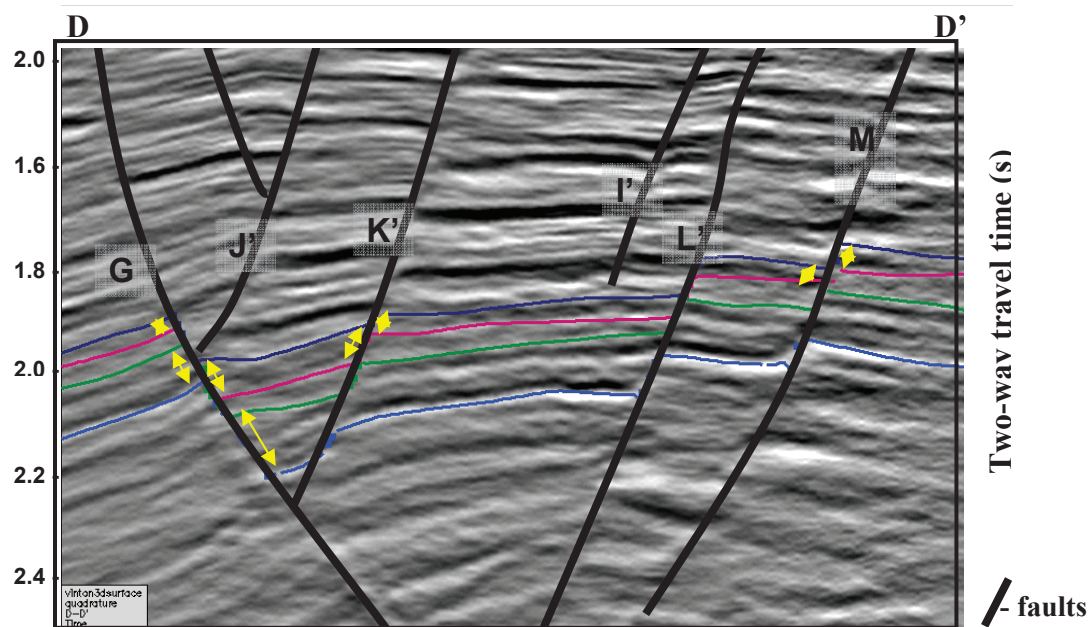


Figure 34: Seismic profile showing the D-D' cross-sections across the west faults.

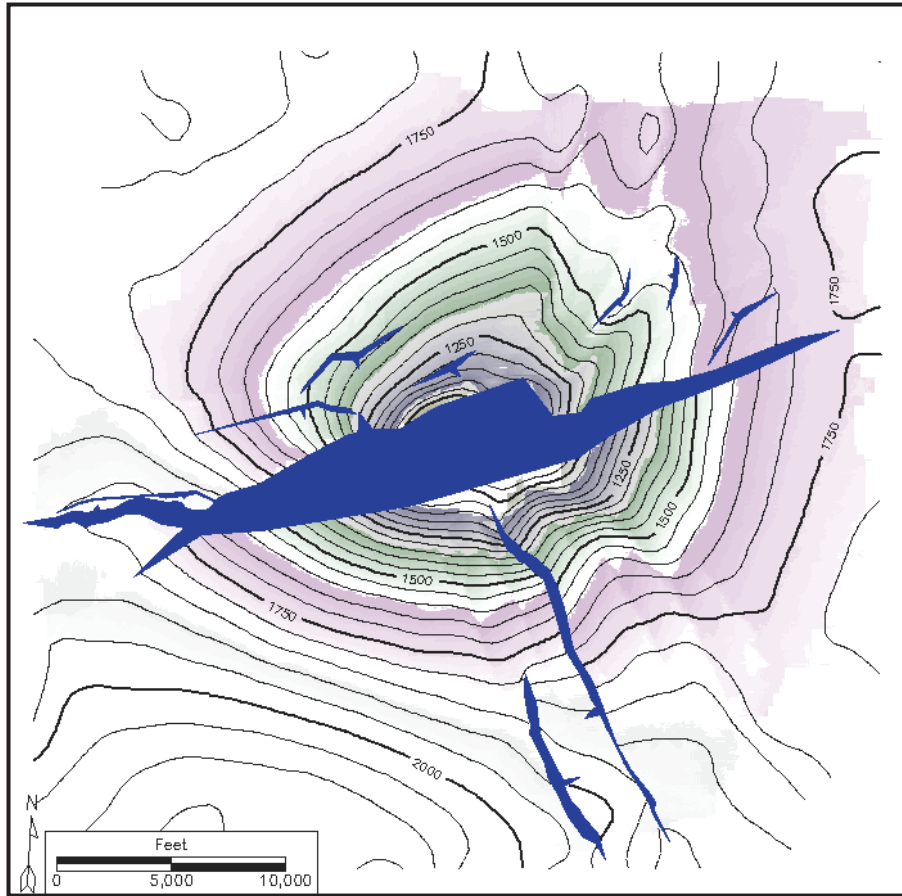


Figure 35: Time structure map of active faults during the Aquitanian, Vinton Dome.

Detailed evaluation of the time dip and azimuth maps of the Upper Oligocene and Lower Miocene horizons indicates consistency in their structural pattern and tilt (Figures 36 & 37). The strata dip away from the salt and had been domed by the effect of upward movement of the salt.

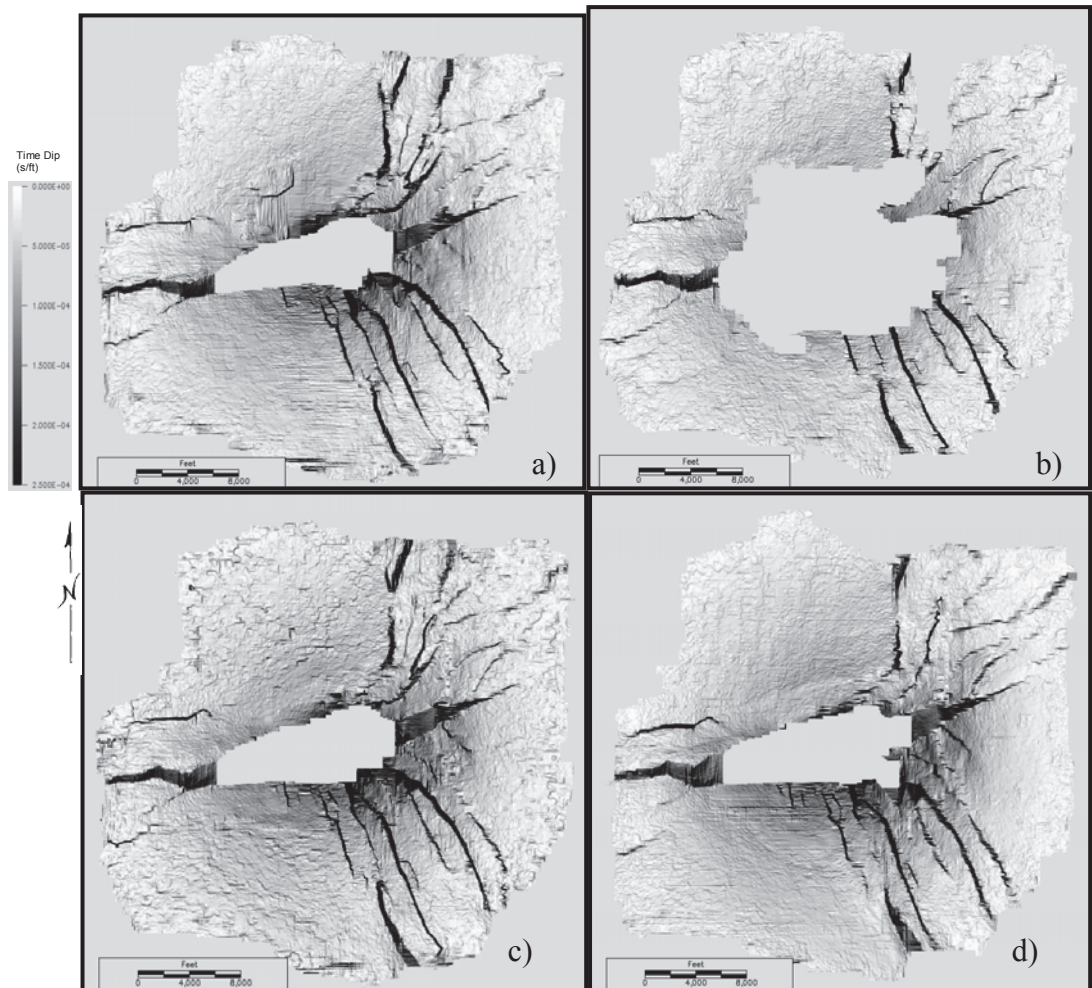


Figure 36: Basemap profile showing time dip (s/ft) of faults in Lower Miocene to Upper Oligocene horizons. (a) *Siphonina davisi*; (b) Top Anahuac (*Discorbis gravelli*); (c) *Heterostegina texana* (d) *Marginulina vaginata*. These are computed in a window of 20ms. Darker grays correspond to steeper dips.



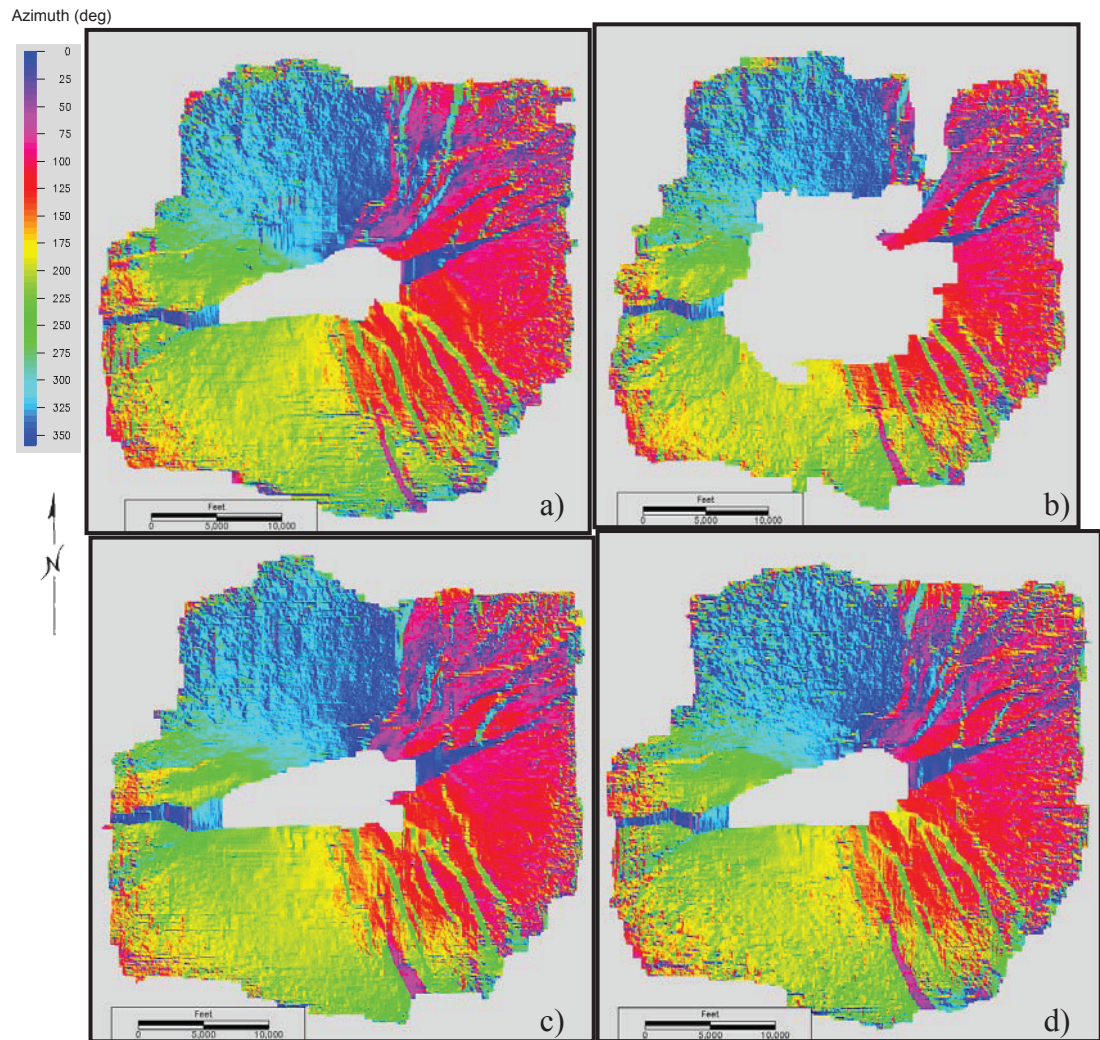


Figure 37: Basemap profile showing dip azimuth (in degrees) of faults in Lower Miocene and Upper Oligocene horizons. (a) *Siphonina davisi*; (b) *Discorbis gravelli* (Top Anahuac); (c) *Heterostegina texana*; and (d) *Marginulina vaginata*.

### 3.2.2.1 Polygonal “Mosaic” Fractures

In the Vinton Dome area, mosaic patterns are observed on all of the four mapped horizons in the Miocene when curvature attributes are applied (Figures 38 & 39). These are multi-directional polygonal features which exist not only in the deep marine sediments, but also on shelf and in the shore zones. They are consistent through the entire survey from the *Marginulina varginata* section in the deepest marine and throughout the entire Miocene section.

Careful observation of these polygonal features (average of 200 ft - ~ 60 m in diameter) reveals that they show no overall preferred direction of either strike or dip, revealing an isotropic nature of the fracture pattern. They are slightly variable, and vary in shapes, sizes and positions. However, there is no observable alteration of intensity of polygons around high dips of salt body when compared to the flanks, and within more bent blocks of faults (such as in the blocks of faults L, J, N, and f). They are also not observable in the conventional 3D seismic amplitude data or in other attribute maps; nonetheless, they appear to be geologically related features. Combination of the regularity of the survey and changes in the polygons suggest their geological authenticity.

The mosaics of different horizons were overlaid on each other (Figure 40). The *Siphonina davisii* and *Discorbis gravelli* horizons display no significant change in polygonal faulting, perhaps due to their closeness in time (~ 50 ms), but reveal change in major faults. These horizons differ considerably from the *Heterostegina texana* and the *Marginulina vaginata* horizons, which are farther in time (A difference of 100 ms and 250 ms respectively from *Siphonina davisii*). The

*Heterostegina texana* horizon displays more radial and linear faulting than the other horizons while the other three horizons display more robust polygons. The *Siphonina davisi* and *Discorbis gravelli* horizons are shale tops while and the *Marginulina vaginata* horizon is sand top, whereas, the *Heterostegina texana* section is a carbonate zone. The importance of a different lithology and sediment loading of the area during the *Heterostegina texana* time may significantly contribute to increased salt movement and consequent slumping of sediments that may be responsible for its increased linear and radial pattern of polygonal faulting. As expected, the polygons change significantly in position, size, and shape when negative curvature of different horizons are compared with their respective positive curvatures, but align more closely when negative curvatures of different horizons are compared.

In the North Sea Basin, overpressured Early Cenozoic mud rock sequences exhibit polygonal features which are unrecognizable in conventional 3D seismic and amplitude time slices, but show up well in coherence slices (Figure 41). Haskell *et al.* (1999) explained that polygonal features can be formed by episodic hydro-fracturing of basin-wide over-pressured compartments. These features are associated with slumps and dewatering structures which may indicate geologic hazards. Consistent polygonal features from deep marine horizons to shallow shelf horizons (750 ms – 2200 ms), and high dip of beds in the Vinton area strongly suggest fracturing of strata as a result of the upward thrust of the salt plug (Figure 28).

Other means by which polygonal faults form include syneresis (Figure 42). Dewhurst *et al.* (1999) defined syneresis as a process in which the pore fluid is expelled from sedimentary gels through the spontaneous action of electrochemical forces. This differs from mud compaction processes in which gravitational forces drive expulsion of pore fluids; rather, it is a process of spontaneous volumetric contraction and concomitant fluid expulsion. However, syneresis had been associated with very fine sediments such as silty mudstones and claystones that are found in slope or basin floor depositional environments (Lovell, 1990; Joy, 1993; & Dewhurst *et al.*, 1999). The continuous presence of the fracture sets throughout the Upper Oligocene and Miocene sections is found in clastic progradational sequences as well as marine sequences. A combination of many processes could also be responsible for the formation of the Vinton Dome polygonal fractures.

The acquisition configuration used for Vinton 3D seismic was a circle and spoke pattern (Figure 43). This may likely introduce some noise of equal pattern to the seismic data. The noise may be interpreted as acquisition or processing footprints. Ideally, the Vinton Dome polygonal features should be calibrated with image logs, given that the patterns are partially variable even though there is strong structural deformation.



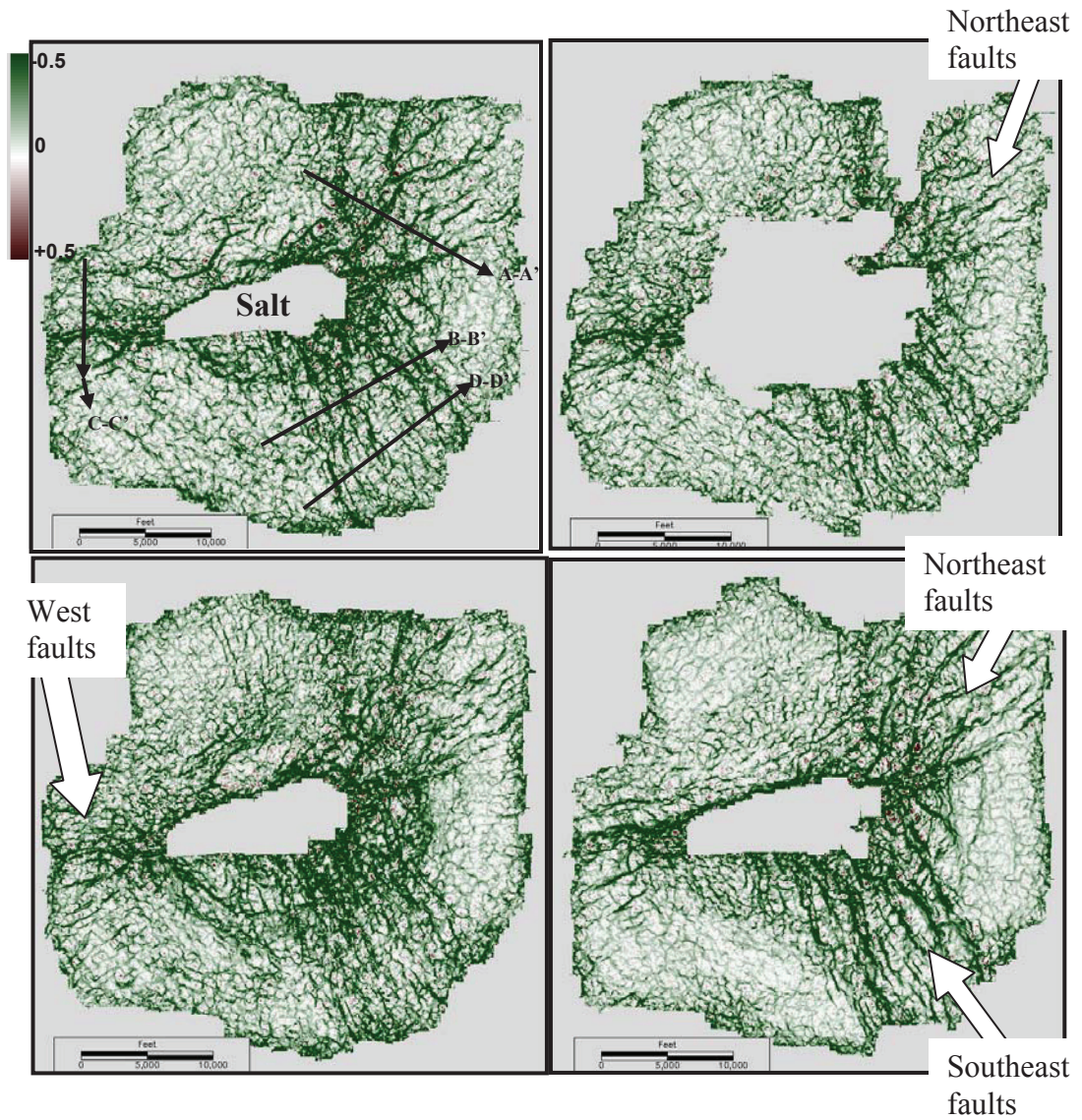


Figure 38: a). Most negative curvature maps of Lower Miocene and Upper Oligocene horizons. (a) *Siphonina davisi*; (b) Top Anahuac (*Discorbis gravelli*); (c) *Heterostegina texana*; (d) *Marginulina vaginata*. Arrow lines on (a) refer to cross-sections across the major faults (Figures 31 – 35 for cross-sectional views).



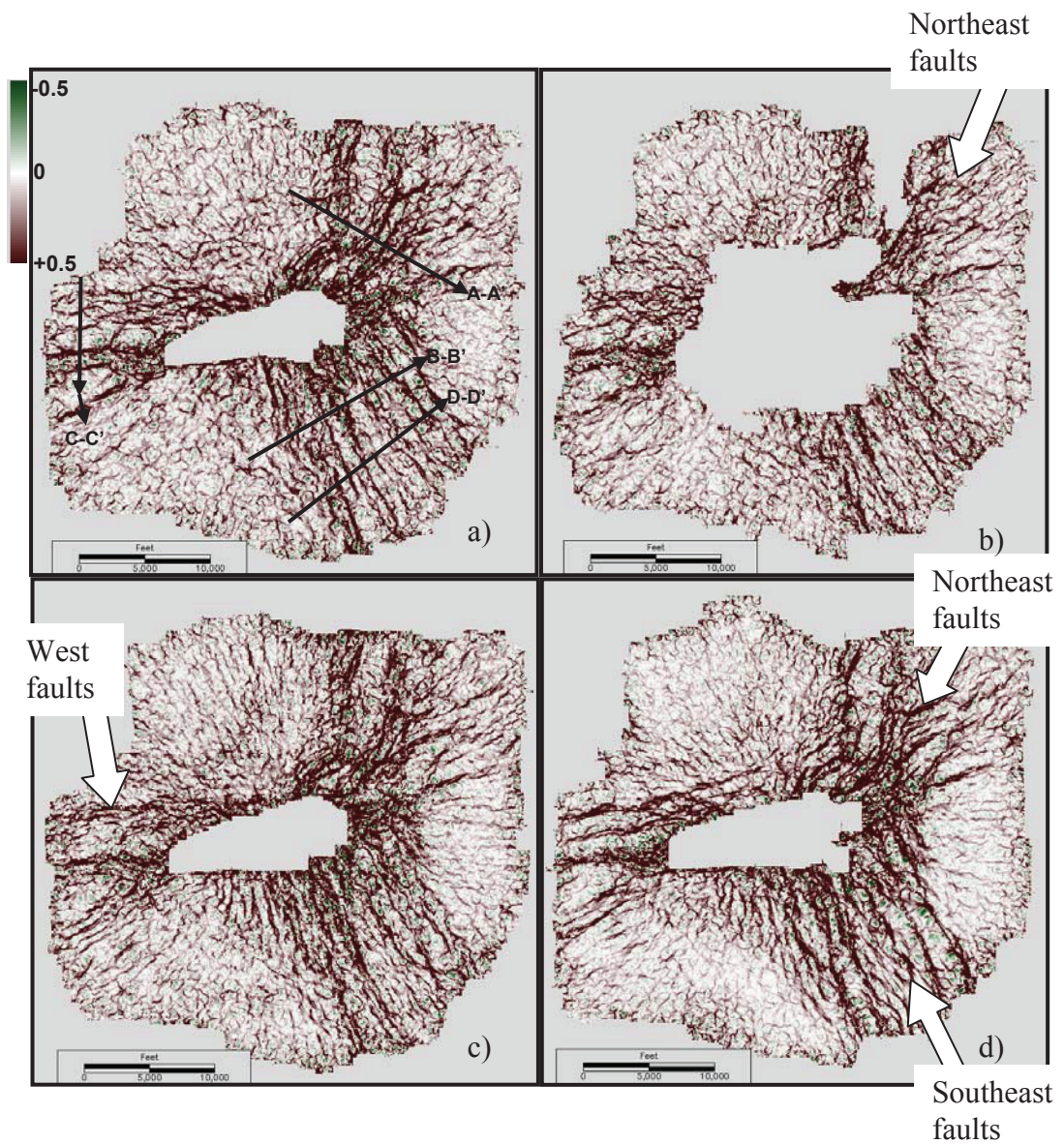


Figure 39: a). Most positive curvature maps of Lower Miocene and Upper Oligocene horizons. (a) *Siphonina davisi*; (b) *Discorbis gravelli* (Top Anahuac); (c) *Heterostegina texana*; (d) *Marginulina vaginata*. Arrow lines on (a) refer to cross-sections across the major faults (Figures 31 – 35 for cross-sectional views).

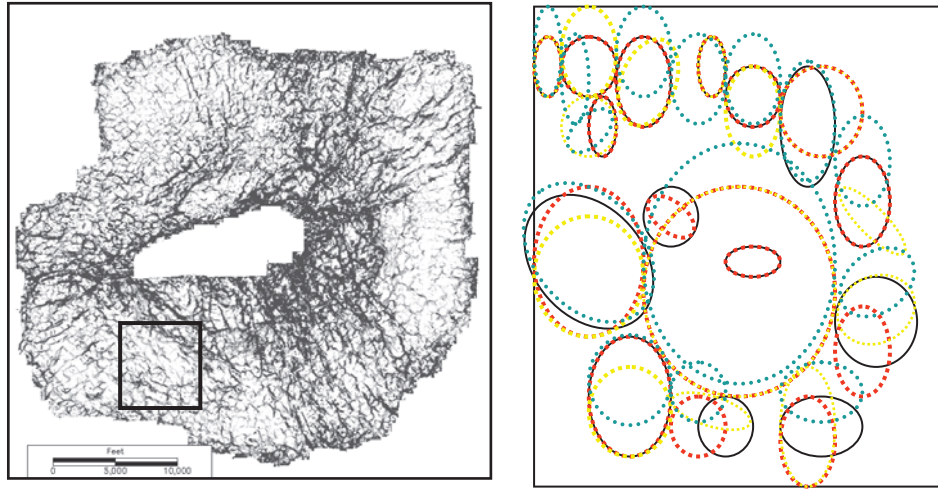


Figure 40: Positions and sizes of some fault polygons represented in the black square on the dome. Change in color represents different horizons. *Siphonina davisii* – Black, Top Anahuac – Red, *Heterostegina texana* – Yellow, *Marginulina vaginata* – pale blue.

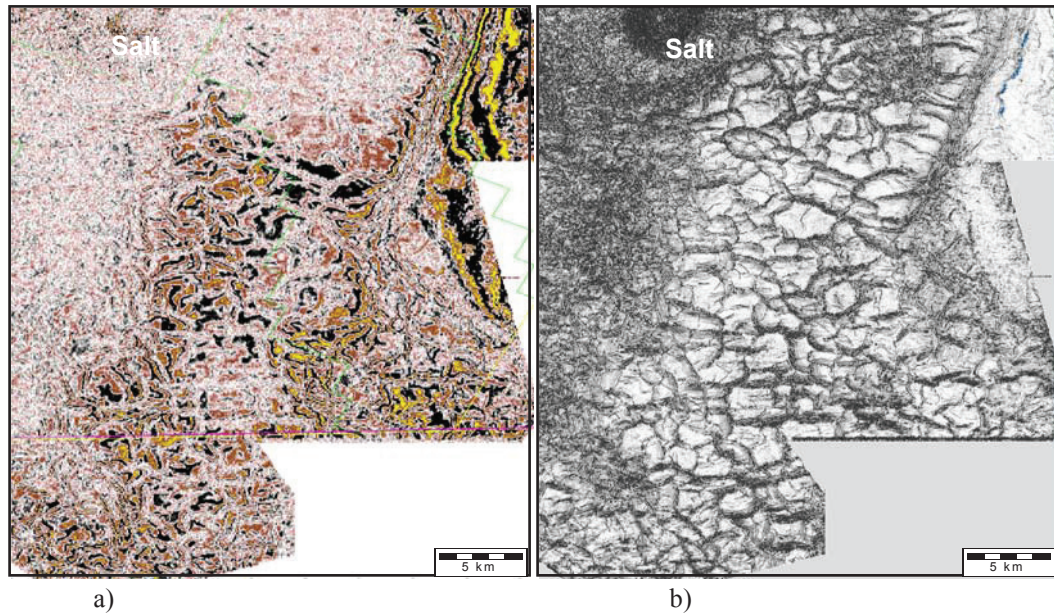


Figure 41: a) Time slice and b) coherency slice at 2800 ms showing polygonal faults caused by dewatering of overpressured shales in the Lower Miocene, Valhall area, North Sea. Polygon size approximate 1-3 km (Haskell *et al.*, 1999).



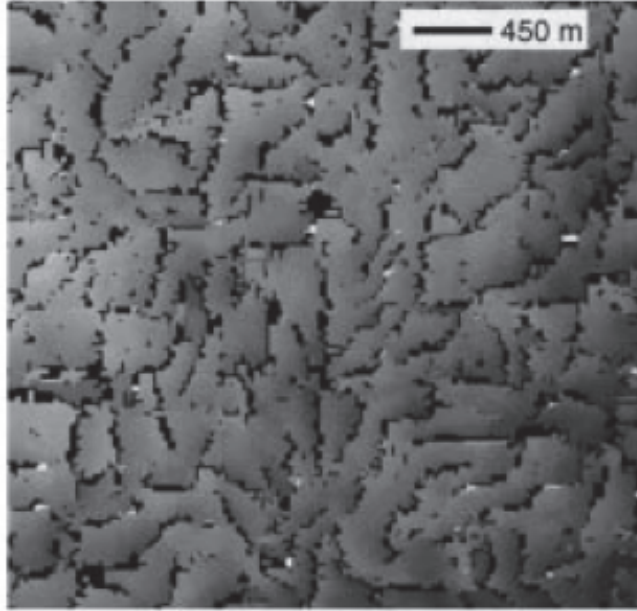


Figure 42: Horizon slice of Lower Miocene, North Sea Basin, showing polygonal faults caused by syneresis. Polygon sizes are 200 – 500m. Time contours 1.18 s (white), 1.29 s (Dark gray) (Dewhurst *et al.*, 1999).

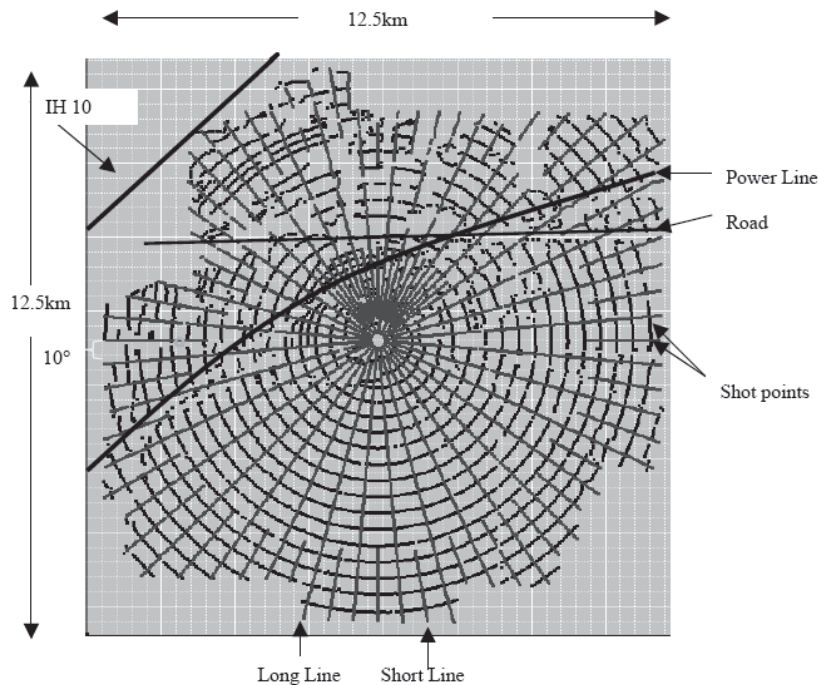


Figure 43: Acquisition pattern for the Vinton Dome survey. Radial lines represent receivers and roughly concentric circles represent shot points. Interstate Highway 10 runs along the northwest of the survey (Constance *et al.*, 1999).

### 3.2.3 Discussion on Faults

Intrinsic factors such as the shape of salt bodies and regional stress significantly influence fault patterns during periods of doming (Parker & McDowell, 1955; Hughes, 1960; and Withjack & Scheiner, 1982). The experimental and analytical models shown for circular and elliptical domes (Withjack & Scheiner, 1982) show that on elliptical domes, normal faults form on the crest which roughly parallel the long axes, but splay outward toward the ends of the long axes near the peripheries whereas, circular domes experience more radial faulting. These models also show that regional extension is usually perpendicular to the direction of normal faults. This pattern is observed on Vinton Dome with divergent faults on the northeast toward the elliptical direction of the salt only, while the other parts of the dome with associated circular salt direction do not have divergent faults. The northeast faults splay in the direction of the salt's ellipsoidal axis and were perhaps caused by regional extension and differential loading of sediments during doming.

The en echelon fault set in the southeast part of the dome is relatively distal and is perhaps linked to early formation of the dome. Regional peripheral Late Jurassic to Miocene fault trends in some Mississippi Salt Basin areas demonstrate that en echelon extensional faults and half grabens are closely associated with early formation and salt flowage (Hughes, 1968; & Mancini *et al.*, 2001). Halokinesis was attributed to have formed this set of faults with associated gravity creep and active differential subsidence. Hughes (1968) also explained that it is possible to have varying rates of deposition over a salt structure rising differentially at a constant rate,

which may result in variations in the increase of fault throws with depth, and different degrees of thinning and thickening of the stratigraphic units in closely associated fault blocks.

I propose that the west faults set were formed by tensional stress due to the formation of secondary peripheral synclines in the downthrown side of the master fault that was driven by sediment loading and salt movement in the north of the dome. Galloway (1986) attributed such faults (but in mega scale) in deltaic environments to gravity induced deformation.

#### **3.2.4 Impact on Sedimentation**

The depositional patterns, structural patterns and salt tectonics are totally inter-dependent. Generally, sediment input is expected from inland (north of the dome) to the Gulf of Mexico basin (south of the dome). Due to low seismic resolution, seismic facies of channels are merely displayed as bird's eyes in conventional 3D seismic vertical section and are not apparent on attribute maps. However, detailed interpretation of the seismic data and tracing of these channel facies reveals channel-flows from the northeastern part of the area indicating sediment transport from the northeast to the west, southwest and southeast parts of the dome (Figure 44).

Deposition in the northern area is structurally controlled by the master fault, *m* (Figure 30). Sediments thicken at the hangingwall of the fault and thin at its footwall indicating that the salt was seated at the hangingwall in the Anahuac.

Stratal thickness in the downthrown side (Late Oligocene section) is approximately 350 ft (107 m) while the upthrown side has only about 100 ft (30.5 m), suggesting evidence of salt creep from the north of the dome to the upthrown side of the fault, creating a graben in the north of the dome, perhaps represented by the rim syncline (Figure 27).

More sediment input at the north of the dome results in more salt withdrawal from the hangingwall to the footwall of the master fault. Consequently, more space is created in the hangingwall of the master fault to accommodate even more sediments. In the Aquitanian, the northeast faults set controlled the sandy feeder channel in the area. The channels, often displayed as bird's eyes (example in Figure 44), were traced in the seismic data. Their obscurity by low seismic resolution has largely contributed to their ambiguity in coherence maps (Chapter 4 for more details). The channels in the northeastern fault blocks converged towards the master fault and merely flowed parallel to the master fault's strike to the west of the dome. Other channels crossed the eastern part of the dome and deposited their contents to the southeast where deposition was observed to be greatest. The graben (Figures 30 & 34) formed by the two compensated faults, K' and G' was an area of sediment ponding which was directly fed by one of these channels. Thickening of strata adjacent to the southeast fault set shows that the active faults strongly control sedimentation during the Early Miocene. The southeast faults on the dome were perhaps linked to salt flowage and early deformation in the area which may cause the varying rates of deposition in the fault blocks (Hughes, 1968).

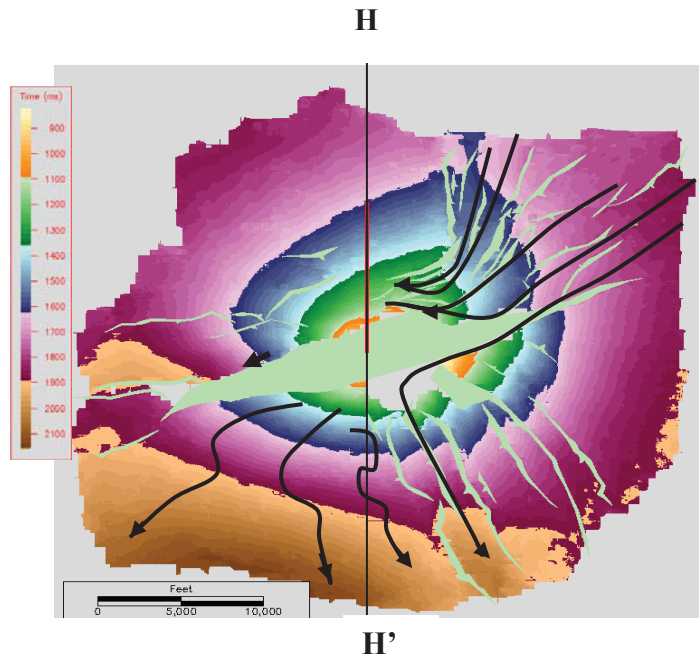


Figure 44 a: Map showing direction of some Early Miocene channels in Vinton Dome area as traced in well and seismic data, i.e. mapped on vertical sections (inlines and crosslines). The channels are not well imaged in coherence image (e.g. Figure 64). Red line indicates crossline position displayed in seismic profile in figure 44 b.

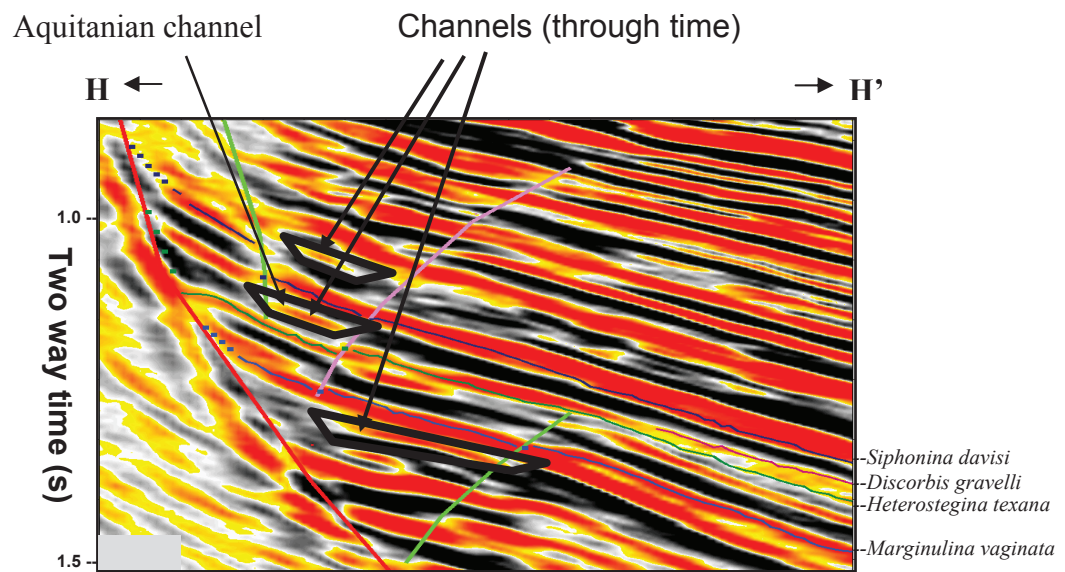


Figure 44 b: Seismic profile of crossline position (Figure 44 a) showing position of some northern channels indicated by “bird’s eyes” seismic facies, flowing in westward direction.

The development of the west faults (Figures 30 and 33) intensify in the Early Miocene indicating increase in sedimentation especially in the northwest and west part of the dome (Appendices A1a – A1d). The increase in intensity of the faults over time from the Late Oligocene to the Early Miocene substantiates increase in sediment loading and perhaps concurrent salt withdrawal in this locality, corresponding to the previously established history of the Cenozoic era (Galloway, 2000). However, decreased thickness of fault heaves in the Top Anahuac section indicates sediment starvation (Appendix A1b). Nonetheless, fault block **P** (Figure 30) continued to receive sediments from the northeastern area.

Peripheral fault sets reveal volume expansion and increased sedimentation with decreased time. A loop cross-sectional view of the Aquitanian strata (Figures 45 and 46) suggests syndeposition of the Early Miocene strata around the dome. The thicknesses of the strata are approximately equal and are well developed at the peripheries of the dome.



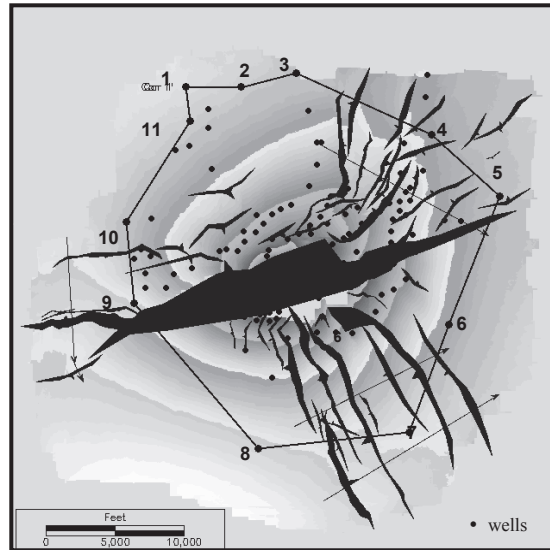


Figure 45: Structural map showing loop x-section around the dome.

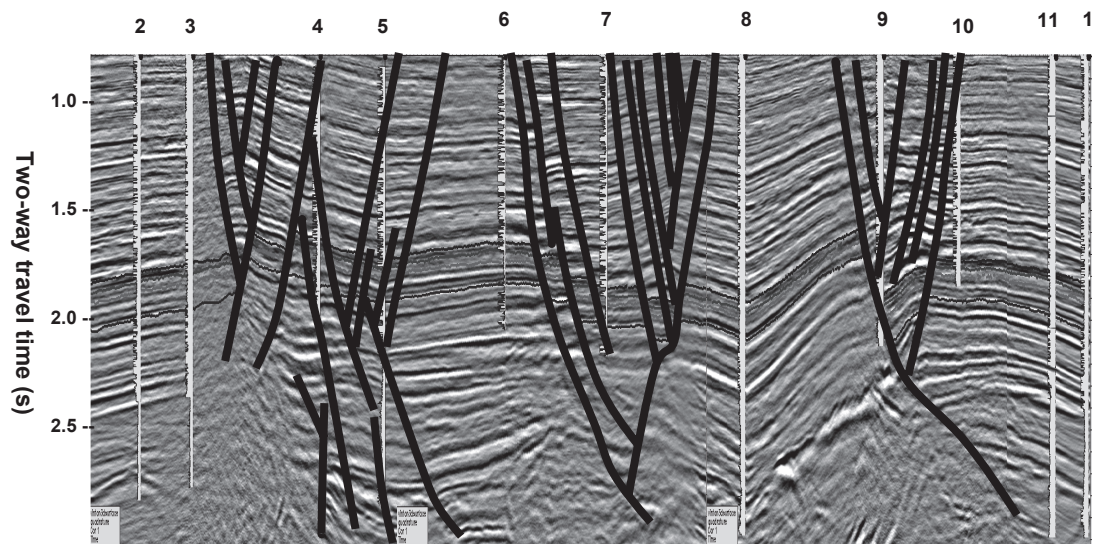


Figure 46: Seismic profile showing loop structural vertical cross-section of SP logs (Figure 45); *Siphonina davisii* - top horizon, Top Anahuac - 2<sup>nd</sup> horizon, *Heterostegina texana* - 3<sup>rd</sup> horizon, & *Marginulina vaginata* – last horizon.

Thickening and thinning of Early Miocene strata within peripheral fault sets provide insights to depositional variations and the history of active faults. The

northeast faults set (Figure 31) shows variations in the degree of sedimentation. Downthrown fault blocks of *m*, E, O, S, and i indicate thickening of strata which coincide with paths of channels in the locality (Figures 30, 31, and 44). Thickening of strata observed on these downthrown blocks support evidence of active sedimentation. However, shortening observed in fault blocks N and J suggests that these blocks were previously horsts, whereas blocks N and S (Figures 30 & 31) were later displaced as a graben.

Little or no change of stratal thickness in the southeast fault set of cross-section B-B' is an indication of by pass deposition, but the D-D' cross-section southwards show thickening in the graben of the G' and K' fault block, indicating a major depositional center for the area (Figures 30, 32, and 34). Equal vertical thickness of *Discorbis gravelli* to *Siphonina davis* strata observed on the southeast fault blocks in B-B' cross-section may indicate equal rate of syndeposition or passive faulting. Vertical thickness variations of *Heterostegina texana* to *Discorbis gravelli* strata, however, are related to active sedimentation that may be associated with salt movement, associated faulting and slumping.

The west faults (Figure 33) signify extensive thickening of the Late Oligocene strata (*Marginulina vaginata* to *Heterostegina texana*) in the fault block c and as compared to the other parts of the dome, which may indicate active salt withdrawal from this locality. The absence of thickening in the Early Miocene section in this locality, however, suggests a post withdrawal stage in the locality.

### 3.2.5 Appendices

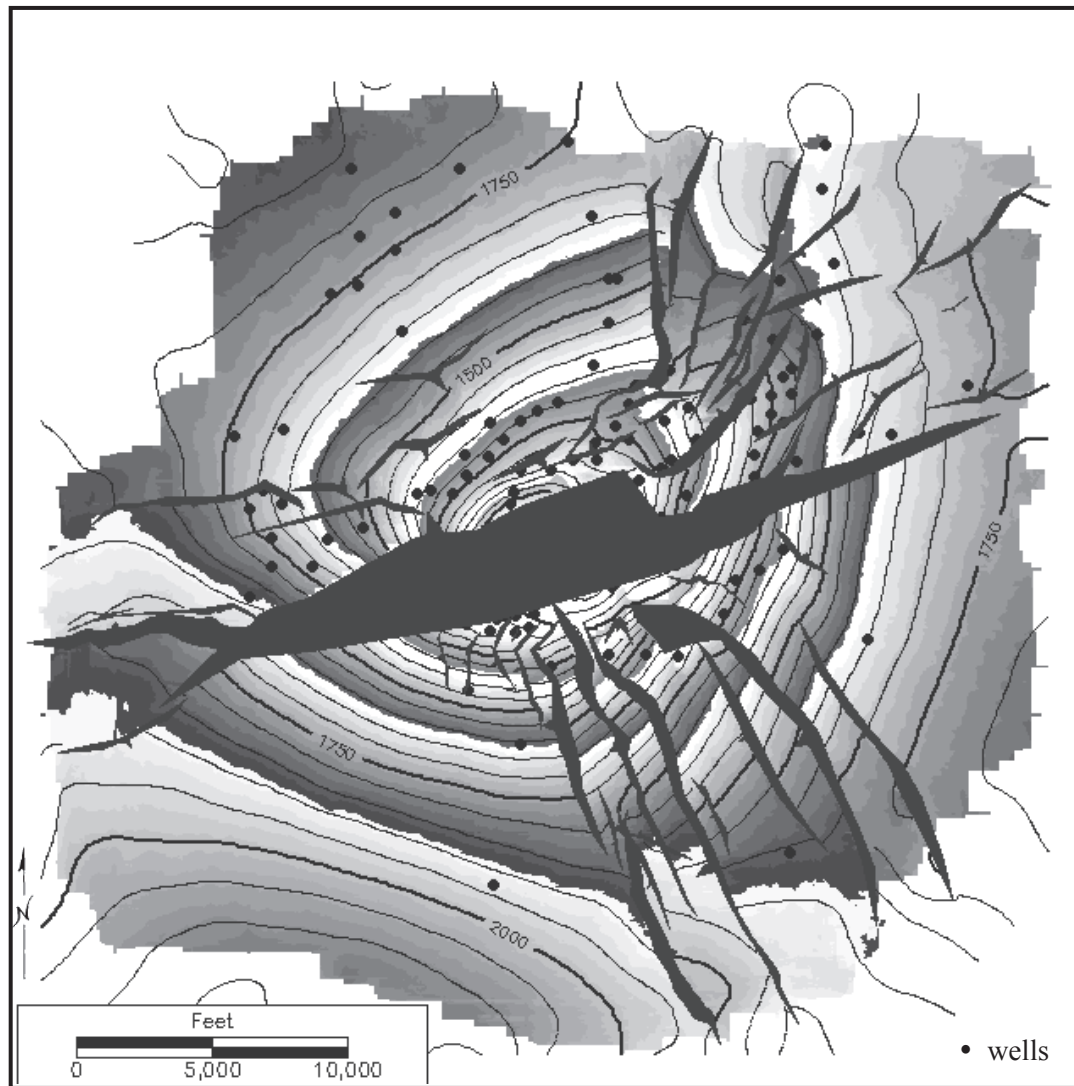


Figure A1a: Time-structure map of *Siphonina davisi* horizon at Vinton Dome

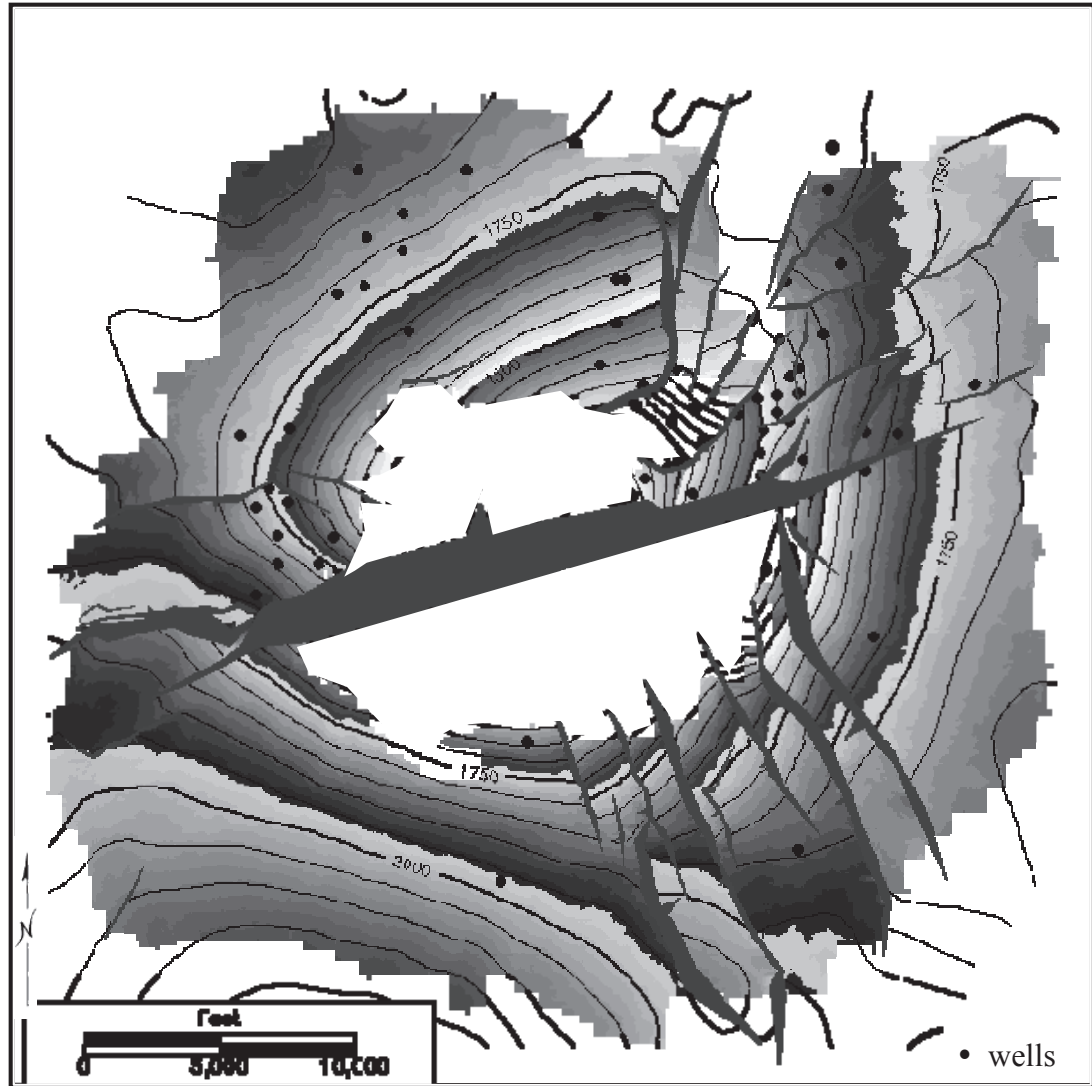


Figure A1b: Time-structure map of Top Anahuac horizon at Vinton Dome

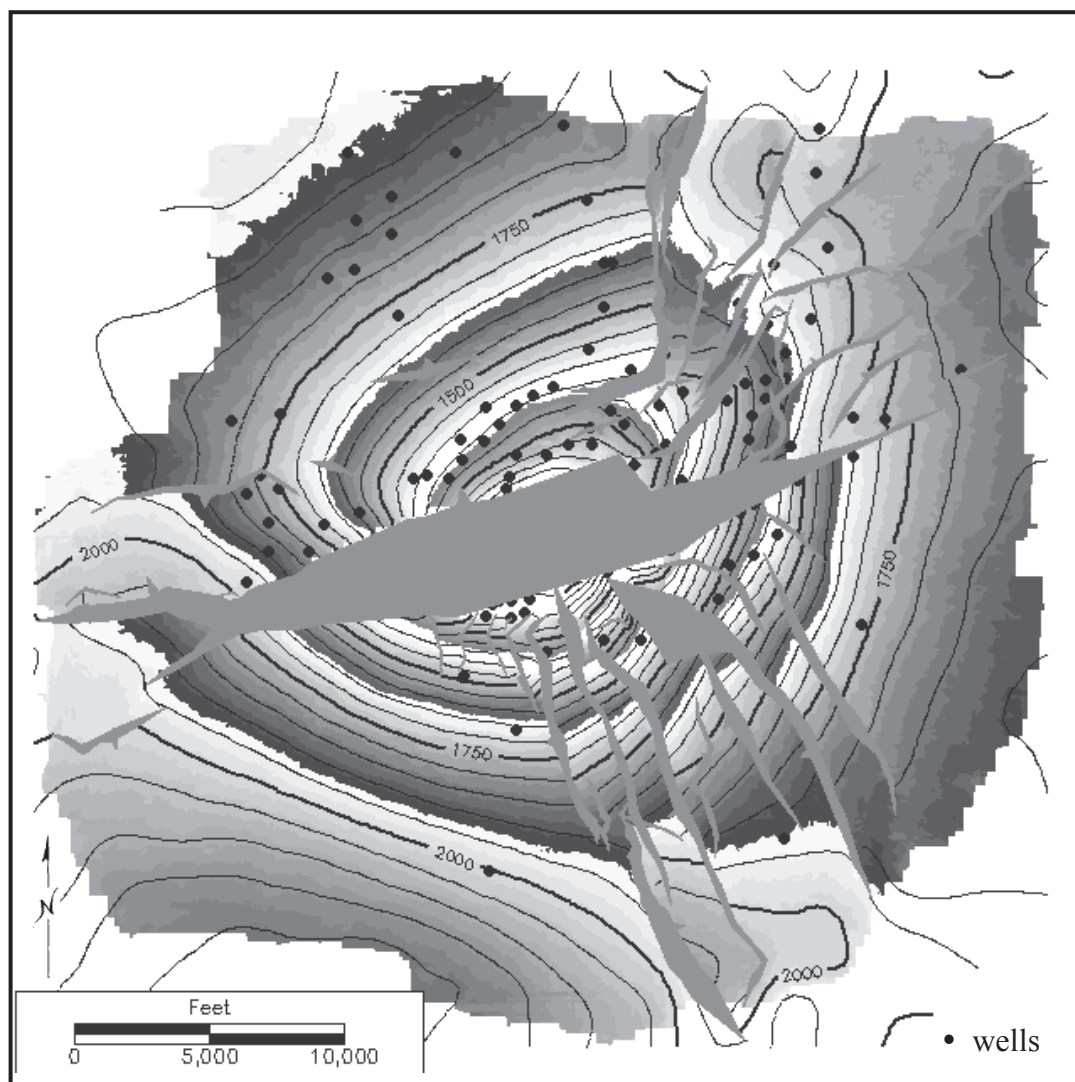


Figure A1c: Time-structure map of *Heterostegina texana* horizon at Vinton Dome

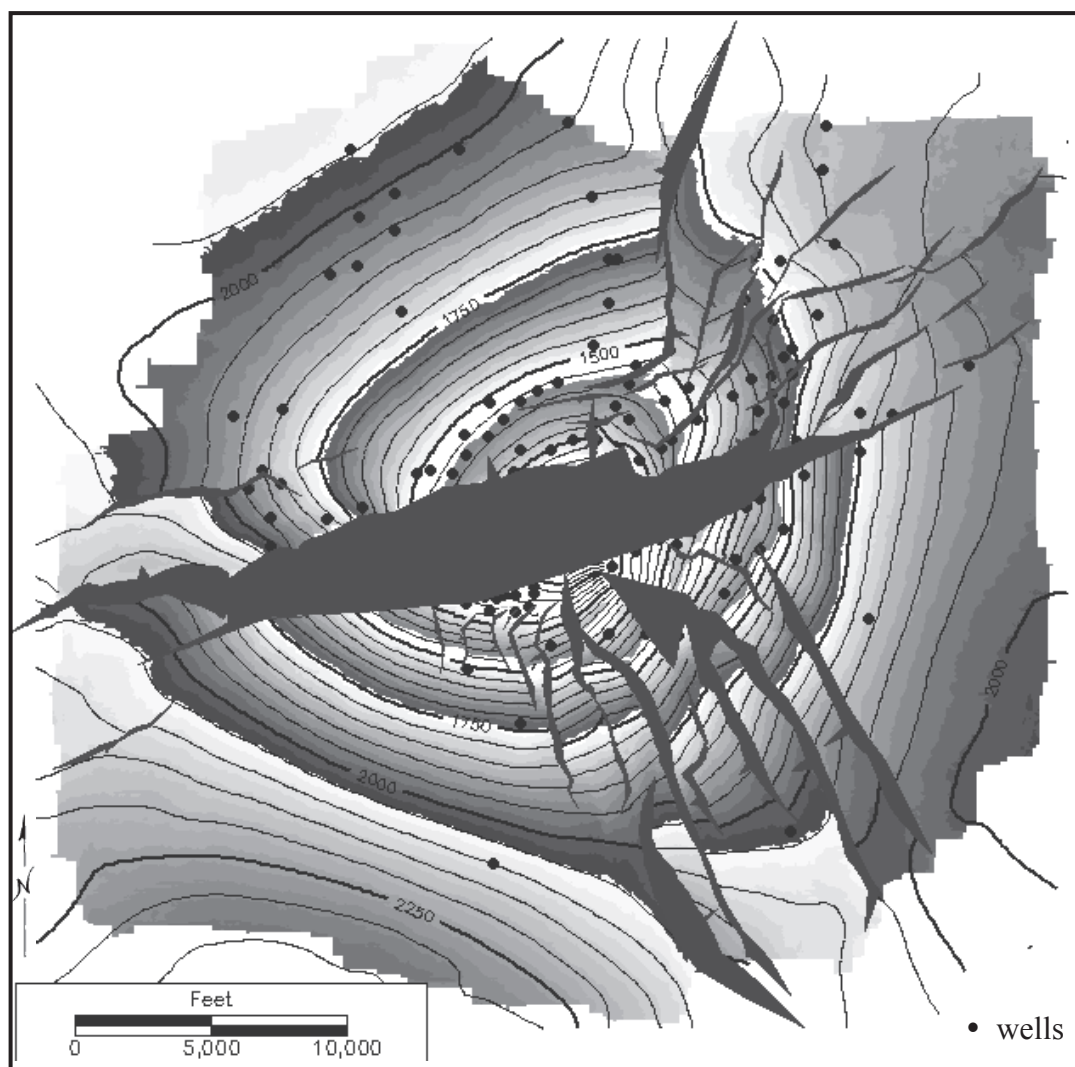


Figure A1d: Time-structure map of *Maginulina vaginata* horizon at Vinton Dome

## CHAPTER FOUR

### INTEGRATED INTERPRETATION

#### 4.1 APPLIED BIOSTRATIGRAPHY

Biostratigraphic data for this project as presented by independent biostratigraphers' archives and operating companies were very limited in the Lower Miocene in the Vinton Dome area. Only twelve wells have foraminiferal planktic and benthic data that include the *Marginulina vaginata*, *Bolivina perca*, *Heterostegina texana*, *Discorbis gravelli* and *Siphonina davisii* in the Oligocene and Miocene sections of the Vinton Dome area. No calcareous nannoplanktic data were available. The scarcity of biostratigraphic data could be due to the strategic paleogeographic position of the Vinton Dome during the Early Miocene or because data has been kept confidential. The Vinton Dome area in the Early Miocene lay in the shallow water environments between the channel belt and the deltaic environment of the ancient Calcasieu River (Galloway, 2000), which could have led to a relatively low probability of preservation of marine fossils in the area and the resultant few picks (Figures 11 - 15). High resolution marine biostratigraphy therefore, may be unattainable in a highly dynamic setting, such as a channel belt on the Miocene shelf.

There are no available records of spore and pollen data. A combination of forams, spores and pollens could have been more diagnostic in the biostratigraphy of the Early Miocene. Lack of spore and pollen data may be due to confidentiality, or because the data were not obtained at the time the wells were drilled, perhaps also



because the resolution of such data were not considered useful and not needed for age-dating the Cenozoic era. Resolution of such data is poor in the Cenozoic era, during which there was high risk of redeposition, especially in the deltaic regions with mud and salt diapirism (Breard, 1996).

Biostratigraphic study of data from Vinton Dome indicates that the Aquitanian alone in the Lower Miocene has few marine fossil records, suggesting that it is the only stage in the Lower Miocene that sustained marine fossil preservation. The overlying Burdigalian and other upper stages in the Miocene record periods of major progradation of fluvial deposits onto the area and have no marine biostratigraphic record. Marine fossil records in the Vinton Dome area are more profuse below the Miocene section.

Due to the absence of high resolution biostratigraphic data, data analysis guided by the Minerals Management Service Biostratigraphic Chart (Witrock *et al.*, 2003) (Figure 7) could only enable the placement of the Aquitanian within the Lower Miocene rock sequences in the previously established Gulf of Mexico 3<sup>rd</sup> order sequence stratigraphic framework (Haq *et al.*, 1988; Fillon *et al.*, 1999; and Zeng & Hentz, 2004). However, interpretation and correlation of logs have enabled interpretation of depositional environments of the Aquitanian on the shelf in the study area.



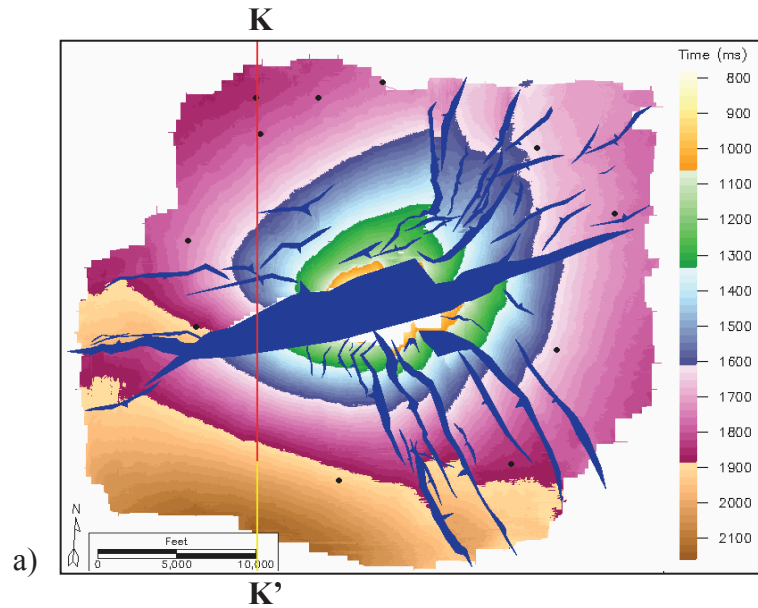


Figure 47a: Basemap showing crossline position of seismic profile of interpreted horizons with integrated biostratigraphic data.

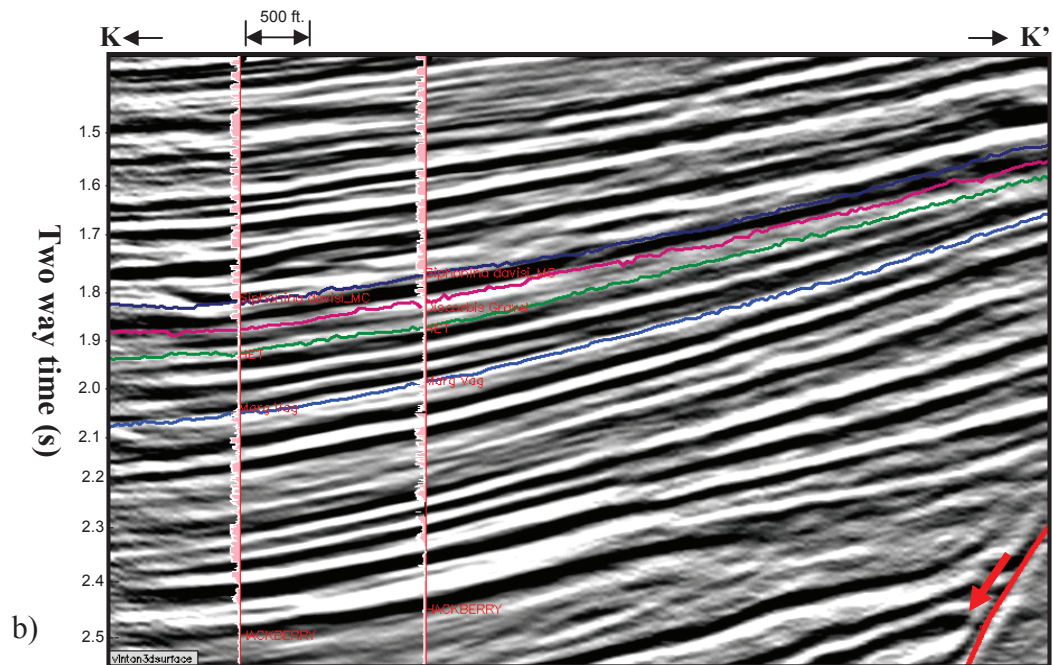


Figure 47b: Seismic section in N-S direction showing interpreted horizons and correlation between well log curves and markers. From upper to lower horizons are *Siphonina davisi*, *Discorbis gravelli*, *Heterostegina texana*, and *Marginulina vaginata*.

The top of the Aquitanian in the Lower Miocene of the Vinton Dome area is recognized by the *Siphonina davisi* zone (Haq *et al.*, 1988; Styzen, 1996; Lawless *et al.*, 1997; & Witrock *et al.*, 2003), and the base by the *Discorbis gravelli* zone, the topmost Oligocene faunal pick that is closest to the base of Miocene (Figures 6 & 7). Four horizons were mapped for the purpose of understanding the evolution of the Aquitanian formation and they included the *Marginulina vaginata*, *Heterostegina texana*, *Discorbis gravelli*, and *Siphonina davisi* zones (Figure 47).

*Heterostegina texana* and *Discorbis gravelli* are fossils that mark the Top Oligocene in the Oligocene-Miocene transitional section and both have served as a control for the base of the Aquitanian in the integration of seismic and well data. The basal Miocene is not an obviously defined section; therefore, the *Discorbis gravelli*, which is the closest fossil to the top of the long Anahuac shale column, has been used to mark the base of the Miocene (Trevino *et al.*, 2003; Witrock *et al.*, 2003). The *Robulus* “A” species, the topmost fossils in Upper Oligocene are not present in the Vinton data and also have been identified as less stratigraphically useful taxa (Breard *et al.*, 1996) (Figure 7).

*Heterostegina texana* has also been recognized by some researchers as a Top Anahuac shale fossil (Ye *et al.*, 1995; Fillon & Lawless, 1999; 2000; Galloway, 2001). However, *Discorbis gravelli* marks the uppermost 3<sup>rd</sup> order sequence within the Anahuac 2<sup>nd</sup> order sequence (Breard *et al.*, 1993; Lawless *et al.*, 1997; Witrock *et al.*, 2003). It is a period of transgression and maximum flooding surface and a correlatable surface in my study area. It terminates away from the salt plug and

therefore, is not well represented in the Vinton dome area. *Heterostegina texana* marks a maximum flooding sequence and a period of carbonate buildup in the Late Oligocene. It is a highly correlatable surface and well represented throughout the study area. *Siphonina davis* marks a period of transgression and a maximum flooding surface on the LM2 depositional episode (Witrock *et al.*, 2003) (Figure 7). It is a relatively correlatable surface of the Lower Miocene 3<sup>rd</sup> order sequences.

Analysis of the biostratigraphic data and their environmental preferences, guided by Breard *et al.* (1993) showed that the Early Miocene strata in the Vinton Dome area were laid down in the inner neritic to middle neritic zones (Figures 6, 7& 10).

Understanding biostratigraphic limitations in dynamic areas such as the Vinton Dome can be very useful in enabling correct spatial placement of rock sequences that contributes to accurate geologic interpretations since stratigraphic correlations depend enormously on biostratigraphic applications for local and regional subdivisions of rock units. Limits in biostratigraphic applications can exist in some wells and may be controlled if they are well understood. Where erroneous reading, such as data mishandling, in fossil depth is suspected, log correlation via log signatures may be employed to facilitate the inference of depositional surfaces and bodies. Correlation between wells in seismic data based on biostratigraphic picks may be challenging for reasons that include the following:

- Due to severe faulting and potential slumping of sediments, redeposition or reworking of faunas from their original environment to deeper zones could contribute a major factor to shifts in biostratigraphic information in well data.
- Picks are facies or environment dependent; however, paleoecologic study has shown that due to migration or evolution, some fossils species show preference to shallower or deeper depths than their counterparts and examples are *Planulina* and *Siphonina* of the Late Eocene and Early Oligocene (Berggren and Miller, 1989; Breard *et al.*, 2003).
- Drilled sandstone cuttings are sampled every 30 to 60 ft meaning that depths are averaged and may lower biostratigraphic data resolution.
- Drilling effects that result in caving up or downfalling of cuttings into boreholes may result in erroneous reading of pick depths which will also lower biostratigraphic data resolution.
- Methods of collecting and analyzing samples.

## 4.2 LOG INTERPRETATION

Twelve wells in my study section have biostratigraphic data and each faunal pick is found in one or at most two wells. Considering the haphazard nature of the faunal data, I correlated the well logs and established stratigraphic surfaces using log signature characters, while simultaneously referencing the faunal picks for appropriate intervals. Biostratigraphic data were integrated with the well data by identifying depths of faunal picks on logs. Lithology and sedimentary character were determined from electric logs and used to identify and correlate a series of previously established maximum flooding surfaces (MFS) surfaces (Fillon *et al.*, 1997; Lawless *et al.*, 1997), such as *Marginulina vaginata*, *Heterostegina texana*, *Discorbis gravelli*, and *Siphonina davisi*. From these, parasequences and the stacking patterns of parasequence sets were established and used to determine the depositional setting of the Aquitanian strata.

First, I prepared a correlation type log for the Lower Miocene (Figure 48) which has a complete stratigraphic section for the Lower Miocene strata in the Vinton Dome area and integrated biostratigraphic data. It shows the most complete unfaulted interval of sediments representative of the thickest and deepest sedimentary section in the field.

The wells with biostratigraphic data, allowed stratigraphic units to be defined and correlated among other wells, and were tied to the seismic data. Seismically defined surfaces were also identified in the wells and correlation was established with other wells. SP logs were correlated using the 'Billard ball' type correlation

(Tearpock & Bischke, 1991), providing a means of closed loop correlation whereby the correlation begins and ends with the same well (Figures 49 & 50).

Shale sections, representing condensed sections, were used for electric log correlation. Closely-spaced well correlations were evaluated to improve the accuracy of the log interpretation, help differentiate between fault cuts and stratigraphic variations, and improve the estimate of the size and depth of identified fault cuts.

The SP logs give a distinctive spiky signature at the limey *Heterostegina texana* (HET) zone that is useful in correlation. The *Siphonina davis* zone is typically a thick shale that overlies stacked sandstones strata underlain by the Anahuac shale column. The *Discorbis gravelli* zone is recognized by the point of change in stacking pattern between the Late Oligocene retrogradationally stacked parasequences to the Early Miocene progradationally stacked parasequences. It is interpreted as the uppermost MFS between the HET and the Lower Miocene stacked sandstone units, which conforms to the previously established maximum flooding surface (Fillon *et al.*, 1997).

Below the *Marginulina vaginata* MFS zone, in the lower Upper Oligocene, is approximately 1400 ft (426.72 m) interval of sandstones, with 50 ft to 300 ft (15.24 m to 91.44 m) thick individual coarsening upward parasequences that are progradationally stacked and bounded by marine flooding surfaces. The lower Upper Oligocene interval is interpreted as consisting of deltaic sandstones, and the 300 ft (91.44 m) sandstone bodies show clinoforms in the associated seismic data.

Variations of fining-upward facies exist within the same interval, in some wells in the northeast parts of the dome, and are interpreted as fluvial facies that suggest fluvial input from the northeast parts to the dome (Figure 49 – wells 4 & 5). The topmost part of this interval is shown in the cross-sections; however, no detailed correlation was attempted in this lower Upper Oligocene interval.

Above the *Marginulina vaginata* section, are approximately 500 ft (152.4 m) of mudstones and siltstones identified by a “railroad track” SP log signature. The outer to inner neritic fossils in well data within the interval suggests marine or shelf deposits. These mudstones and siltstones are overlain by the limey *Heterostegina texana* zone, a carbonate zone representing the maximum flooding section in the middle Late Oligocene (Breard *et al.*, 1994; Galloway *et al.*, 2000). Approximately, six parasequences were correlated around the dome in the *Marginulina vaginata* and *Heterostegina texana* interval. Each parasequence averages 75 ft (22.86 m), except in the northeast, where there is thinning of parasequences ranging between 25 ft (7.62 m) and 50 ft (15.24 m). Parasequences show funnel-shaped SP log pattern and are stacked as coarsening upward retrogradational parasequences, bounded by marine flooding surfaces.

Above the *Heterostegina texana* zone, are approximately 300 ft (91.44 m) of additional mudstones and siltstones indicated by “railroad track” SP log signature that are terminated by much more coarser sediments in the Early Miocene, and gradationally marked by the Aquitanian coarsening-upward shoreline sandstones (Figures 49 & 50). Inner neritic fossils in well data within the interval suggest

marine, shelf, or prodelta mudstones and siltstones. Three parasequences are correlated around the dome in the *Heterostegina texana* and *Discorbis gravelli* interval. Each parasequence averages 100 ft (30.5 m) and also shows funnel-shaped SP log patterns. They are coarsening upward and retrogradationally stacked parasequences, bounded by marine flooding surfaces. The top of these parasequences is tied to a maximum flooding surface, referred to as the Top Anahuac Shale, and marked by the *Discorbis gravelli* zone.

The Aquitanian section exhibits 2 to 3 coarsening upward progradational parasequences, each ranging between 50 ft (15.24 m) to 100 ft (30.48 m) and bounded by marine flooding surfaces (Figure 49). The sandstones are separated from each other by 20 to 40 ft (6.1 to 12.2 m) thick proximal shale. They individually range from 20 to 150 ft (6.1 to 45.7 m) thick and are thickest in the northwest and southeast corner of the dome (Figure 49). I labeled the sandstone units that are below the shale as the Lower Aquitanian sandstones and the sandstone units above the shale as the Upper Aquitanian sandstones. There are no biostratigraphic data to help differentiate between the LM1 and LM2 depositional episodes but the separating proximal shale suggests that the two episodes correspond respectively to the Lower and Upper Aquitanian shoreline deposits.

The Upper and Lower Aquitanian sandstones consist of shoreline facies and presence of stacked, upward-fining fluvial deposits in the northern edge of the dome (Figures 49 & 50). Well 2 (Figure 50) depicts a 60 ft (18.3 m) channel deposit sharply truncating another channel deposit, leaving a remnant of 40 ft (12.2 m) of the



older channel deposit, and both have incised the Aquitanian shoreline deposits indicating that they are younger than the Aquitanian sandstones. I interpret these as “incised” channels that were rejuvenated as a result of sudden increase in discharge, a major avulsion, or sea level fall (Olariu & Bhattacharya, 2006). The base of the stacked channels directly overlies the Early Miocene prodelta, shelfal, or marine mudstones and siltstones. This sudden change in vertical facies succession suggests a basinward shift in facies that was perhaps due to a forced regression (Figure 49).

A local unconformity is interpreted below a 150 ft (45.7 m) sharp-based fining-upward fluvial package overlying distal marine mudstones that is associated with the graben in the southeast part of the dome. The extent of the unconformity can only be correlated to the south, southwest, west and northwest parts of the dome where valley fills overlay, or incised the proximal shale that divides the Upper Aquitanian from the Lower Aquitanian sandstones (Figure 49). However, the Upper and Lower Aquitanian sandstones have both been incised in the south whereas the Lower Aquitanian sandstones are preserved in the west and northwest, indicating that the unconformity (Figure 49 - wells 7 to 11) is younger than the Lower and Upper Aquitanian sandstones.

Thinning of the Upper Oligocene strata is associated with the salt body and several units appear to onlap toward the center of the dome (Figure 50). Relatively, constant stratal thickness is observed in the Aquitanian, except at the center of the dome, where there is onlap of the strata against the salt body.

In the north - south longitudinal cross-section across the dome, well 8 shows only 25 ft (7.62 m) of a top-eroded shoreline Lower Aquitanian sandstone that can be correlated in nearby northern wells whereas, the proximal shale that separates the Upper and Lower Aquitanian sandstones, and the Upper Aquitanian sandstone units are not present and are presumed to have been eroded off. The absence of faults in this section of the well, the presence of a nearby unconformity, and a thick fluvial unit in the next southern well suggest a by-pass zone with deposition to the south or a ravinement surface (Figure 50).

Approximately 50 ft (15.24 m) of *Siphonina davis* shale drapes the Aquitanian sandstones throughout the entire dome suggesting that the unconformity was tectonically-influenced in the Early Miocene and may have resulted from increased sediment supply and salt withdrawal processes (Figure 49 - wells 7, 8, 9, 10, and 11).

Lateral well facies variations around the dome show that the Aquitanian consists of deltaic sandstones in the northwest, north and northeast parts of the dome which have been eroded by younger fluvial or valley-fill facies in the north, east, southeast, southwest and west parts of the dome (Figures 49 & 50).

Blocky, sharp-based channel-like log signatures above the *Siphonina davis* shale indicate predominantly fluvial deposits in the Burdigalian section.

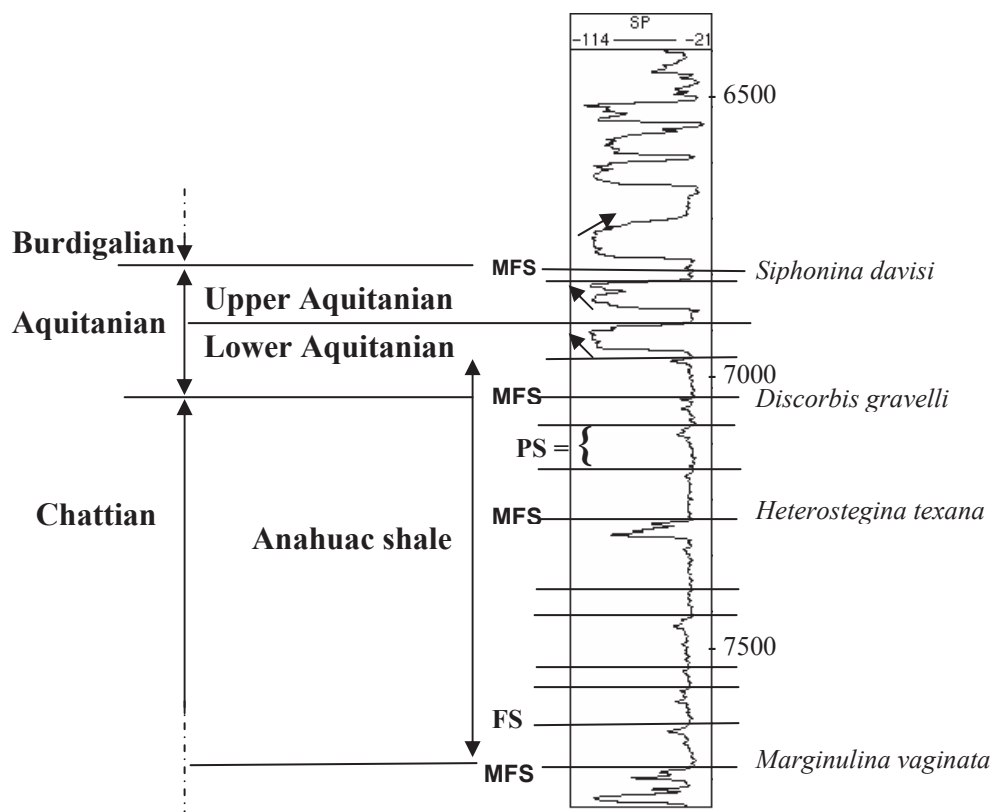


Figure 48: A Type log of Upper Oligocene to Lower Miocene, Vinton Dome. Interval PS = Parasequence; FS = Flood surface; Depth in feet.

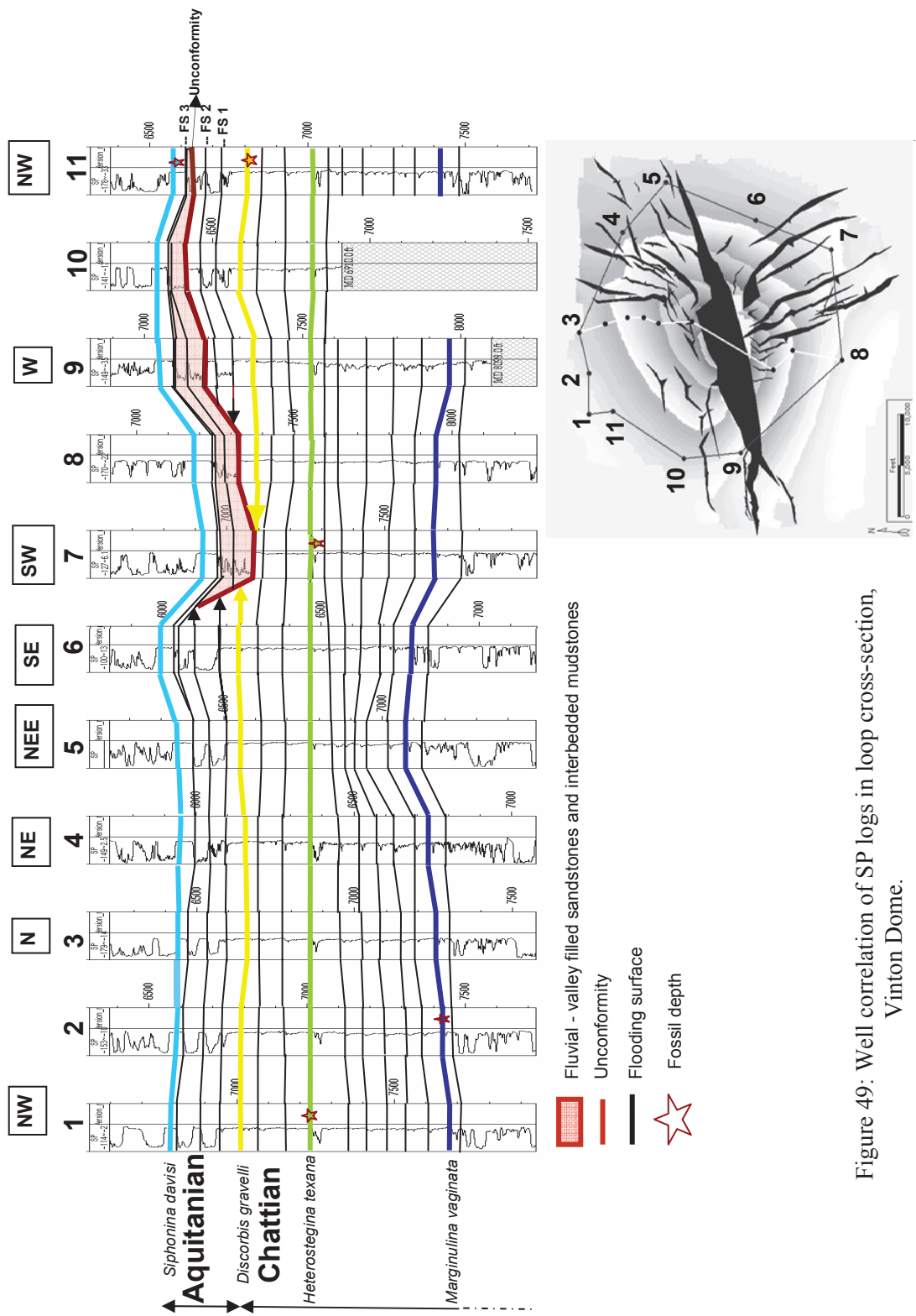


Figure 49: Well correlation of SP logs in loop cross-section, Vinton Dome.

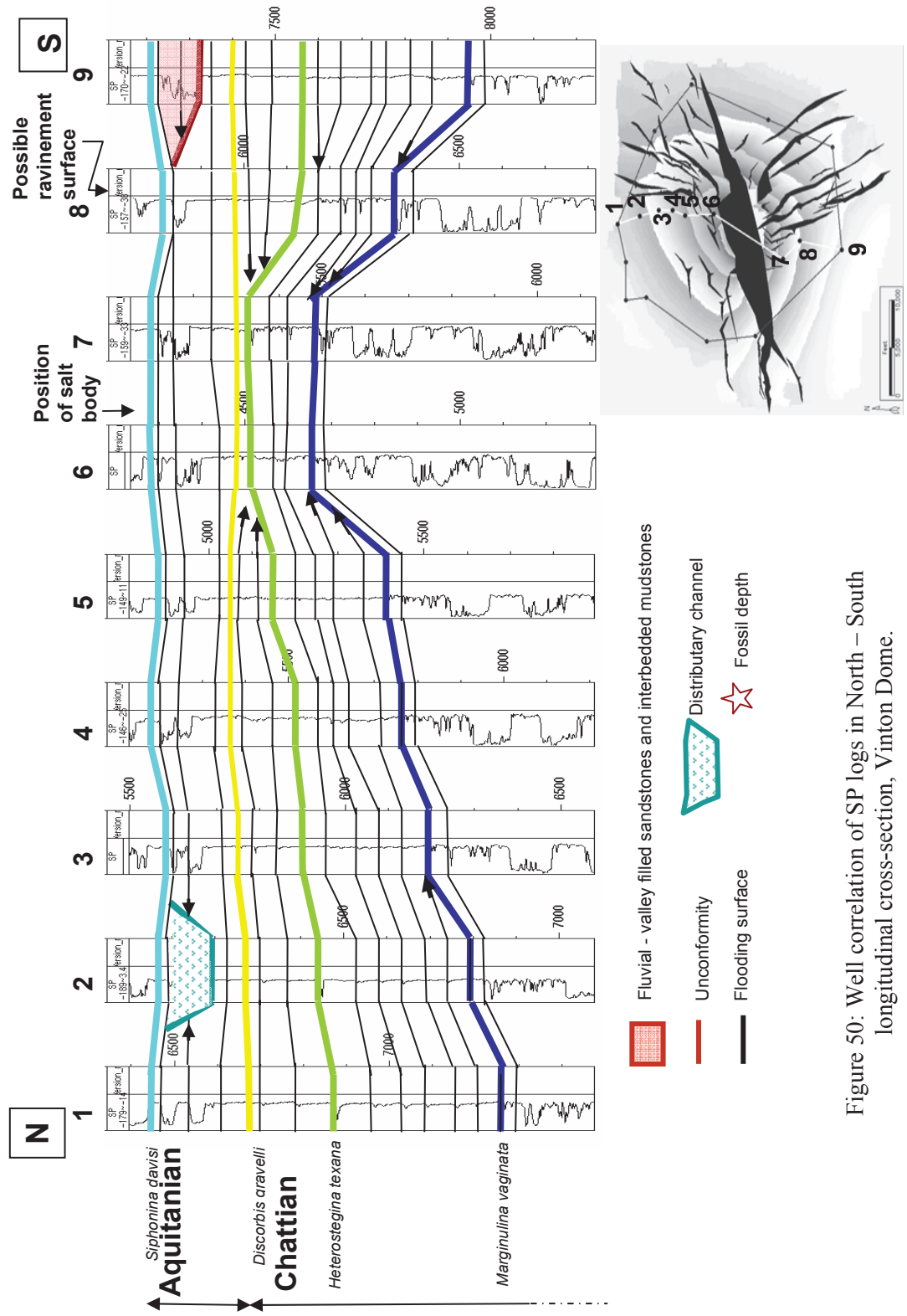


Figure 50: Well correlation of SP logs in North – South longitudinal cross-section, Vinton Dome.

Fluvial facies dominate the northwest and the south of the dome and are mostly overlying the Aquitanian deltaic facies whereas, the deltaic facies dominate only the northern part of the dome. Using well data control, an incised valley is drawn representing most of the northwest and the south of the dome (Figure 51).

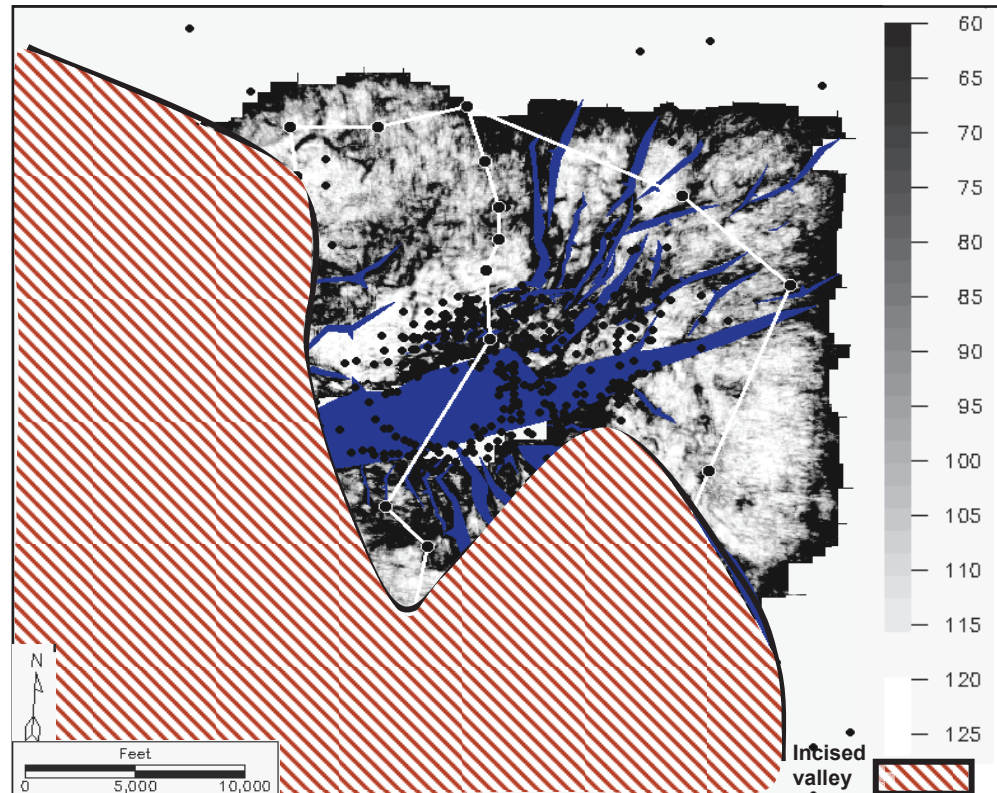


Figure 51: Basemap showing the position of the Aquitanian incised valley based on well control.

### 4.3 SEQUENCE STRATIGRAPHY

Well data interpretation and integration with seismic data provided some assistance in mapping the Aquitanian stage, which show two parallel reflections that delineate its top and base. The Aquitanian stage consists of two previously established 3<sup>rd</sup> order maximum flooding surfaces (MFS), marked by *Lenticulina jeffersonensis* and *Siphonina davisi*. These are inner to outer neritic fossils, thereby placing the Vinton Dome area on the Miocene shelf. Integration of biostratigraphic and log data with the seismic data has allowed the delineation of the *Siphonina davisi* surface, while the *Lenticulina jeffersonensis* surface is not identified suggesting that it is merged or eroded in the seismic profile. The top of the *Discorbis gravelli* MFS, however serves as the base of the Aquitanian.

Seismic facies of higher order sequences often have low vertical resolution that may be due to low accommodation that is characteristic of shelf, where younger tracts generally invade into older ones, thereby offering thin and tight-packages (Zeng & Hentz, 2004). Higher order systems tracts then become irresolvable in seismic profiles, and at best show as 3<sup>rd</sup> order composite seismic responses with indistinct 4<sup>th</sup> order top, base, and internal reflections. Robust seismic facies such as clinoforms, downlaps, onlaps, and toplaps that usually characterize slope environments are absent in the Aquitanian section, except onlap of strata toward the salt body. Moreover, seismic tools that offer additional information for analyzing depositional systems such as reflection amplitude and coherence have limited success in higher resolution sequence stratigraphy (Zeng & Hentz, 2004). In the

light of limitations presented by seismic resolution, well log cross-section provided the highest resolution and the best tool in the sequence stratigraphic evaluation of the area.

#### **4.3.1 Sequence Stratigraphic Analysis by Well Logs**

Analyses were executed by applying the following basic methods for log and sequence stratigraphic evaluation. Sequence boundaries represent points on the SP logs, within coarsening upward sequences, which separate the highstand systems tracts from the lowstand systems tracts, and are identified in the neritic zones as abrupt shallowing or abrupt basinward shift in facies, for example, the base of a blocky sand log signature. Transgressive surfaces are represented by the first significant flooding surface that separates parasequences. Maximum flooding surfaces represent the major condensed sections that typically mark the top of the transgressive systems units, and often include the distal highstand systems tract. They are correlatable surfaces that separate fining upward transgressive systems tracts from the coarsening upward highstand systems tracts. A maximum flooding surface is identified as the shaliest point on the SP log where the fining upward pattern changes to a coarsening upward pattern (Figures 49 & 50).

Stacking patterns of parasequences have been used to define parasequence sets, which in turn define system tracts (Wagoner *et al.*, 1990). Previously established 3<sup>rd</sup> order maximum flooding surfaces (MFS) permits the recognition of highstand systems tract below the *Marginulina vaginata* MFS, shown as clinoforms



(Figures 49, 50 & 52). Each of the clinoforms is 50 ft (15.24 m) to 300 ft (91.44 m) thick, with an average of 80 ft (24.38 m) indicating that the Vinton Dome area had been a deltaic environment. Thick deltaic and fluvial sandstones were observed in logs throughout the area, but the progradational clinoforms are observed only in the southwestern part of the dome.

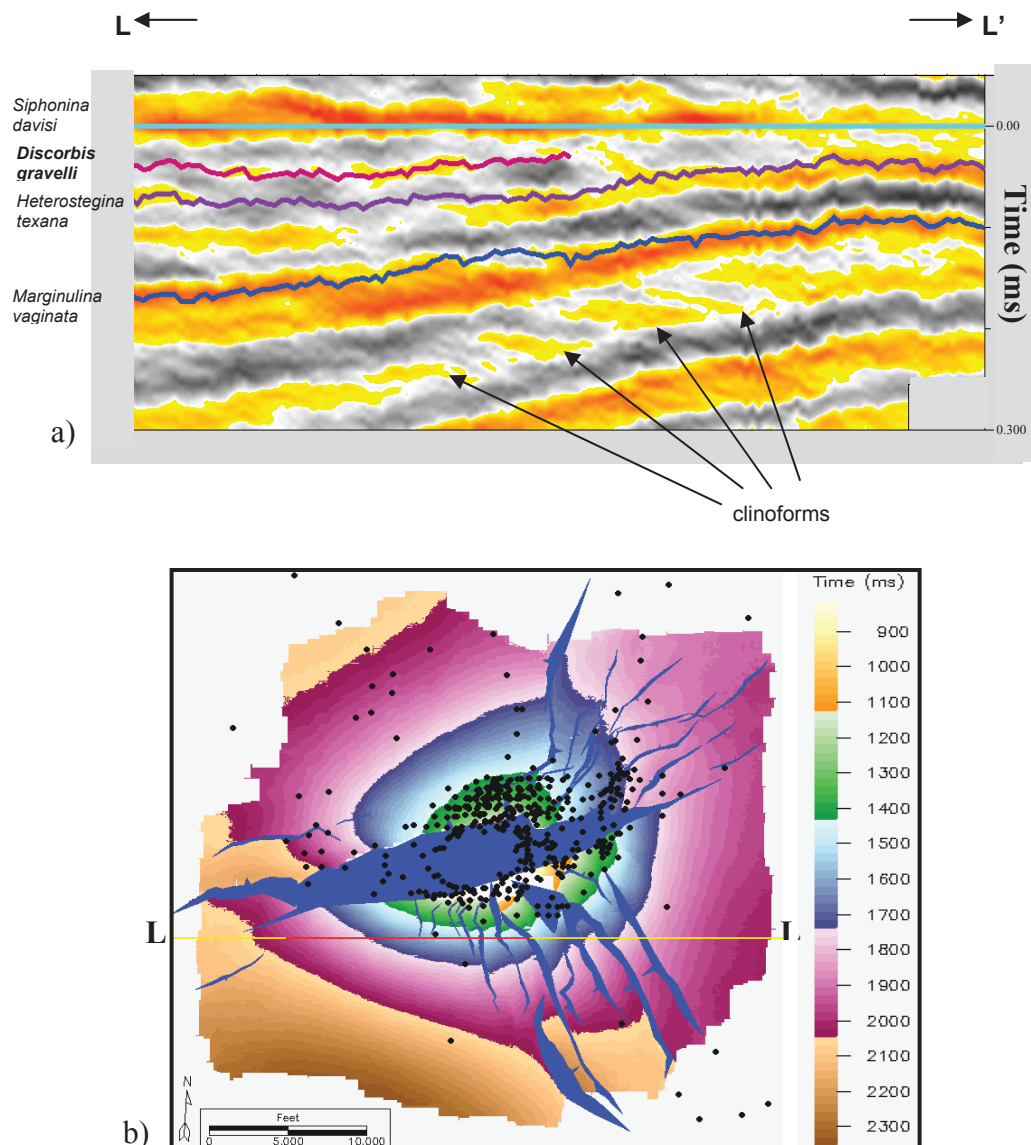


Figure 52: a) Seismic profile and b) basemap showing clinoforms below the *Marginulina vaginata* strata and evidence of progradation in the southwest area, Vinton Dome.

Above the *Marginulina vaginata* MFS, there is a major unconformity, recognized by onlap of reflections from beneath the *Heterostegina texana* strata to *Siphonina davisii* strata, against an immediate older reflection in the south of the dome (Figure 53).

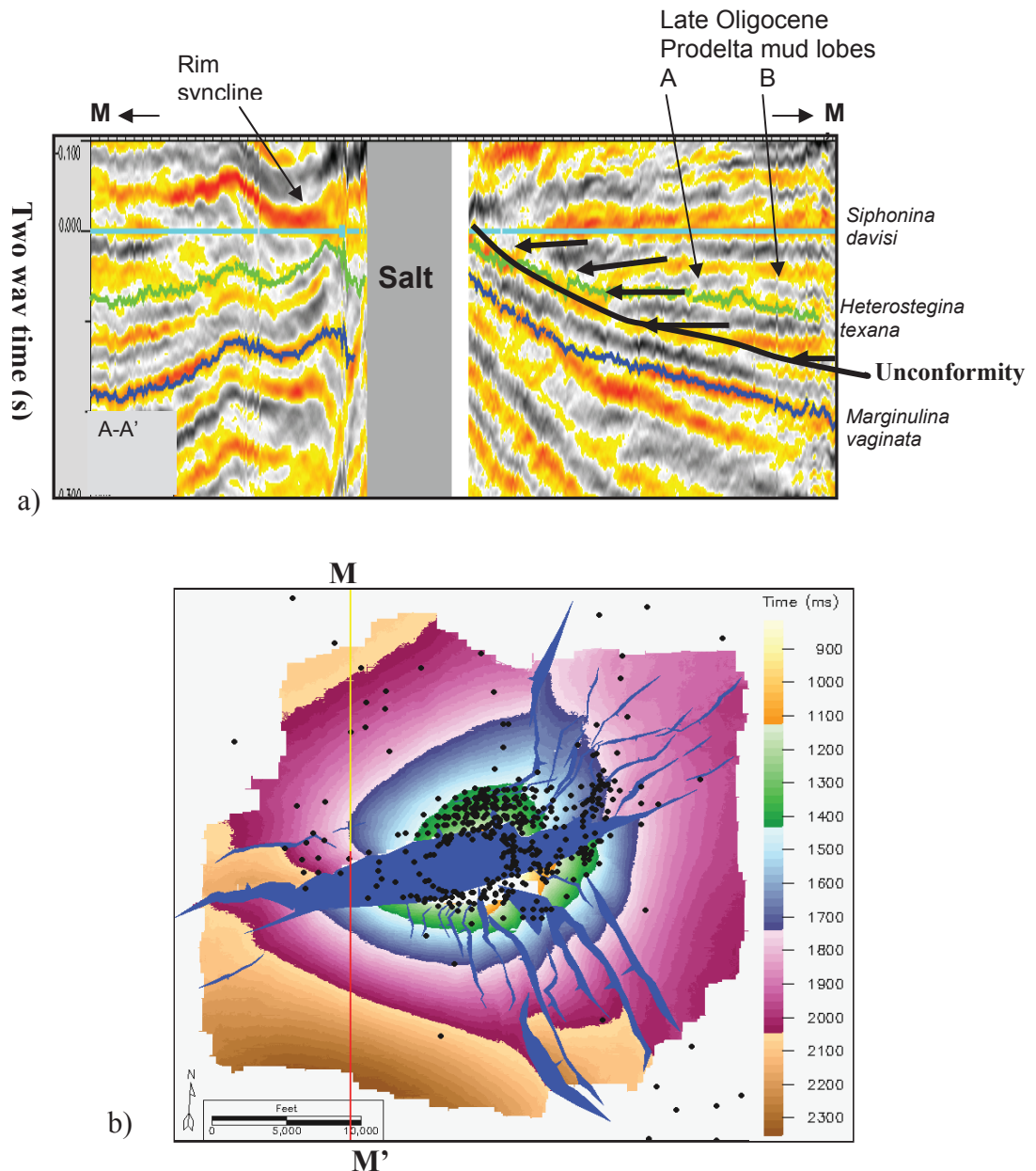


Figure 53 a & b: a) Seismic profile and b) basemap; showing the unconformity and onlap of the Late Oligocene to Early Miocene strata. Red line indicates position of seismic profile.

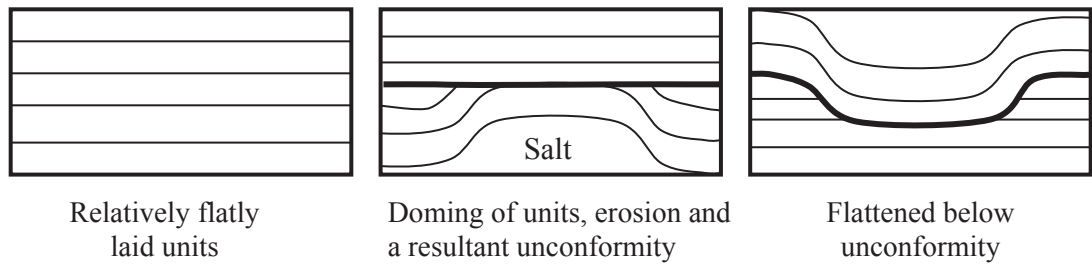
The unconformity does not satisfy the criteria for sequence boundary since it can only be locally defined (Wagoner *et al.*, 1990). This unconformity is perhaps related to salt withdrawal processes and may have been tectonically impacted.

The transgressive systems tracts above the *Marginulina vaginata* MFS are represented in my dataset, as retrogradational parasequence sets below the transgressive parasequence sets of the *Heterostegina texana* to *Discorbis gravelli* interval (Figures 49 & 50). However, aggradational and progradational parasequence sets of shelf deposits may co-exist with the retrogradational parasequence sets at the same depth as a result of erosion after sea level falls (Zeng & Hentz, 2004). At the south of the dome, a 45 ms interval bearing buried prodelta turbidites within the *Heterostegina texana* and *Discorbis gravelli* MFS surfaces may represent a thin phase of a highstand or lowstand sequence above the *Heterostegina texana* MFS zone.

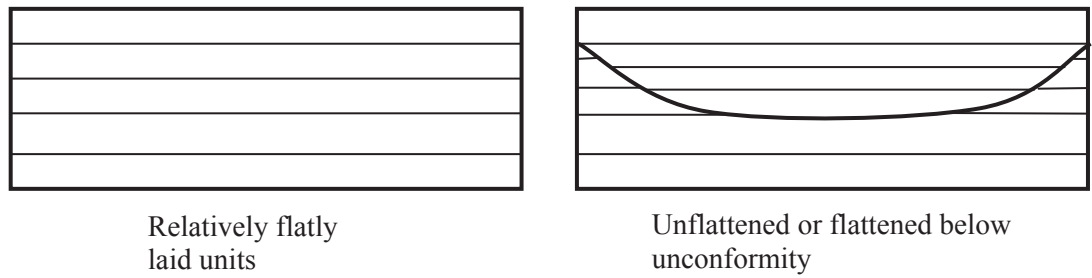
The Early Miocene has been characterized as a period of substantial evolution in sediment dispersal in the northern Gulf of Mexico (Edwards, 1994; Fillon & Lawless, 1999; 2000; Galloway *et al.*, 2000), and high sediment influx is expected to the top of the Anahuac shale. The prograding parasequences of the Aquitanian shoreline deposits, therefore, represents the highstand systems tract that was deposited on top of the *Discorbis gravelli* MFS. An abrupt change and basinward shift in facies is recognized locally in some wells between the Anahuac shale and the Aquitanian sandstones indicating a relative sea level fall (Figure 49, wells 1 & 5; Figure 50). Lack of evidence for subaerial exposure and erosional

truncation suggests that there are no incised valleys in the Oligocene - Miocene interface. Rather, the abrupt seaward translated marine, shelfal, or prodelta facies in the Oligocene to the Lower Miocene shoreline facies, suggests that there was a eustatically-induced forced regression that may indicate a sequence boundary in the Oligocene – Miocene interface (Posamentier *et al.*, 1990; 1992; Posamentier & Allen, 1999; & Soria *et al.*, 2003). This is in accordance with the lowermost Miocene sequence, previously reported as deposits of a second order eustatic sea level fall (Fillon & Lawless, 2000) (Figure 3).

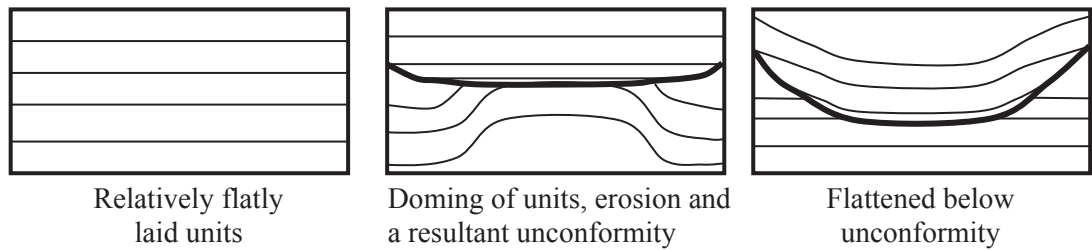
The *Siphonina davis* sequence, however, has been reported as deposits within the second order relative sea level rise in the Lower Miocene supersequence (Figure 4). The prograding to aggrading shoreline deposits of the Upper Aquitanian sandstones may have indicated imprints of the relative sea level rise and a resultant normal regression pattern, as a result of high sediment influx to the basin. Above the Upper Aquitanian sandstones, the presence of an unconformity in the south of the dome, some evidence of sedimentary by-pass that are closely located and more northern to the unconformity, and the draping of the *Siphonina davis* shale suggest that there was a combined eustatically-induced forced regression and a tectonically-induced forced regression that may have been impacted by salt withdrawal-driven subsidence and tectonic uplift of the adjacent area (Figure 54).



(a) Tectonically-impacted



(b) Eustatically-impacted



(c) Combined

Figure 54: Schematic illustration of settings before and after flattening a horizon below a sequence boundary (a) tectonically-impacted scenario in salt dome environments, (b) eustatically-impacted scenario and (c) combination of both tectonically and eustatically-impacted scenario as seen in figure 49. Thick lines represent unconformity.

#### 4.4 SEISMIC INTERPRETATION

The 60 Hz. resolution 3D surface seismic data applied to this study allowed imaging of merged 3<sup>rd</sup> order sequences that represent the Aquitanian, but the higher order sequences are limited by vertical resolution and their seismic responses are therefore unresolved. Instead, log data interpretation aided the identification of the 3<sup>rd</sup> order sequences (Figures 47 & 49). Each of the two 3<sup>rd</sup> order sequences between the Top Anahuac and *Siphonina davisii* range from 25 ft (7.6 m) near salt to 280 ft (85 m) thick at the periphery of dome, and constitute the LM1 and LM2 chronozones (Figure 7). These 3<sup>rd</sup> order sequences have composite seismic response of higher order sequences (Figure 47).

The depositional pattern of the Aquitanian strata is dependent on the structural pattern and salt tectonics. Isochore maps and phantom slices of amplitude maps of the *Marginulina vaginata* to *Heterostegina texana* strata show evidence of equal thickness with a ring pattern of deposition around the peripheries of the dome that suggests syndeposition with the growth of the salt dome (Figures 55-58). Onlap of strata towards the dome suggests a period of active salt movement (Figures 55 and 56). The uneven distribution of the strata makes distinct correlation of depositional bodies exceedingly difficult. Thickening of the strata at the hangingwall of the master fault and thinning at the footwall is evidence that the salt was seated at the footwall of the fault in the Late Oligocene, which suggests salt creep from the downthrown block to the upthrown block of the fault (Figures 59 and 60). In the Early Miocene, thickening or thinning of strata in the hangingwall is masked by the

absence of the Top Anahuac strata at the salt flank. However, thinning observed at the hangingwall may be due to the displacement of more salt bodies as more sediments are deposited at the northern part of the dome.



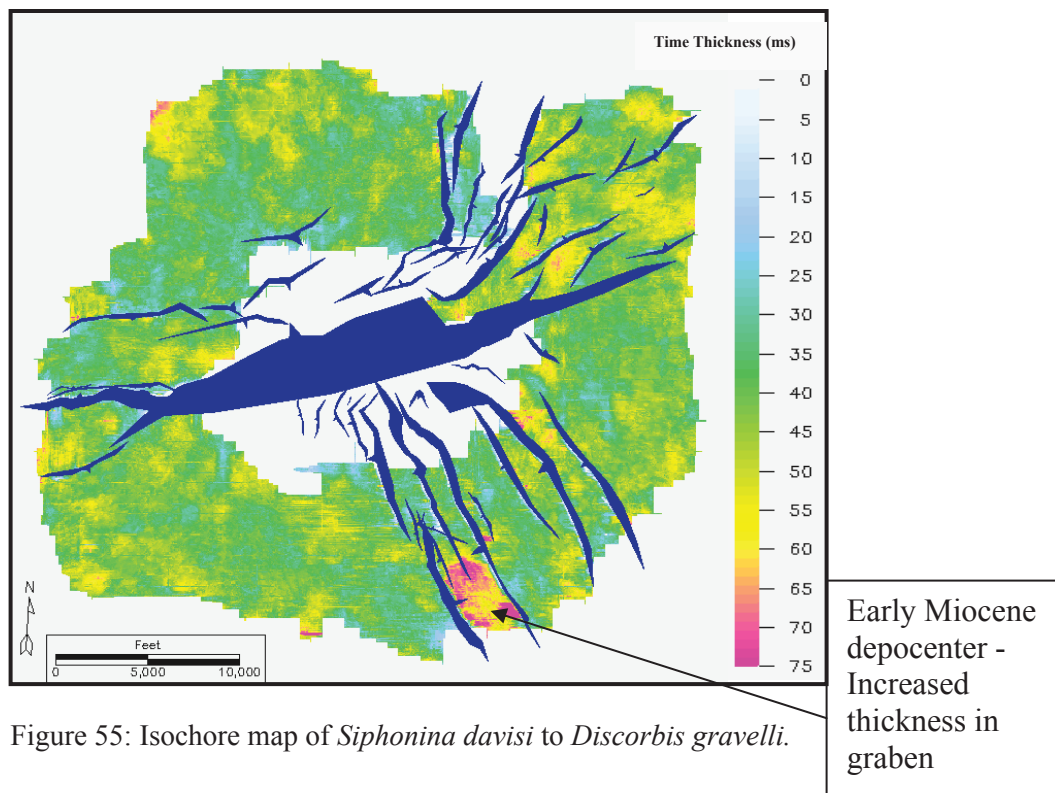


Figure 55: Isochore map of *Siphonina davisi* to *Discorbis gravelli*.

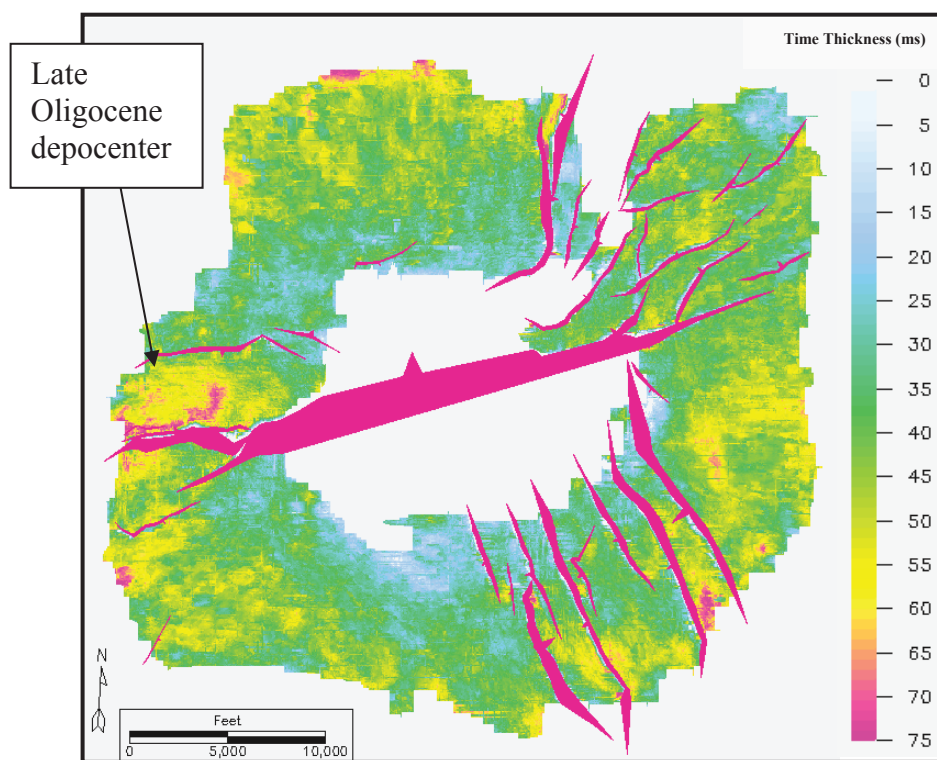


Figure 56: Isochore map of *Discorbis gravelli* to *Heterostegina texana*.

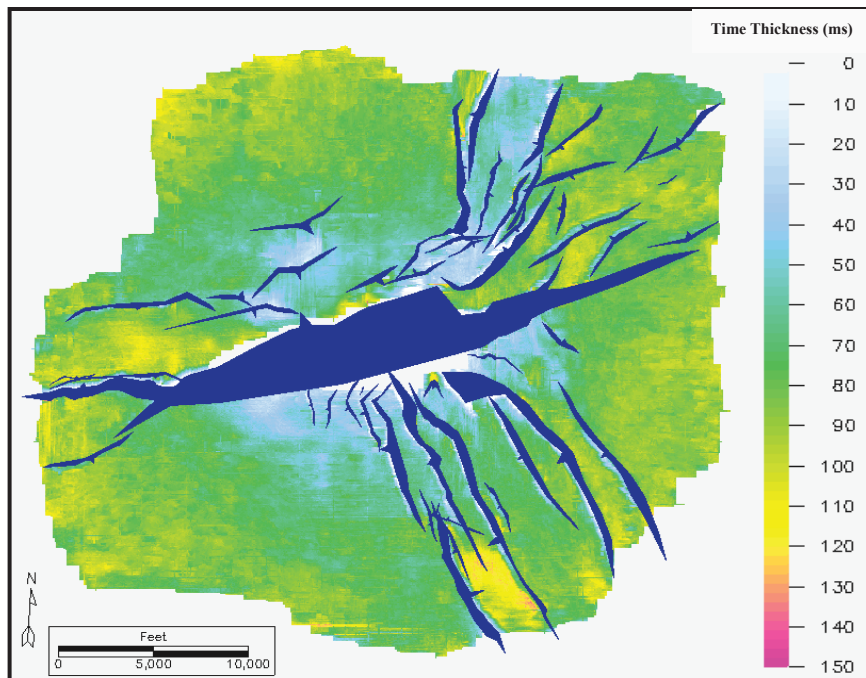


Figure 57: Isochore map of *Siphonina davisi* to *Heterostegina texana*.

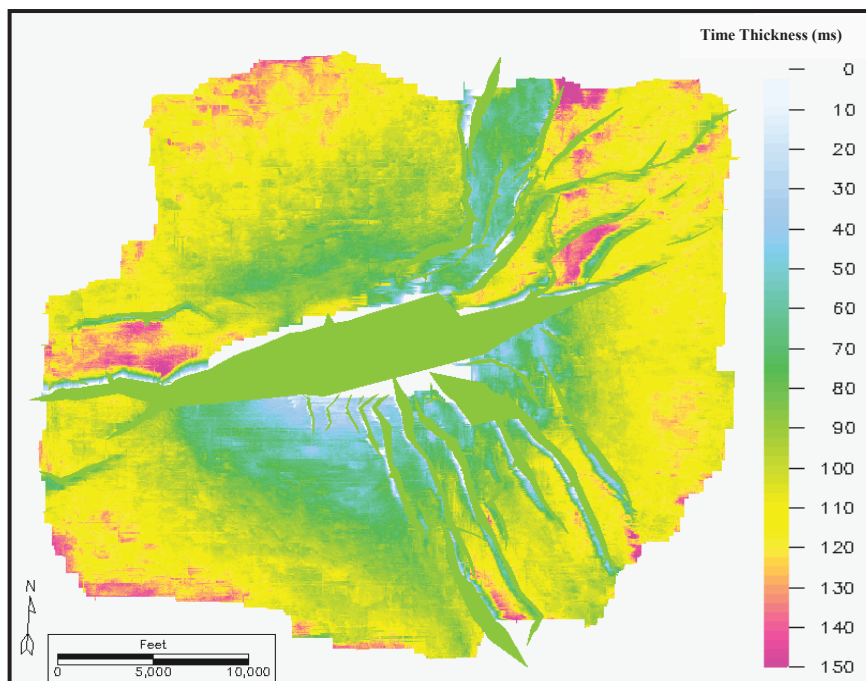


Figure 58: Isochore map of *Heterostegina texana* to *Marginulina vaginata*.

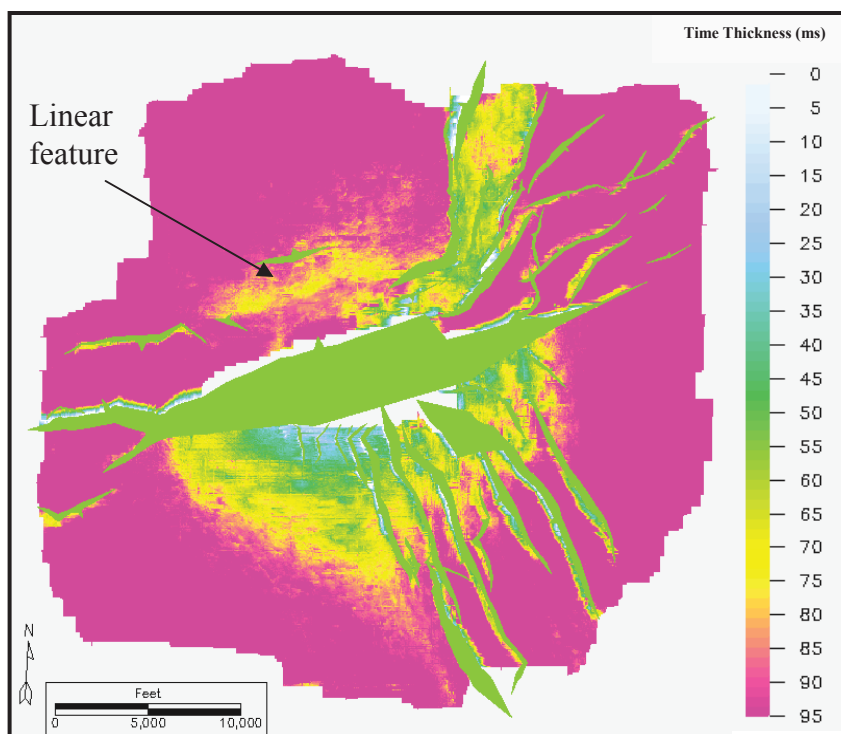


Figure 59: Isochore map of *Heterostegina texana* to *Marginulina vaginata*, focusing on salt position. Linear feature is due to thinning as a result of turtle structure anticline.

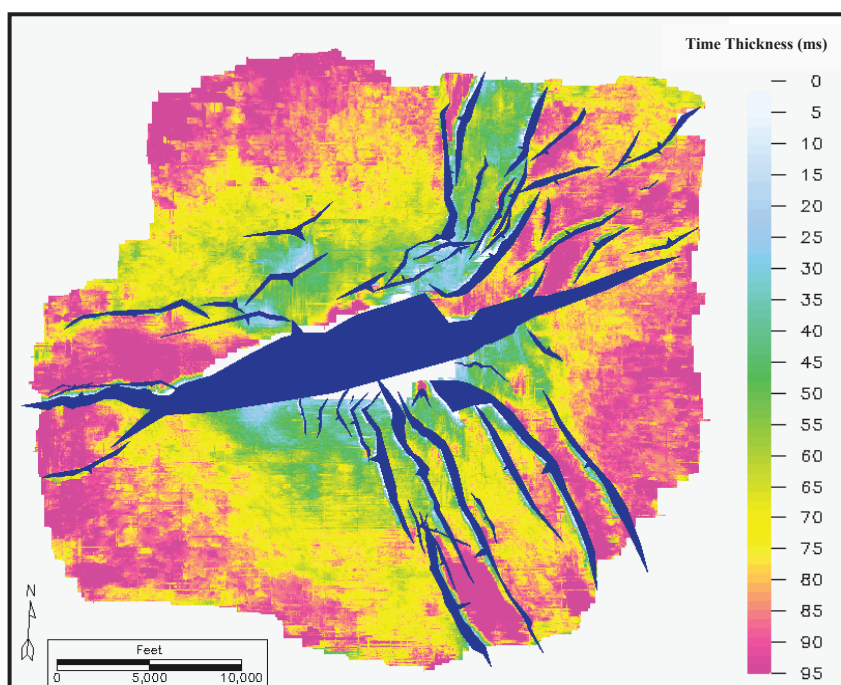


Figure 60: Isochore map of *Siphonina davisi* to *Heterostegina texana*, focusing on salt position.

A linear feature that strikes parallel to the master fault at the north of the dome reveals the thinning of the Late Oligocene strata near the salt body as a result of the effect of the turtle structure anticline (Figures 27 & 58). There is no observable fault in the vicinity of the linear feature on the seismic section and the negative and positive curvatures did not image such a linear feature as a fault. The syncline thus created by the adjacent anticline may have formed a collection area for sediments downfalling as a result of the upward movement of the salt body. The Late Oligocene *Marginulina vaginata* to *Discorbis gravelli* strata, as revealed by well logs, are mainly mudstones and siltstones. Considering that the northern part of the dome is a hangingwall of a major fault, relative movement of the fault block may likely have caused deformation structures such as the curvy features present in the axis of the rim syncline (Figures 61 & 62). The curvy features could easily be misinterpreted as fluvial bodies, but abundant well data in the area show that these are within thick prodelta to shelf mudstones and could not be fluvial features.

Coherence maps revealed shale deformation features in the southwest and south of the dome (Figures 63 - 68). The outer neritic *Heterostegina texana* to *Discorbis gravelli* section contains channel-like features and their associated lobe-shaped features that were not intersected by many wells. They occur in an interval of approximately 45 ms and some of the channel belts are up to 3500ft (1 km) wide and 165 ft (50 m). Each of the lobes average 3 km wide, meaning they are above the tuning thickness and are part of the siltstones and mudstones of the Upper Oligocene section. They are coherent, stratigraphically confined between the *Heterostegina*



*texana* and *Discorbis gravelli* surfaces, uncorrelated to faults, and sinusoidal in shape ((Figures 66 & 67). They have been revealed by seismic data and coherence maps; however, they are not observable in time slices. Since the closest well log to these lobes has characterized the Late Oligocene strata as mudstones and siltstones (Figure 49 – well 8) and the fossils have classified the environment as an inner to outer neritic zone, I interpret the features as prodelta subaqueous turbidites (Bhattacharya & Walker, 1992; Pattison, 2005; Olariu & Bhattacharya, 2006). These features are common in subaqueous prodelta environment as areas of instabilities. Instabilities can be generated by storm events, river flooding, high rates of sedimentation, earthquakes, or salt movement. Large quantities of mud or silt debris along well-defined gullies may be constantly fed from a source area undergoing rotational slumping and subsidence, which may be deposited in a composite depositional area. The complexity of the arrangement of the Late Oligocene southwestern lobes may indicate evidence of numerous slumping of debris, high area of sedimentation, instability and excess pore fluid pressure (Coleman & Prior, 1982). Salt movement in close proximity could have created slope gradient that may have launched these features.

The Late Oligocene isochores (Figures 55 & 56) showed that deposition was more focused to the western side of the dome, whereas, the southeast graben received more sediments in the Early Miocene. The western and southeastern depocenters may have been created as a result of salt evacuation and movement to the center of the dome or away to a nearby salt body. In the Early Miocene, channel

facies that were traced around the dome also revealed stratigraphically confined features at the north of the dome, in the path of the rim syncline. This was a channel that flowed parallel to the strike direction of the master fault. This channel received sediment supply from the feeder channels at the northeast of the dome (Figures 43 & 44) and transported it, perhaps in a confluence, westward and parallel to the master fault. Evidence of this channel in the Early Miocene can be seen on seismic and well data. The channel belt is positioned near the salt body and coherence map of the Aquitanian suggests presence of crevasse splay in the hangingwall of the master fault, which further suggest that the area was in a lower delta plain environment (Figure 67) (Coleman & Prior, 1982). Further southward, toward the salt body, the channel may have meandered or split into distributary channels. Subject to the limit of the survey and the presence of the salt body, evidence of channels in the same vicinity in the southwest part of the dome suggests distributaries of the northern channel.

Evidence of a deltaic environment in the Early Miocene during the *Discorbis gravelli* - *Siphonina davisi* time can only be inferred from the logs. Presence of sandy, upward coarsening units indicates deltaic sands, and bell-shaped, fining-upward log motifs indicate fluvial deposits in the north, northeast, southeast and western parts. In the Aquitanian, the presence of numerous channels in the southwest part and the unconformity in the southeastern part suggest evidence of bypass deposition further seaward during lowstand of sea level (Figures 49, 50, 68 & 69). There are few wells in the south and southwest part of the survey with which to

confirm the information on logs. However, the closest well in the vicinity reveal 150 ft (45.72 m) of fluvial deposits, as a result of the unconformity in the Aquitanian section (Figure 49- well 7). Therefore, I interpret the south and southwest depositional area as a subaqueous delta front. Its accommodation may have been provided by salt withdrawal, further away from the dome, in the southern part of the dome. The channels associated with these depositional lobes did not appear to incise the underlain Oligocene strata (Figures 49, 68, & 69). In the Early Miocene, during the *Discorbis gravelli* - *Siphonina davisii* time, a channel crossed directly from the northeast, over the salt, to the south where it deposited its load into the graben formed by faults G and K (Figures 30 & 34). The graben is the thickest section of the Aquitanian strata.



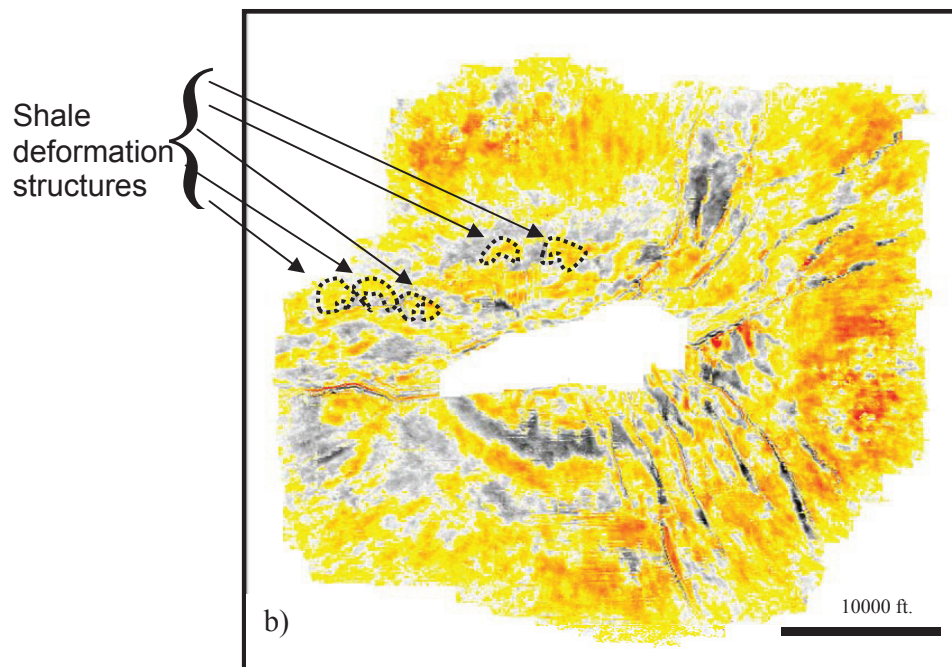
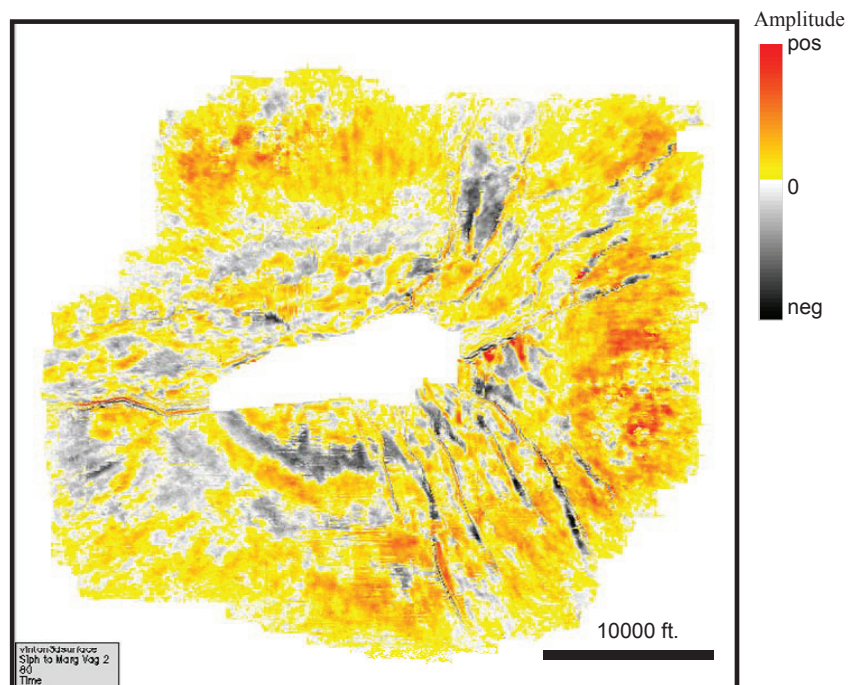


Figure 61: a). Uninterpreted and b). interpreted stratal slices of amplitude map of *Heterostegina texana* – *Discorbis gravelli* section at 80 ms below flattened *Siphonina davis* horizon.

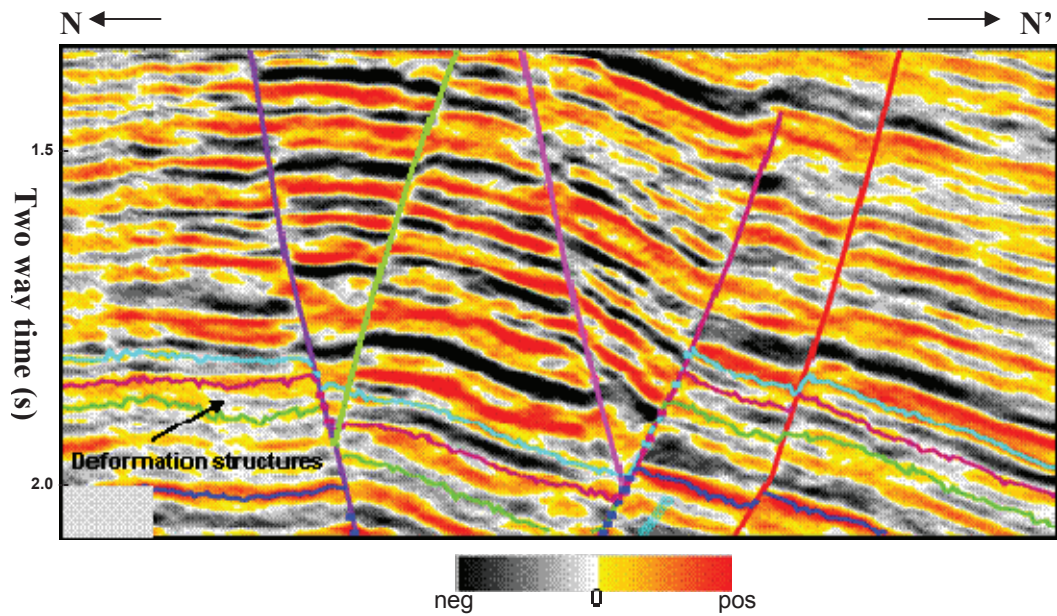


Figure 62 a: Seismic profile showing one of the deformation features along the crossline direction between the Top Anahuac and the Heterostegina texana strata.

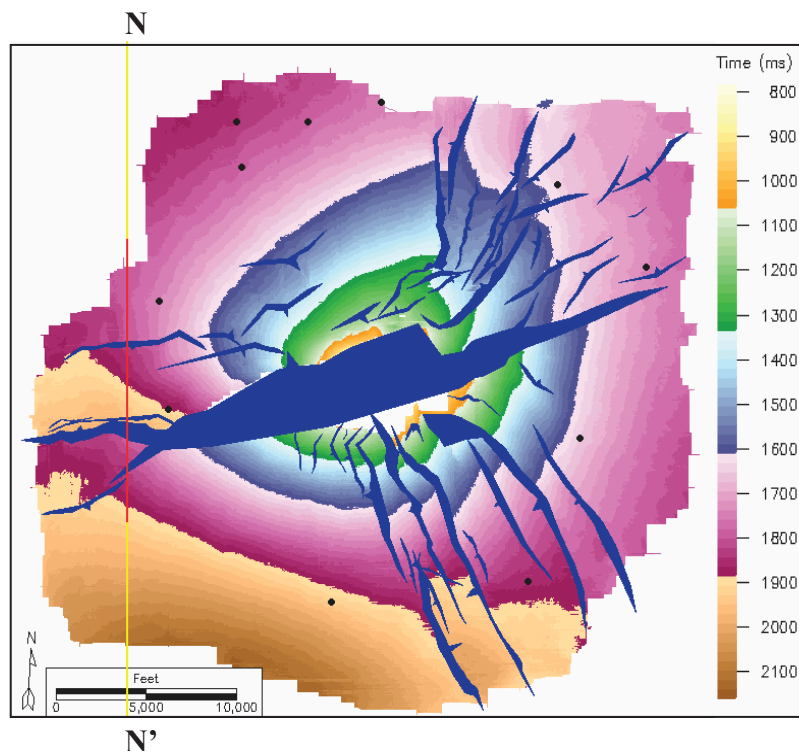


Figure 62 b: Basemap showing crossline profile. Deformation structures are in the rim syncline in the hangingwall of the master fault in the northern part of the dome. Red line indicates the position of the seismic profile.



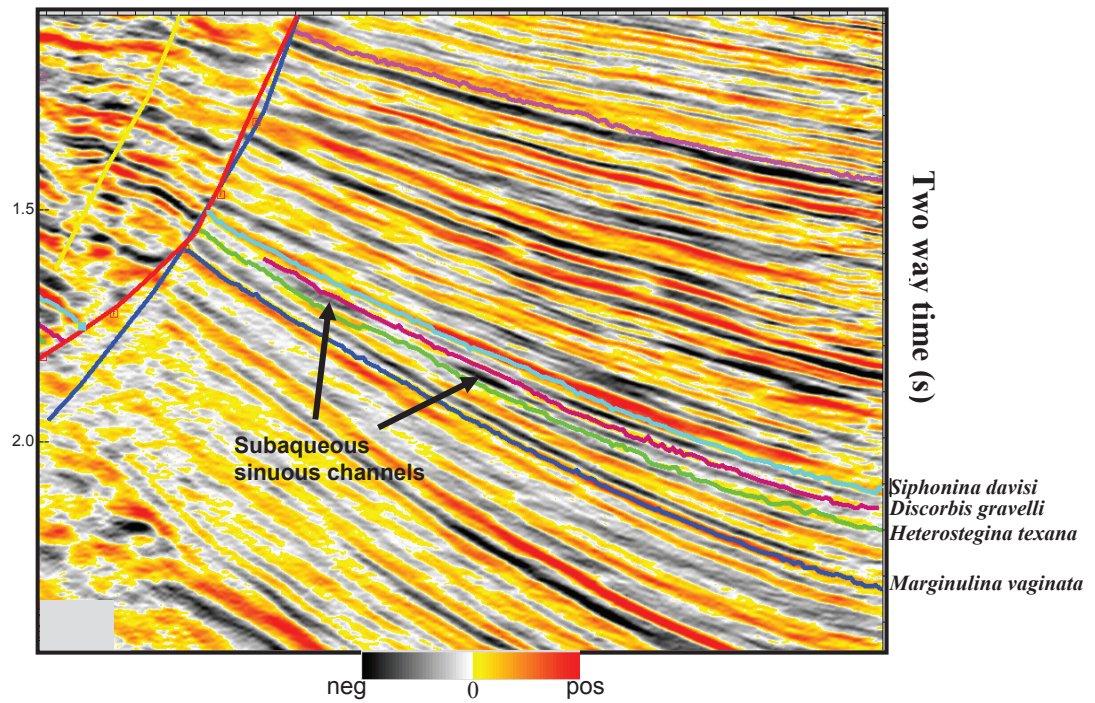


Figure 63 a: Seismic expression of crossline showing the presence of Late Oligocene sinuous subaqueous channels as bird's eyes.

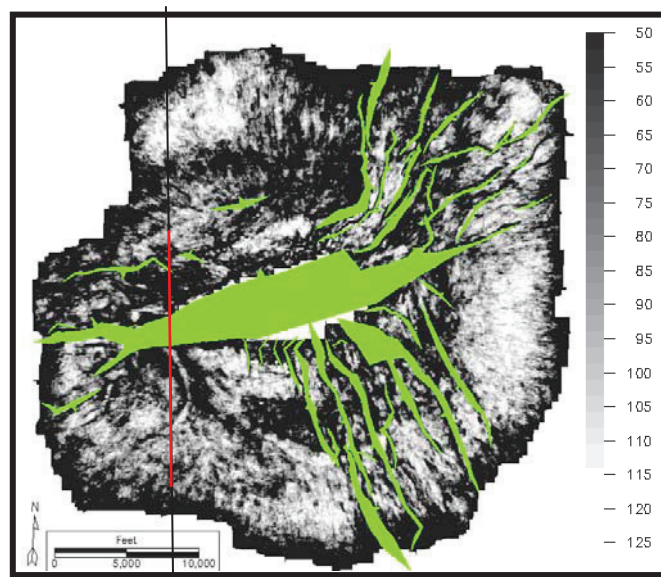


Figure 63 b: Coherence map showing crossline profile on sinuous subaqueous channels. Red line shows position of seismic profile.

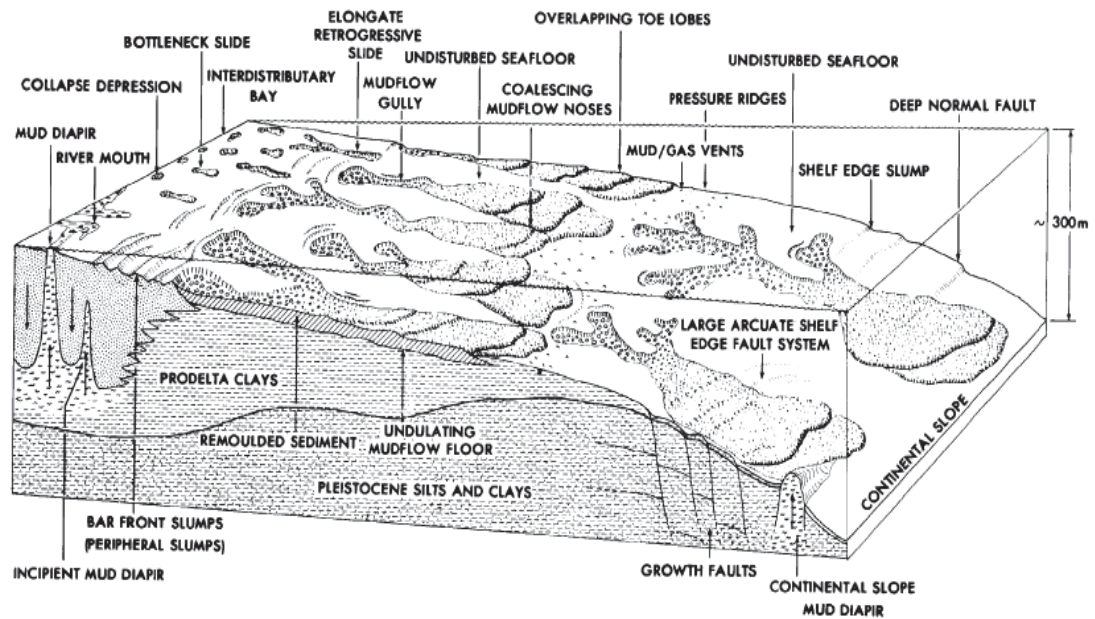


Figure 64: Schematic analog illustration showing subaqueous depositional environment and processes such as major types of submarine landslides, diapirs, and contemporary faults in the Mississippi River delta (Coleman & Prior, 1982).

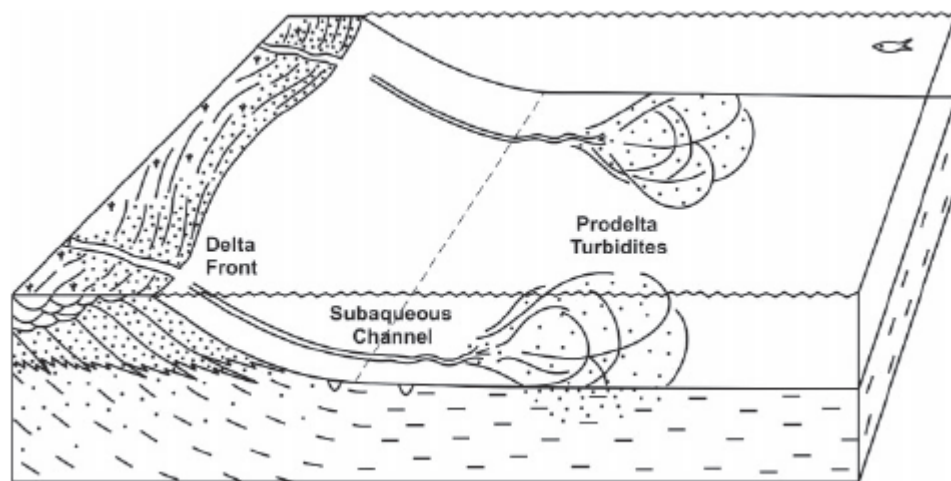


Figure 65: Schematic analog of a three component shoreface to shelf depositional model – Delta front, subaqueous channels and prodelta turbidites (Pattison, 2005).



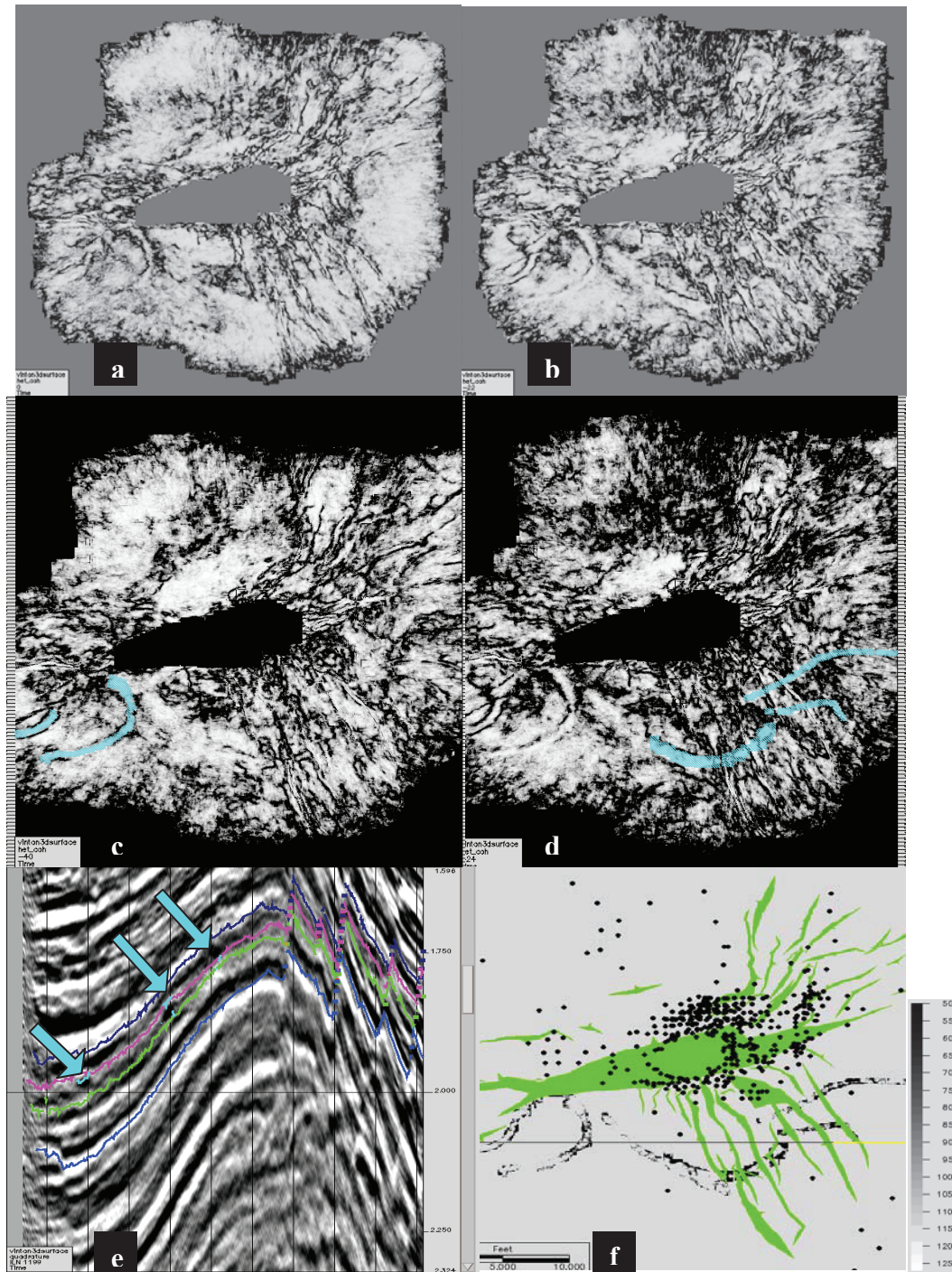


Figure 66: A series of interpretative maps showing sinusoidal (cyan color) and lobe features in the Late Oligocene section, in the southwest and south of the dome. (a) and (b) are uninterpreted while (c) and (d) are interpreted coherence maps. Seismic section (e) displays cyan arrows pointing to the positions of the cyan-colored painted features within the same stratigraphic unit. Basemap (f) shows the overall result of the painted sinusoidal features at different times within the coherence cube, above the flattened *Heterostegina texana* surface.

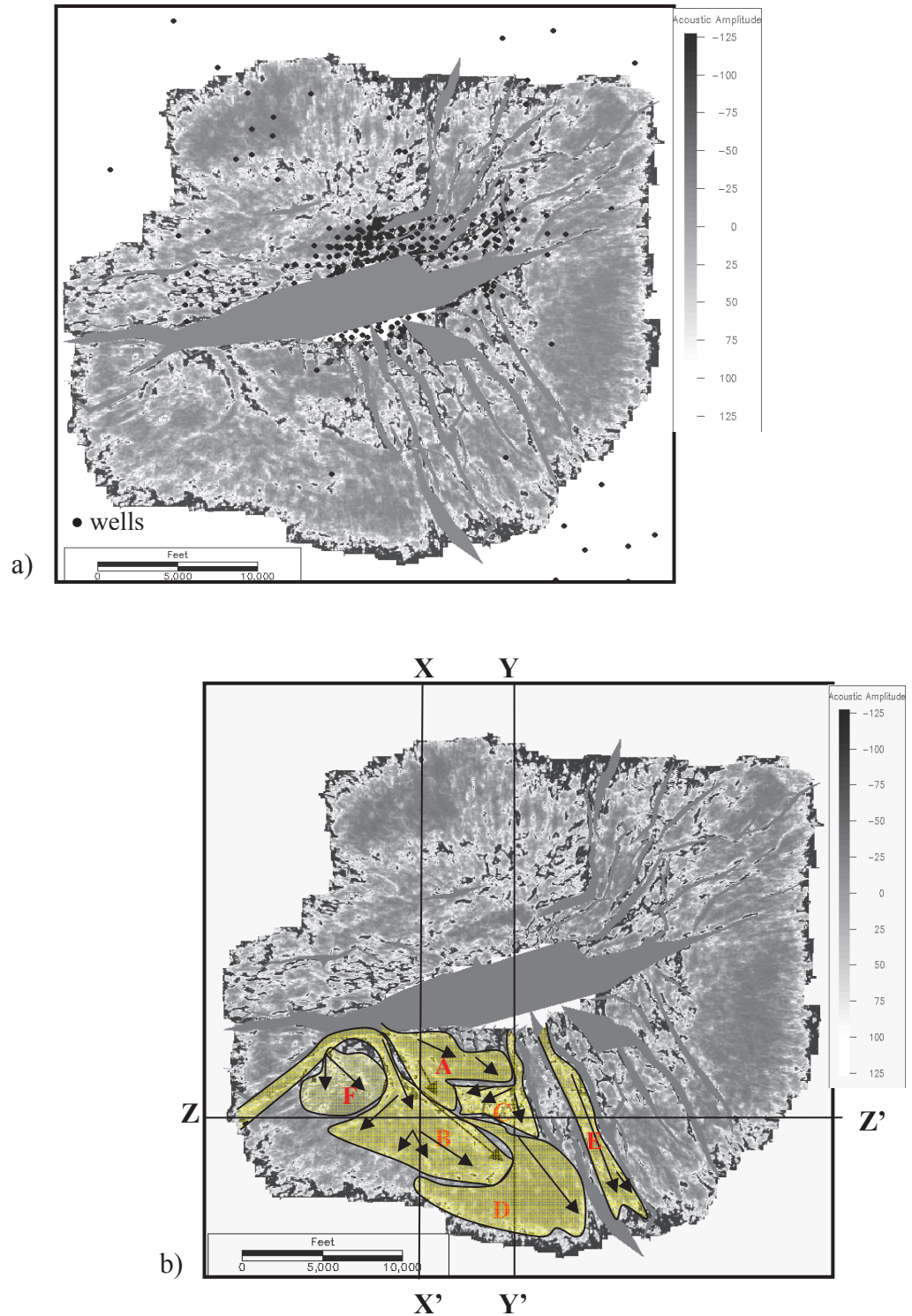
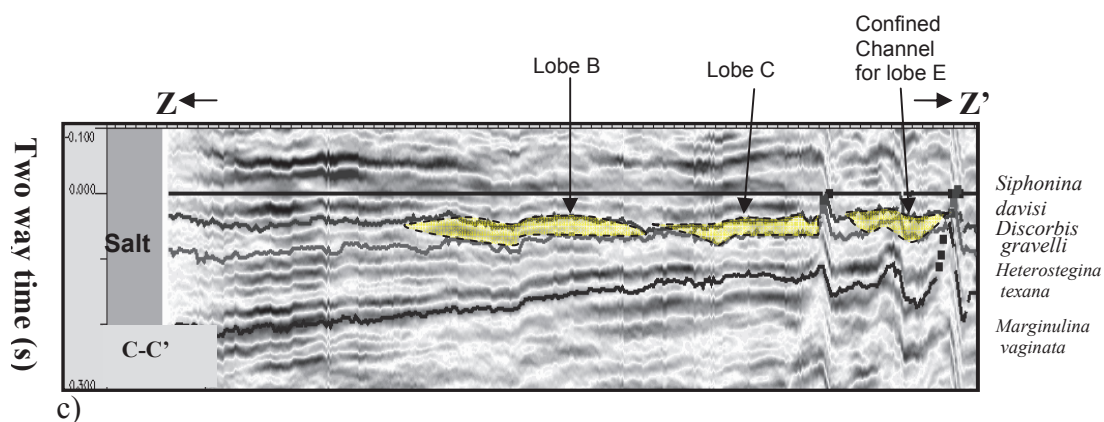
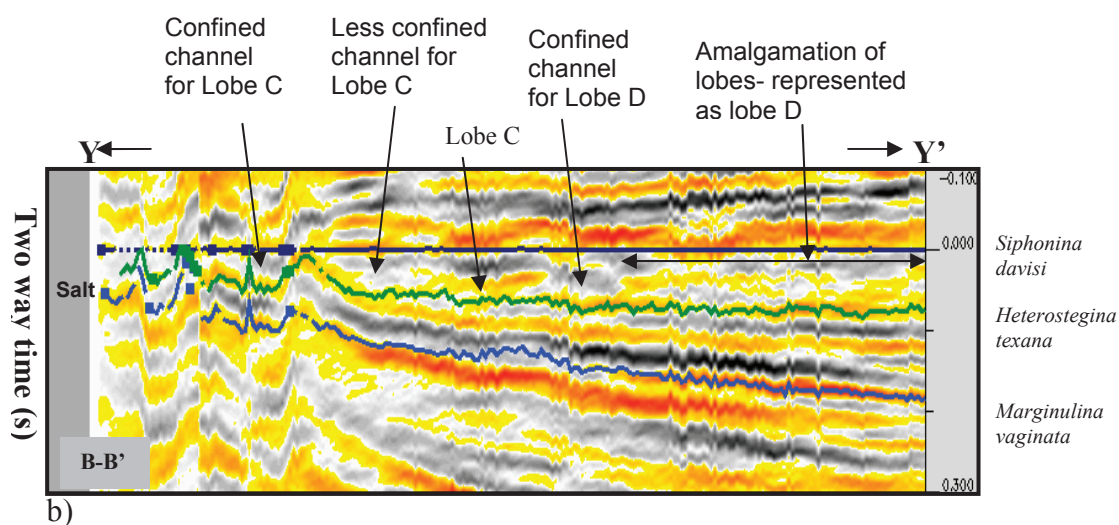
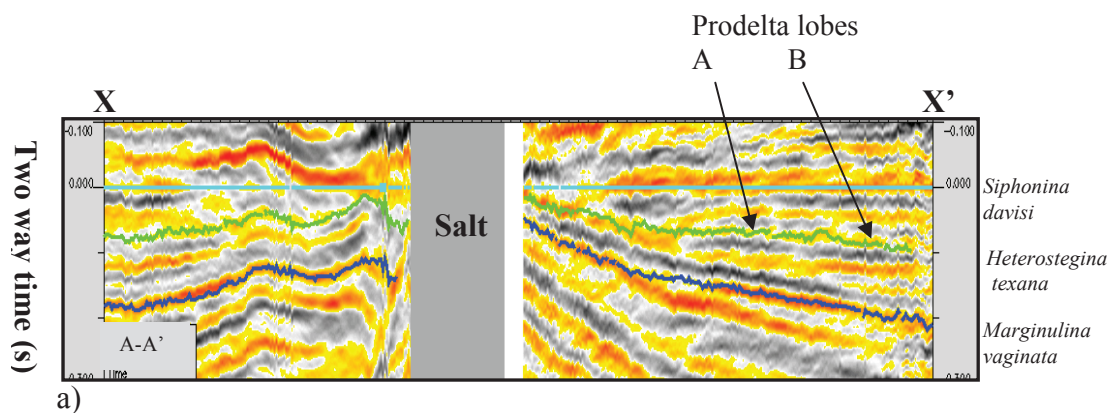


Figure 67: a) Un-interpreted and b) interpreted coherence maps of the *Heterostegina texana* – *Discorbis gravelli* section showing depositional lobes. I interpret these as subaqueous channels and prodelta turbidites. Seismic profiles of crosslines X-X' and Y-Y' and inline Z-Z' across lobes are shown in figures 68 a-c.





Figures 68 a, b & c: Seismic profiles X-X', Y-Y' and Z-Z' flattened on *Siphonina davisi* horizon reveal Late Oligocene subaqueous channels and associated lobes. Figure 68 b illustrates that lobe C appears to have been eroded by another channel. Lobe D is an amalgamation of older lobes. Lobe C is younger than lobe B.



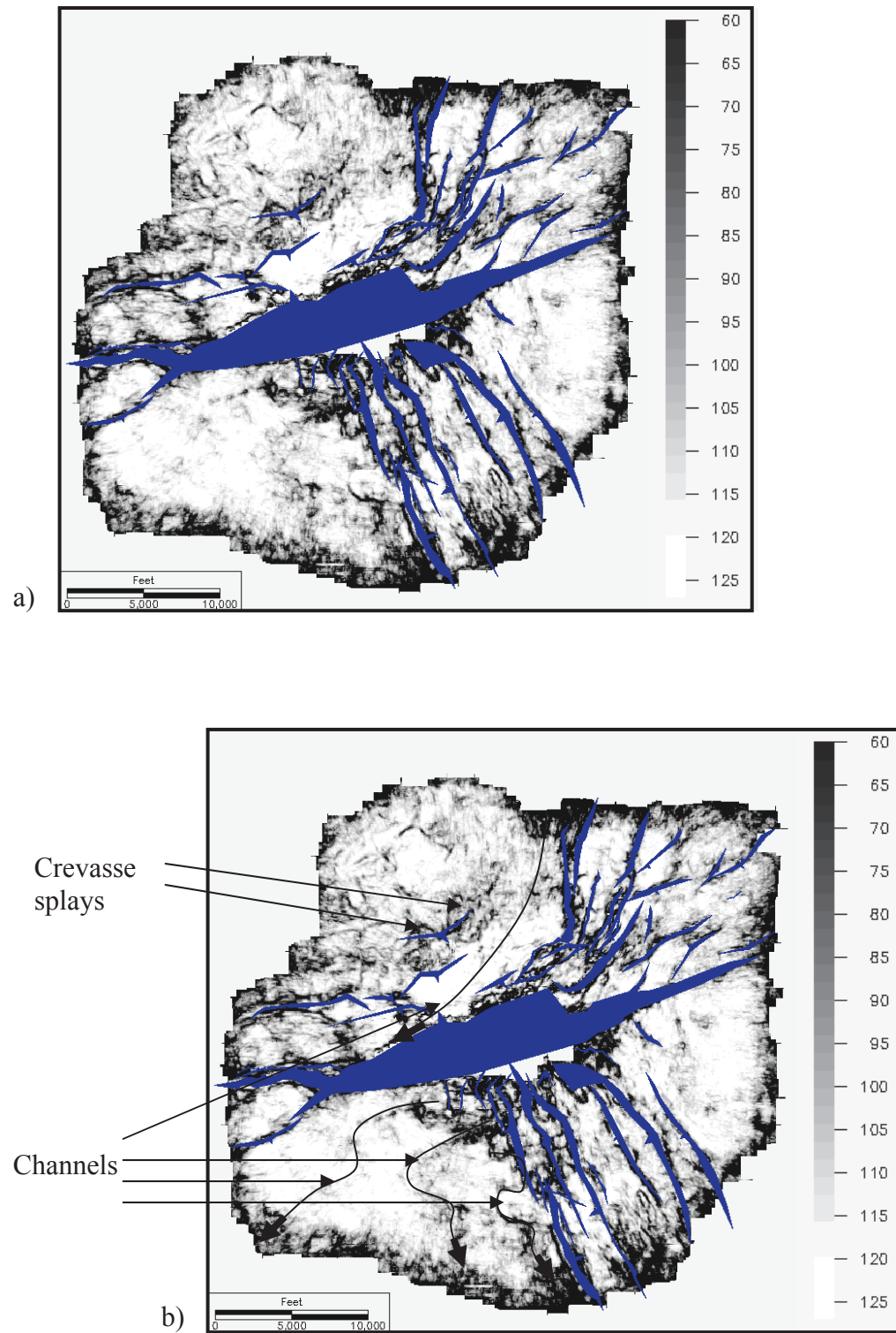


Figure 69: a). Un-interpreted and b). interpreted coherence maps of the Aquitanian section showing evidence of channels.

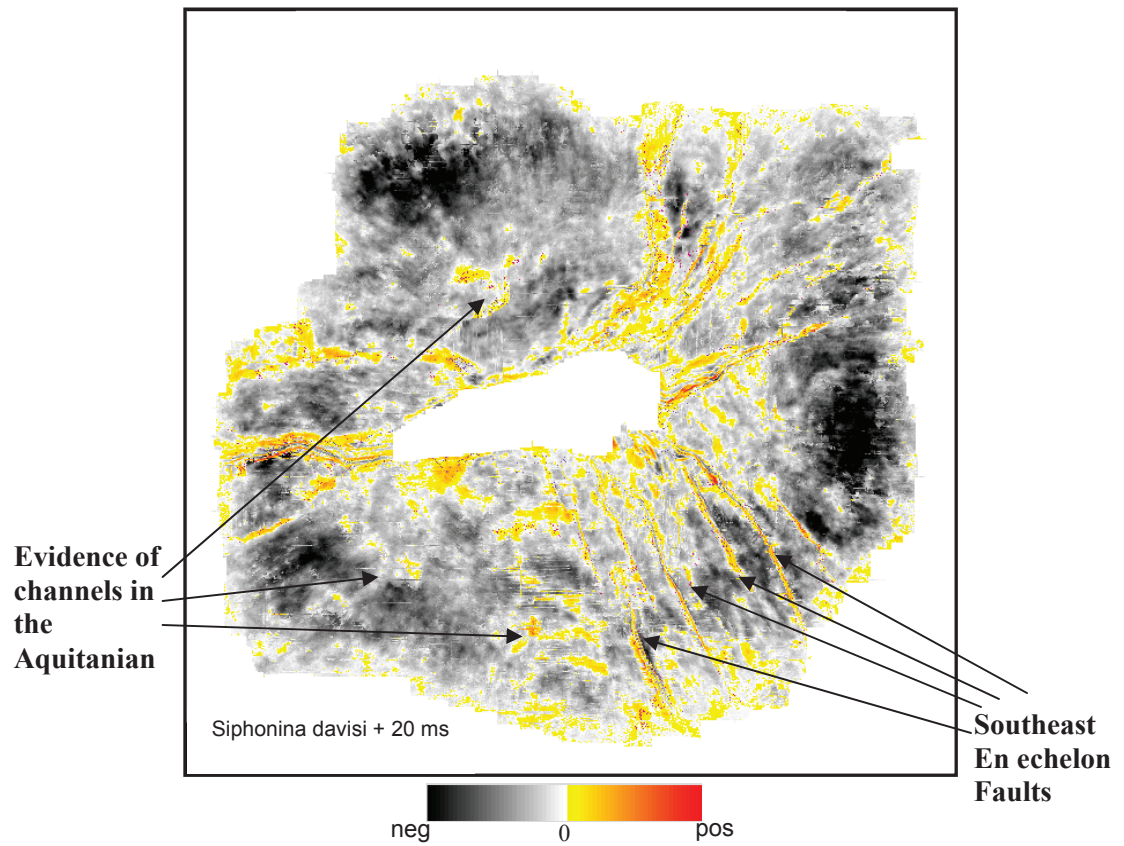


Figure 70: Stratal slice of amplitude map of the Aquitanian, Vinton Dome

## CHAPTER FIVE

### CONCLUSIONS

The stratigraphy and the depositional regime of the Aquitanian were controlled by the structural pattern and salt tectonism. Accommodation in the northern part of the dome was regulated by the inter-relationship of tectonic subsidence and sediment dispersal. Evolution of the Aquitanian was better understood by its comparison with the preceding Oligocene strata.

Salt shape largely controlled the structural pattern in the Late Oligocene to Early Miocene. The dome contained complex fault systems that controlled the depositional systems. The dome consists of a counter-regional fault, three peripheral fault sets, and isotropic polygonal fault system in the entire dome. This is probably the first documentation of fine scale polygonal faults in the Gulf of Mexico basin. The North Sea basin, however, has numerous reports of larger scale polygonal faults. Vinton polygonal faults are fracture sets and can be formed by dewatering processes, syneresis, deformation by salt movement, and/or by episodic hydrofracturing of basin-wide over-pressured compartments.

Aquitania strata were deposited with the rising salt and the depocenter distribution was controlled by unconformity, growth along the active faults, and perhaps also by salt withdrawal processes. The Late Oligocene strata however, were characterized by slumping.

Deltaic sandstones and younger fluvial deposits characterize the Aquitanian. The Top Aquitanian fossils and their environmental preference suggest that the area was on the inner neritic shelf. Presence of crevasse splays and numerous fluvial deposits indicate that the Aquitanian environment was a lower delta plain. Fluvial input from the northeastern part of the dome to the south and west parts may have created overloading of sediments and a resultant unconformity, perhaps activated by salt withdrawal processes. Thick fluvial deposits, perhaps more than 150 ft (46 m), are present in the southeast depocenter, which has a gross thickness of about 280 ft (85 m). The draping of the *Siphonina davisi* shale on the Aquitanian sandstones indicates that the unconformity was partly tectonically impacted.

The Upper Oligocene Anahuac section contains mudstones and siltstones with fossils that indicate inner to outer neritic shelf. Presence of deformation structures along the rim syncline in the north, subaqueous channels and their accompanying turbidites in the south suggests a prodelta environment. The major depocenter in the Late Oligocene occurred in the west and the major shift to the southeast in the Aquitanian was controlled by salt withdrawal processes. Presence of clinoforms below the *Marginulina vaginata* section indicates that the area was previously a delta front environment.

Highstand sedimentation of the Aquitanian on top of the transgressive sedimentation of the Late Oligocene suggests a sea-level fall, which corresponds to the previously established 2<sup>nd</sup> order sea level fall. Accommodation on shelf is typically thin, that may make shelf tracts to co-exist at the same depth. However,

two unconformities have been identified; one in the Early Anahuac, above the *Marginulina vaginata* MFS zone and the other in the Aquitanian, above the deltaic sandstones.

New acquisition and interpretation technology have provided better imaging of the complexly-faulted Vinton Dome strata and an opportunity to further decipher its depositional systems. Seismic attributes further provided finer scale structural architecture of the dome and salt tectonics has been better understood on the Miocene shelf. The study highlighted some of the stratigraphic complexities of delta systems and depositional bodies formed in shallow water under conditions of limited accommodation and salt influence.

## REFERENCES

- Arenson J. D., Medvin, E. A., & Maione, S. J., 1999, Interpretation of Coherence Cube Processing in the 3-D Workspace: American Association of Petroleum Geologists: vol. 49, p. 74-81.
- Barnes, A., 2006, Too many seismic attributes?: CSEG Recorder: p. 40-45.
- Berggren, W. A. & Miller, K. G., 1989, Cenozoic bathyal and abyssal calcareous benthic foraminiferal zonation: Micropaleontology: vol. 35, p. 308-320.
- Bhattacharya, J. P. & Walker, R. G., 1992, Deltas. *In* Walker, R. G., and James, N. P. (eds), Facies Models: Response to Sea-level Change: Geological Association of Canada, p. 157-177.
- Blood, T. E. & Crastley, 1995, Evidence for additional type 1 sequences in the lower Miocene of the Gulf of Mexico: Annual Meeting Abstracts - American Association of Petroleum Geologists: vol. 4, p.10.
- Breard, S.Q., Callender, D. A., & Nault, M. J., 1993, Paleoecologic and Biostratigraphic Models for Pleistocene through Miocene Foraminiferal Assemblages of the Gulf Coast Basin: Gulf Coast Association of Geological Societies Transactions: vol. 43, pp. 493-502.
- Breard, S.Q., Nault, M. J., & Callender, A. D., 1994, Biostratigraphy and Paleoecologic Tolerances of Oligocene through Paleocene Foraminiferal Assemblages of the Gulf Coast Basin: Gulf Coast Association of Geological Societies Transactions: vol. 44, p. 111-116.
- Breard, S.Q., Callender, D. A., & Nault, M. J., 1996, Local Foraminiferal Faunas: The Key to Enhanced Stratigraphic Resolution of Expanded Cenozoic Sections in the Gulf Coast Basin: Gulf Coast Association of Geological Societies Transactions: vol. 46, p. 55-62.
- Brown, A. R., 1996, Seismic attributes and their classification: The Leading Edge: vol. 15, p. 1090.

Brown, A. R., 2005, Pitfalls in 3-D Seismic Interpretation: Search and Discovery Article: #40145.

Chopra, S. & Marfurt, K., 2005, Seismic Attributes – a historical perspective: Geophysics: vol. 79, p 3SO- 28SO.

Chopra, S. & Marfurt, K., 2006, Seismic Attributes – a promising aid for geologic prediction: CSEG: 2006 Special Edition: p. 110-121.

Coleman, J. M. & Prior, D. B., 1982, Deltaic Environment of Deposition: American Association of Petroleum Geologists: vol. M31: Sandstone Depositional Environments, p. 139-178.

Combellas-Bigott, R. I., & Galloway, W. E., 2002, Depositional history and genetic sequence stratigraphic framework of the middle Miocene depositional episode, south Louisiana: Gulf Coast Association of Geological Societies Transactions, vol. 52, p. 139-150.

Constance, P. E., Holland, M. B., Roche, S. L., Bicquart, P., Bryans, B., Gelinsky, S., Ralph, J. G., & Bloor, R. I., 1999, Simultaneous acquisition of 3D surface seismic data and 3C, 3D VSP data: 69<sup>th</sup> Ann. International Meeting, SEG, Expanded Abstracts, 104-107.

Curtis, D. M., 1970, Miocene deltaic sedimentation, Louisiana Gulf Coast: *in*, Morgan, J. P., edition, Deltaic sedimentation, modern and ancient: SEPM Special Publication: 15, p. 293-308.

Dewhurst, D. N., Cartwright, J. A., & Lonergan, L., 1999, The development of polygonal fault systems by syneresis of colloidal sediments: Marine and Petroleum Geology: vol. 16, p. 793-810.

Edwards, M. B., 1994, Enhancing sandstone reservoir prediction by mapping erosion surfaces, Lower Miocene Deltas. Southwest Louisiana, Gulf Coast Basin: Gulf Coast Association of Geological Societies Transactions: vol. 44, pp. 205-215.



- Fails, T. G., 1990, Variation in Salt Dome Faulting, Coastal Salt Basin: Gulf Coast Association of Geological Societies Transactions, vol. 40, p. 181-193.
- Fillon, R. H. & Lawless, P. N., 1999, Miocene Deposition and Petroleum Geology, Northern Gulf of Mexico: Petroleum Technology Transfer Council, Eastern Gulf Region- Technology Workshop, Jackson, Mississippi, November 10, 1999.
- Fillon, R. H. & Lawless, P. N., 1999, Paleocene – Lower Miocene Sequences in the Northern Gulf: Progradational Slope Salt-Basin Deposition and Diminishing Slope-Bypass Deposition in the Deep Basin: Gulf Coast Association of Geological Societies Transactions: vol. 49, p. 224-241.
- Fillon, R. H. & Lawless, P. N., 2000, Lower Miocene – Early Pliocene Deposystems in the Gulf of Mexico; Regional Sequence Relationships: Gulf Coast Association of Geological Societies and Gulf Coast Section SEPM, 47<sup>th</sup> annual meeting: vol. 50, pp.411-428.
- Galloway, W. E., 2001, Cenozoic evolution of sediment accumulation in deltaic and shore-zone depositional systems, Northern Gulf of Mexico Basin: Marine and Petroleum Geology: vol. 18, p. 1031-1040.
- Galloway, W. E., Ganey-Curry, P., Li, X., & Buffler, R. T., 2000, Cenozoic depositional evolution of the Gulf of Mexico Basin: American Association of Petroleum Geologists: vol. 84, p. 1743-1774.
- Galloway, W. E., Jirik, L. A. Morton, R. A., & Dubar, J. R., 1986, Lower Miocene (Fleming) depositional episode of the Texas coastal plain and continental shelf: structural framework, facies, and hydrocarbon resources: University of Texas at Austin, Bureau of Economic Geology Report of Investigations: vol.150, 50 p.
- Galloway, W. E., 1986, Growth faults and Fault – Related Structures of Prograding Terrigenous Clastic Continental Margins: Gulf Coast Association of Geological Societies Transactions: vol. 36, p. 121-128.
- Hamiter, R., Lowrie, A., MacKenzie, M., & Guderian, E., 1997, Origin of Salt-Withdrawal Mini-Basins, Proven Producers Aling Present and Paleo-Louisiana

- Slope: Gulf Coast Association of Geological Societies Transactions: vol. 47, p. 185-191.
- Haq, B. U., Hardenbol, J., & Vail, P. R., 1988, Mesozoic and Cenozoic Chronostratigraphy and Eustatic Cycles: SEPM Special Publication, 42, Tulsa, 71-108.
- Haskell, N., Nissen, S., & Hughes, M., 1999, Delineation of geologic drilling hazards using 3-D seismic attributes: The Leading Edge: vol. 18, no. 3, p. 373-382.
- Hentz, T. F. & Zeng, H., 2003, High-Frequency Miocene sequence stratigraphy, offshore Louisiana: Cycle framework and influence on production distribution in a mature shelf province: American Association of Petroleum Geologists: vol. 87, no. 2, p. 197-230.
- Hughes, D. J., 1960, Faulting Associated with Deep-Seated Salt Domes in the Northeast Portion of the Mississippi Salt Basin: Gulf Coast Association of Geological Societies Transactions: vol. 10, p. 155-173.
- Hughes, D. J., 1968, ERRATA Salt Tectonics as Related to Several Smackover Fields Along the Northeast Rim of the Gulf of Mexico Basin: Gulf Coast Association of Geological Societies Transactions: vol. 18, p. 320-330.
- Hunt, J. L. & Burgess, G., 1995, Depositional Styles from Miocene Through Pleistocene in the North-Central Gulf of Mexico: An Historical Reconstruction: Gulf Coast Association of Geological Societies Transactions: vol. 45, p. 275-284.
- Joy, A. M., 1993, Comments on the pattern of post-rift subsidence in the central and northern North Sea Basin, *in* Williams G. D., & Dobb, A., Tectonics and seismic sequence stratigraphy: Geological Society Special Publications: vol. 71, p. 123-140.
- Krutack, P. R. & Beron, P., 1990, Heterostegina zone – a shallow Anahuac (Late Oligocene – Early Miocene) oil frontier in southern Louisiana and Mississippi: Transactions GCAGS: vol. 40, p. 397-409.

- Lawless, P. N., Fillon, R. H., & Lytton, III, R. G., 1997, Gulf of Mexico Cenozoic Biostratigraphic, Lithostratigraphic, and Sequence Stratigraphic Event Chronology: Gulf Coast Association of Geological Societies Transactions: vol. 47, p. 271-282.
- Lerche, I., Malloy, S., Petersen K., & Lowrie A., 1996, Lateral Variations of Sub-salt Overpressure Build-up in the Gulf of Mexico: Gulf Coast Association of Geological Societies Transactions, vol. 46, p. 271-280.
- Liu Q., Buffler R. T., & Galloway, W. E., 1997, Seismic Expression and Depositional Environments of a Late Oligocene/Earliest Miocene Carbonate Unit, Offshore Mississippi and Alabama: Gulf Coast Association of Geological Societies Transactions: vol. 47, p. 291-297.
- Lovell, J. P. B., 1990, Cenozoic, *in* Glennie, K. W., An introduction to the petroleum geology of the North Sea, Oxford: Blackwell Scientific Publications: p. 273-293.
- Mancini, E. A., Puckett, T. M., Parcell, W. C., & Llinas, J. C., 2001, Smackover Petroleum System (Source, Reservoir, Seal and Trap) And Underdeveloped Smackover Reservoirs in the Mississippi Interior Salt Basin: Topical Reports: vol. 5-8.
- Marfurt, K. J., 2005, Robust Estimates of 3-D Reflector Dip and Azimuth: submitted to Geophysics.
- Martin P. A. Jackson & William E. Galloway, 1984, Fault Patterns Around Salt Domes: American Association of Petroleum Geologists: Special Volumes: Vol. A159, p. 95 – 101.
- Marton, G. & Buffler, R.T., 1993, Application of simple-shear model to the evolution of passive continental margins of the Gulf of Mexico Basin: Geology: vol. 21, p. 495-498.
- McBride, B.C., Weimer P., & Rowan M.G., 1998, The evolution of allochthonous salt along a megaregional profile across the Northern Gulf of Mexico: American Association of Petroleum Geologists: vol. 82, no. 5B, p. 1037-1054.

- Mohriak, W.U., Macedo, J.M., Castellani, R.T., Rangel, H.D., Barros, A.Z.N., Latg, M.A.L., Mizusaki, A.M.P., Szatmari, P., Demercian, L.S., Rizzo, J.G., & Aires, J.A., 1995, Salt tectonics and structural styles in the deepwater province of the Cabo Frio region, Rio de Janeiro, Brazil: American Association of Petroleum Geologists Memoir: vol. 65, p. 273-304.
- Nettleton, L. L., 1934, Fluid Mechanics of Salt Domes: American Association of Petroleum Geologists Bulletin, vol. 27, p. 51-63.
- Olariu, C., & Bhattacharya, J. P., 2006, Terminal Distributary Channels and Delta Front Architecture of River-Dominated Delta Systems: Journal of Sedimentary Research: vol. 76, no. 2, p. 21-233.
- Parker, T. J. & McDowell, A. N., 1955, Model Studies of Salt Dome Tectonics: American Association of Petroleum Geologists Bulletin: vol. 39, no. 12, p. 2384 – 2470.
- Pate, K. A., & Dunbar, J., 2000, Evolution of faulting Styles around Salt Domes: American Association of Petroleum Geologists Bulletin, vol. 2000, p. 112.
- Pattison, S. A. J., 2005, Storm Influenced Prodelta Turbidite Complex in the Lower Kenilworth Member at Hatch Mesa, Book Cliffs, Utah, U.S.A.: Implications for Shallow Marine Facies Models: Journal of Sedimentary Research: vol. 75, no. 3, p. 420 - 439.
- Pirson, S. J., 1977, Geologic Well Log Analysis: Book: 2<sup>nd</sup> Edition, Gulf Publishing Company.
- Posamentier, H. W., James, D. P., & Allen, G. P., 1990, Aspects of sequence stratigraphy: recent and ancient examples of forced regressions: American Association of Petroleum Geologists Bulletin: vol. 74, p. 742.
- Posamentier, H. W., Allen, G. P., James, D. P., & Tesson, M., 1992, Forced Regressions in a Sequence Stratigraphic Framework: Concepts, Examples, and Exploration Significance (1): American Association of Petroleum Geologists Bulletin: vol. 76, p. 1687-1709.

- Posamentier, H. W. & Allen, G. P., 1999, Siliciclastic Sequence Stratigraphy – Concepts and Applications: SEPM Concepts *in* Sedimentology and Paleontology #7.
- Rader, B., & Medvin, E., 2002, Shallow hazard detection in the near-surface, a coherence cube processing application: The Leading Edge: vol. 21, p. 672-674.
- Rekoske, K., & Hicks, D., 1992, Synthetic Seismograms: Part 7. Geophysical Methods: American Association of Petroleum Geologists: Special Volumes: vol. AO95, p. 390-391.
- Rijks, E. J. H. & Jauffred, J. C. E. M., 1991, Attribute extraction: An important application in any detailed 3D interpretation study: The Leading Edge: vol. 10, p. 11-19.
- Roberts, A., 2001, Curvature attributes and their application to 3D interpreted horizons, First Break, **19**, 85-100.
- Rowan, M., 2000, Modern Salt Tectonics: Workshop sponsored by Petroleum Technology Transfer Council's Eastern Gulf Region on July 26, 2000, Jackson, Mississippi.
- Salvador, A., 1987, Late Triassic-Jurassic paleogeography and origin of Gulf of Mexico basin: American Association of Petroleum Geologists: vol. 71, no. 4, p. 419-451.
- Seni S. J. & Jackson M.P., 1983, Evolution of Salt Structures, East Texas Diapir Province, Part 1: Sedimentary Record of Halokinesis: American Association of Petroleum Geologists: vol. 67, no. 8, p. 1219-1244.
- SONRIS Database Access, 2006, Louisiana Department of Natural Resources: [sonris.com](http://sonris.com)
- Soria, J. M., Fernandez, J., Garcia, F., & Viseras C., 2003, Correlative Lowstand Deltaic and Shelf Systems in the Guadix Basin (Late Miocene, Betic Cordillera, Spain): The Stratigraphic Record of Forced and Normal Regressions: Journal of Sedimentary Research: vol. 73, no. 6, p. 912-925.

- Styzen, M. J., 1996, Late Cenozoic Chronostratigraphy of the Gulf of Mexico: Chart (In progress), Shell Offshore Inc.
- Taner, M. T. & Sheriff, R. E., 1977, Seismic Stratigraphy - Applications to Hydrocarbon Exploration: Memoir 26: A165, p. 301-327.
- Tearpock, D. J. & Bischke, R. E., 1991, Applied subsurface geological mapping: Prentice-Hall, N.J., 648 p.
- Thompson, S. A. & Eichelberger, O. H., 1928, Vinton Salt Dome, Calcasieu Parish, Louisiana: American Association of Petroleum Geologists: vol. 12, no. 4, p. 385-394.
- Trevino, R. H., Loucks, R. G., Brown, F. L. & Remington, R. L., 2003, General Geology of the Mid-Tertiary Block 889 Field Area, Offshore Mustang Island, Texas: Gulf Coast Association of Geological Societies Transactions: vol. 53, p. 808-819.
- Trusheim, F., 1960, Mechanism of Salt Migration in northern Germany: American Association of Petroleum Geologists Bulletin, vol. 44, p. 1519-1540.
- Vendeville, B. C., 2002, A New Interpretation of Trusheim's Classic Model of Salt-Diapir Growth: Gulf Coast Association of Geological Societies Transactions, vol. 52, p. 943-952.
- Vendeville, B. C., Fouad, K., & Knox, P. R., 2003, Radial faulting above salt-diapir overhangs; natural example, and physical and kinematic models: Gulf Coast Association of Geological Societies Transactions: vol. 53, p. 828-835.
- Wagoner, J. C., Mitchum, R. M., Campion, K. M., & Rahmanian, V. D., 1990, Siliciclastic Sequence Stratigraphy in Well Logs, Cores, and Outcrops: American Association of Petroleum Geologists Methods in Exploration Series: no 7.
- Watkins, J. S., Bradshaw, B. E., Huh, S., Li, R., & Zhang, J., 1996, Structure and Distribution of Growth Faults in the Northern Gulf of Mexico: OCS: vol. 46, p. 63-77.

Watkins, J. S., Bryant, W. R., Buffler, R. T., staff and students of the Gulf of Mexico Structural and Stratigraphic Synthesis Project, Department of Geology, Texas A&M, 1996, Structural Framework Map of the Northern Gulf of Mexico: Gulf Coast Association of Geological Societies: vol. 46, p. 95-98.

Welper O. J., 2000, The Use of Coherence Cube Visualization in Picking Seismic Processing Parameters and Post Processing Hybrid Visualization Products: American Association of Petroleum Geologists, vol 50, p. 485-494.

White, R., & Simm, R., 2003, Tutorial: Good practice in well ties: First Break: vol. 21, p. 75-83.

Withjack, M. O. & Scheiner C., 1982, Fault Patterns Associated with Domes – An Experimental and Analytical Study: American Association of Petroleum Geologists Bulletin: vol. 66 no. 3, p. 302-316.

Witrock, R. B., A. R. Friedmann, J. J. Galluzzo, L. D. Nixon, P. J. Post, and K. M. Ross, 2003, Biostratigraphic chart of the Gulf of Mexico offshore region, Jurassic to Quaternary, U. S. Department of the Interior, Minerals Management Service, New Orleans.

Worall, D.M. & Snelson, S., 1989, Evolution of the northern Gulf of Mexico, with emphasis on Cenozoic growth faulting: The Geology of North America: vol. A, pg. 97-136.

Vail, P. R., & Wornardt, W. Jr., 1991, An Integrated Approach to Exploration and Development in the 90s: Well Log-Seismic Sequence Stratigraphy Analysis: Transactions GCAGS/GCSSEPM: vol. 61, p. 630-650.

Yin, H. & Groshong, R. H., Jr., 2003, Geometric Properties of Active Piercement Structures: Geologic Insights from 3-D Kinematic Models: Transactions GCAGS/GCSSEPM, vol. 53, p. 888-900.

Zeng, H., & Hentz, T. F., 2004, High-Frequency sequence stratigraphy from seismic sedimentology: Applied to Miocene, Vermilion Block 50, Tiger Shoal area, offshore Louisiana: American Association of Petroleum Geologists: vol. 88, no. 2, p. 153-174.